A STUDY OF NON-LINEAR RAREFIED GAS FLOW PROBLEMS

A THESIS

Presented to

The Faculty of the Graduate Division

by

Danny Lynn Hartley

In Partial Fulfillment

of the Requirements for the Degree

Doctor of Philosophy

in the School of Aerospace Engineering

Georgia Institute of Technology

September, 1967

A STUDY OF NON-LINEAR RAREFIED GAS FLOW PROBLEMS

Approved:

Chairman

Date approved by Chairman: 9/15/67

In presenting the dissertation as a partial fulfillment of the requirements for an advanced degree from the Georgia Institute of Technology, I agree that the Library of the Institute shall make it available for inspection and circulation in accordance with its regulations governing materials of this type. I agree that permission to copy from, or to publish from, this dissertation may be granted by the professor under whose direction it was written, or, in his absence, by the Dean of the Graduate Division when such copying or publication is solely for scholarly purposes and does not involve potential financial gain. It is understood that any copying from, or publication of, this dissertation which involves potential financial gain will not be allowed without written permission.

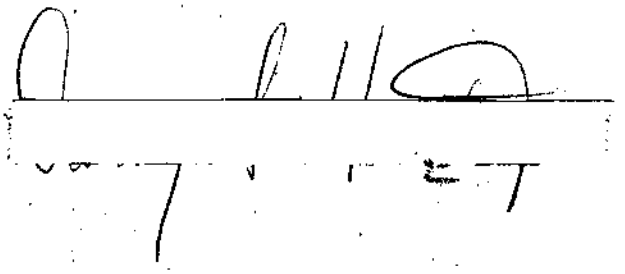

3/17/65

ACKNOWLEDGMENTS

I would like to express my appreciation to Dr. A. Ben Huang for his suggestion of the topic and for his cooperation, counsel, and constructive suggestions during the investigation. I would also like to thank the other members of my reading committee, Dr. Arnold L. Ducoffe and Prof. James E. Hubbartt, for their patient examination of the manuscript.

I am grateful to Mr. T. Taz Bramlette for numerous discussions on the kinetic theory aspects of this research as well as for his critical study of the rough manuscript. Also, I received invaluable advice from Dr. Kenton D. Whitehead and Dr. Jerry A. Sills on the various numerical and computational aspects of the problem. I thank Mr. Robert K. Sigman for his contributing comments. The assistance of Mr. P. F. Huang and of Mr. Y. J. Lin in helping carry out much of the computation in deriving the new quadrature and in testing the Couette flow formulation cannot go unnoticed. I am especially grateful for the generosity of Mrs. Rena Austin for typing the rough draft on this thesis.

I am grateful for the financial aid of an NDEA fellowship and of Ford loans for easing my financial situation during the graduate work.

Finally I thank my parents, Mr. and Mrs. Edward L. Hartley, for their foresight, guidance, encouragement, and unselfish sacrifice in helping me pursue my education and my wife Barbara for her patience, understanding, and encouragement during my years of graduate work.

TABLE OF CONTENTS

LIST OF ILLUSTRATIONS

LIST OF SYMBOLS

a	normal direction transformation constant
B	Gauss-Seidel iteration matrix
C	Chapman-Rubesin constant
C_f	skin friction coefficient, $\frac{\tau}{\frac{1}{2}\rho_\infty U_\infty^2}$
C_h	heat transfer coefficient, $\frac{-q}{\rho_\infty U_\infty c_p (T_w - T_{aw})}$
C_p	pressure coefficient, $\frac{(\frac{p}{p_\infty} - 1)}{\frac{1}{2}\rho_\infty U_\infty^2}$
c_p	specific heat at constant pressure
d	width between plates in Couette flow
D	given matrix in Gauss-Seidel iteration formulation
E	error term in quadrature formulation
f	local distribution function
F	local Maxwellian equilibrium distribution function
g	first transformed distribution function
G	equilibrium form of first transformed distribution function
h	second transformed distribution function
H	equilibrium form of second transformed distribution function
j	third transformed distribution function
J	equilibrium form of third transformed distribution function
k	Boltzmann's constant
k_i	quadrature coefficient

Kn	Knudsen number
m	molecular mass
M_∞	free stream Mach number
n	density, integer defining number of discrete points used in quadrature
P_{ij}	stress tensor
p	pressure
P_i	Lagrange polynomial
Pr	Prandtl number
$\bar{q}$	heat flux vector with components q_x, q_y, q_z
r	recovery factor, reference point for finite difference formulation
R_{n-1}	Lagrange error term
Re_x	Reynold's number at local x station
S	viscosity-temperature exponent
t	time
T	temperature
$\bar{u}$	macroscopic velocity with components u_x, u_y, u_z
U_∞	free stream velocity
$\bar{v}$	microscopic velocity with components v_x, v_y, v_z
V_1	characteristic velocity, Equation 9, Chapter II
V_∞	characteristic velocity, Equation 11, Chapter III
$\bar{V}_{\infty,x}$	rarefaction parameter, $M_\infty(C/Re_x)^{1/2}$
w	discrete ordinate spacing
w'	optimum discrete ordinate spacing
W	velocity of upper plate for Couette flow
$\bar{x}$	position vector with components x, y, z

α_i	discrete ordinate
β	inverse of most probable molecular velocity, $(m/2kT)^{1/2}$
γ	ratio of specific heats
$\bar{\varepsilon}$	error vector with components ε_i
η	transformed normal position vector
λ	mean free path
$\lambda_{G.S.}$	Gauss-Seidel eigenvalue
μ	viscosity
ν	collision frequency
ρ	gas density
$\rho(B)$	spectral radius of matrix B
τ	collision time
$\tau(y)$	universal coordinate
$\bar{\chi}_{\infty,x}$	hypersonic interaction parameter, $M_\infty^3(C/Re_x)^{1/2}$

Superscript

$\pm$	indicates the positive and negative directions of v_y

Subscripts

aw	adiabatic wall condition
G.S.	Gauss-Seidel
o	stagnation condition
s	slip condition
w	wall condition
1	lower plate condition
2	upper plate condition
∞	free stream condition
σ	evaluated at x-component of microscopic velocity associated with σ discrete point

δ	evaluated at y-component of microscopic velocity associated with δ discrete point

SUMMARY

The application of the discrete ordinate method to non-linear rarefied gas flows is presented. The governing equation is taken to be the Boltzmann transport equation with the Bhatnagar-Gross-Krook model of the collision integral. The discrete ordinate method has previously been applied to linearized problems, and it proved to give accurate solutions over a wider range of Knudsen numbers for a given amount of computational effort than any other known existing analytic method. For non-linear problems the quadratures used in the linearized problems are no longer suitable due to the non-equilibrium forms of the velocity distribution function. A new quadrature based on "odd" and "even" equally spaced discrete ordinates is presented. The significant features of the proposed quadratures and their flexibility for adaptation to non-linear problems are discussed.

The method is first applied to the problem of non-linear Couette flow with heat transfer (whose numerically exact solution is available) to calibrate the usefulness and accuracy of the method. The method is then applied to the previously unresolved sharp leading edge problem. The complete flow field near the leading edge is generated and all surface quantities (pressure, skin friction, heat transfer, and slip velocity) are compared to existing theoretical and experimental results.

The general results of the investigation may be summarized in the following conclusions:

1. The discrete ordinate method has been shown to give accurate

solutions over a wider range of Knudsen numbers for a given amount of computational effort than any other known existing method applied to the non-linear BBGK equation.

2. The flexibility of the discrete ordinate method, which has been extended to solve problems previously considered unapproachable from a computational standpoint, has been demonstrated in the solution of the leading edge problem. The results of the leading edge solution offer considerable insight into the behavior of a rarefied gas flow as it traverses the complete spectrum of flow regimes from near-free molecular to continuum, and presents a meaningful connection between the first-collision kinetic theory solutions at the leading edge and the extended continuum theories in the interaction regimes.

3. The successful extension of the method of discrete ordinates to non-linear problems is due to the development of the equally spaced quadratures.

4. The flow field generated for the leading edge problem presents a reasonable picture of the macroscopic properties and their special variations. The results indicate that the effect of wall temperature is confined to the boundary layer region and significantly influences only the density and temperature profiles. The thickness of the shock wave is in qualitative agreement with the theory of Gilbarg and Paolucci [66] and of Liepman, et. al. [64]. The shock front position is slightly below the Mach wave, which agrees with the trend of Butler's numerical solution [60].

5. The surface pressures generated for the leading edge problem agree with the second order weak interaction theory of Hayes and Probstein

[43] in the weak interaction range $\bar{V}_{\infty,x} \lesssim 0.15$. The pressure results have the correct trend as indicated by available experimental data at nominal Mach numbers [40,48]. The pressure peak noted by several experimental investigators [47,48,49] is confirmed and, in fact, occurs in the transition range, $0.4 \leq \bar{V}_{\infty,x} \leq 0.6$, as pointed out by Becker and Boylan [48] and by Moulic [40]. The solution at the leading edge, $\hat{x} = 0$, does not achieve the free molecule limit and indicates that no true free molecule region exists. This was also pointed out by Kogan [62] and by Bird [63].

6. The skin friction results for the leading edge problem are in qualitative agreement with the Blassius solution in the interaction regime, $\bar{V}_{\infty,x} \lesssim 0.3$. The present solution also yields qualitative agreement with the experimental results of Wallace and Burke [51] and of Moulic [40] for the interaction and merged regimes, $\bar{V}_{\infty,x} \lesssim 0.5$. The present results do not exhibit a "peak" of maximum skin friction behind the leading edge, but merely a reduction in slope of the skin friction curve as the leading edge is approached. This behavior agrees with the theoretical predictions of Mirels [67].

7. The heat transfer results for the leading edge problem are in good agreement with boundary layer theory [35] for $\bar{V}_{\infty,x} < 0.1$. The application of Reynold's Anology as corrected by Li and Nagamatsu [56] gives excellent results for $\bar{V}_{\infty,x} \lesssim 0.35$. The present results exhibit a heat transfer peak in the transition region, $0.4 \leq \bar{V}_{\infty,x} \leq 0.6$, which agrees with the experimental data of Nagamatsu, et. al. [47], of Wallace and Burke [51], and of Vidal and Wittliff [50].

8. The wall slip velocity for the leading edge problem agrees

quite well with the theory of Chow [68] and of Oguchi [59], and with the experimental results of Becker and Boylan [48] for $\bar{V}_{\infty,x} < 1.0$. Nearer the leading edge, however, the gas does not exhibit pure slip, $u_w = U_\infty$, but rather a near-free molecular value, $u_w = U_\infty/2$ for $T_w = T_\infty$. The magnitude of the slip velocity is seen to increase almost linearly with increased plate temperature as predicted by Oguchi [59].

CHAPTER I

INTRODUCTION

Background and Review of Recent Literature

Man's recent success in attaining high altitude vehicular activities has presented to the aerodynamicist a new regime in the flight spectrum. One must now contend with the motion of a body through a gas of arbitrary rarefaction, or Knudsen number. Theoretically this problem can be analyzed by solving the Boltzmann equation for the molecular distribution function which describes the state of the gas. However, in general, the Boltzmann equation is a very complicated non-linear integro-differential equation. There is, to date, no mathematically rigorous method of solving this equation analytically for the typically non-linear problems of interest in high speed, high altitude aerodynamics. To obtain a solution for all flow regimes from free molecular to continuum by using a single method would be of great practical importance.

For the continuum regime, approximate solutions to the Boltzmann equation have been determined independently by Chapman and by Enskog [1]. In their solution the Navier-Stokes equations of macroscopic gasdynamics are obtained as first approximations to the full conservation equations, and thus the velocity distribution function is developed in terms of its first five moments (density, velocity, and temperature) and their space gradients. The Navier-Stokes equations which govern the phenomena in this regime have been well substantiated by numerous experiments and applications.

For the slip and transition regimes, attempts have been made to solve the Boltzmann equation using higher order macroscopic equations such as the Burnett equations [2] and the Grad (thirteen moment) equations [3]. However, the mathematics involved in these higher order equations is extremely complex, and there is little evidence that they yield results significantly better than those obtained by the Navier-Stokes equations. Also, these higher order macroscopic equations cannot be extended into the transition and near-free molecular regimes without appreciable error as is evidenced by the work of Yang and Lees [4].

The velocity moment method, which is based on an expansion of the velocity distribution function as a series of orthogonal polynomials in velocity space, has also been applied to the linearized Boltzmann equation. The full-range moment method has been applied to the linearized problem of shear flow and heat transfer between parallel plates by Mott-Smith [5] and by Wang Chang and Uhlenbeck [6]. The convergence of these solutions for large Knudsen numbers (near-free molecular flow) is generally poor. Gross, Jackson, and Ziering [7] improved this technique by expressing the distribution function as one which possesses a two-stream character and thus devised the half-range moment method. This improvement is based upon the fact that the velocity distribution function is discontinuous at the boundary. However, even this modification does not allow the moment method to yield accurate solutions in the near free molecular and early transition regimes with a reasonable amount of computational effort. This slow convergence is evidenced by the work of Huang and Stoy [8], who applied the half-range moment method to the problem of channel flow between two parallel plates.

Very recently, this moment method was generalized by Mintzer [9], who proposed to expand the distribution function in a set of velocity polynomials which are orthogonalized with respect to a zero-order distribution function characteristic of a collisionless gas. The application of the method to various gasdynamic problems is currently under extensive investigation.

The moment method has also been applied to various rarefied gas flows in a different way by Lees [10], who used Maxwell's original integral equations rather than the Boltzmann equation for the velocity distribution function itself. As pointed out by Willis [11], Lees' method may give reasonable over-all results for both linearized and non-linear problems when the Knudsen number is not very large. However, for very large Knudsen numbers (or in the near-free molecular flow regime) Lees' method may lead to significant error.

Krook [12] has also used the moment method to formulate the equivalent continuum equations for various rarefied gasdynamic problems and has pointed out that if the effects of molecular collisions are described by the simplest of the hierarchy of statistical models (the BGK model [13]), exact numerical solutions of many rarefied gasdynamic problems can be obtained. Recently, these numerical solutions for Couette flow and shock-wave structure have been obtained by Anderson [14]. The approximate solutions for some problems based on the Krook's equivalent continuum equations [12] have also been obtained by Macomber [15]. These results are very useful and will be used for comparisons later.

In the near-free molecular flow regime the most useful analytic method, both from the standpoint of accuracy and ease of application, is

the iteration method developed by Willis [16]. This technique consists of an iteration with the zeroeth iteration usually being taken as the collisionless solution. The accuracy thus decreases as Knudsen number decreases, and the method is generally difficult to apply to the transition regime since iterations of higher order than the first are extremely difficult to obtain. Also, convergence of the iteration scheme has not been proven in general.

Very recently, the variational approach has successfully been applied to linearized problems in rarefied gases [17]. No examples on non-linear cases based on this approach are available as yet.

Chu [18, 19] has developed a numerical scheme for solving the non-linear Boltzmann equation with the BGK model by using an initial-value analogy for the spacial derivatives. Chu expands the distribution function in a Taylor series in collision time and eliminates all but first order terms. He has applied this technique to the shock wave structure problem [18] for $1.2 < M_{\infty} < 1.7$ and to Rayleigh's problem [19].

The above discussed methods are all restricted to one-(space) dimensional problems. Thus far, there is no analytical or numerical method available for the two-(space) dimensional (linearized or non-linear) Boltzmann equation.

Discussion of the Method

This thesis will mainly be concerned with the application of a systematic method to solve the Boltzmann equation or its substitute equations. In this thesis it will be shown that the method has sufficient flexibility for adaptation to many practical situations which may arise in physical problems. The method proposed is the discrete ordinate

method which has been extensively and successfully applied to solve the (linear) integro-differential equations of the theory of radiative transfer [20]. It has also been applied to the linearized Boltzmann equation with BGK model by Huang and Giddens, who solved the linearized steady and unsteady Couette flow problem [21,22,23], the linearized Rayleigh's flow problem [24,25], the slip velocity problem [26], and the evaluation of the integral $\int_0^\infty u^m e^{-u^2-x/u} du$ [27]. The applications reveal that the discrete ordinate method with an appropriate quadrature yields accurate results over a wider range of Knudsen numbers for a given amount of computational effort than any of the other existing approximate analytic techniques. Most of the applications of the method to the linearized problems have also been discussed in Reference [28]. Very recently, the method has also been generalized for a much wider class of rarefied gas-dynamic problems by Huang [29]. The technique consists of replacing the integration over velocity space of the distribution function in the Boltzmann equation by an appropriate quadrature. This requires approximating the velocity dependence of the distribution function by a set of functions, each evaluated at appropriate discrete points in velocity space. The number of discrete points taken depends on the degree of approximation desired. Thus, instead of solving a linear or non-linear integro-differential equation for a function of space, time, and velocity, the problem is transformed to a system of linear or non-linear, first order differential equations in a set of functions which are continuous in space and time (if time-dependent problems are considered) but are point-functions in velocity space. This set is then solved simultaneously as an approximation to the true distribution function. In the moment method an essential ingredient

is the assignment of a specific form to the distribution function in its dependence on certain of the independent variables $\bar{x}$, $\bar{v}$, and t. This is not necessary in the present method. Thus, in contrast to the previous moment method, the approximation to the Boltzmann equation is made only in the sense of numerical truncations. An interesting and useful feature of applying the quadrature method to the velocity dependence of the distribution function is that the macroscopic properties of interest are all formed by taking velocity moments of this function. Hence, these moment integrations can be evaluated using the same quadrature by which the distribution function is originally solved, resulting in an extremely convenient form for calculation.

The success of the application of the discrete ordinate method to linearized problems of gasdynamics is wholly based on the nature of the linear problem. Namely, macroscopic velocities are small, resulting in a distribution function essentially centered about a zero velocity; the temperature is constant, or nearly so, thus giving an essentially constant "shape" to the distribution function; and the principle of superposition (a characteristic of linear problems) allows the use of quadratures which have irrationally spaced discrete ordinates (for instance, the Gauss-Hermite and Modified Gauss-Hermite quadratures [30]). For the non-linear problems, however, these quadratures are no longer suitable due to the non-equilibrium forms of the distribution function, f(v), with strongly varying temperatures and large macroscopic velocities. In order to extend the discrete ordinate method to non-linear problems, Huang and Hartley [31] developed a quadrature based on equally spaced discrete ordinates. The development of the "odd" and "even" equally spaced quadratures is presented in Appendix A.

Several significant features of the proposed quadratures are:

(1) The proposed quadratures can be applied to calculate the collision integral of the non-linear Boltzmann equation with the hard sphere model and of the BGK model without resorting to any interpolating procedure in the numerical computation.

(2) The singularity difficulty in the collision integral of the Boltzmann equation with the hard sphere model can be avoided by applying the "odd" and "even" equally spaced quadratures alternately.

(3) The molecular velocity coordinate can be linearly transformed according to the local flow velocity if equally spaced discrete ordinates are used. This important feature always enables the discrete points to be placed under the significant part of the distribution function. Consequently, any macroscopic moments of interest can accurately be calculated.

(4) The quadrature coefficients can be calculated according to the local value of temperature, and thus the quadrature is optimally cognizant of the "shape" of the distribution function $f(v)$.

It will be seen that it is this tool (the equally spaced quadrature) which is responsible for the successful extension of the discrete ordinate method to the solution of non-linear gasdynamic problems.

Purpose of the Research

It is the purpose of this thesis to establish the usefulness of the discrete ordinate technique with the equally spaced quadrature (Appendix A) as applied to the solution of the non-linear Boltzmann equation with the

BGK model.

The method is first applied to the problem of Couette flow with heat transfer (whose numerically exact solution is available [14]) to calibrate the usefulness of the method for solving non-linear boundary value problems. Then the method of discrete ordinates, along with the techniques learned from the Couette flow problem, is applied to the solution of the flow field at the leading edge of a thin flat plate submerged in a viscous, supersonic gas stream.

CHAPTER II

NON-LINEAR COUETTE FLOW WITH HEAT TRANSFER

Background of the Problem

In this chapter the discrete ordinate method using the equally spaced quadrature is applied to the solution of non-linear Couette flow with heat transfer in order to calibrate the proposed method against the known standard solution. The continuum solution for this problem is available in Schlicting [35]. However, the cases of high Knudsen numbers (slip, transition, and near-free molecular regimes) must be solved from kinetic theory analyses.

Early kinetic theory solutions have applied the various techniques described in Chapter I to the solution of the linearized Boltzmann equation. The full-range moment method was applied by Mott-Smith [5], and by Wang-Chang and Uhlenbeck [6]. The half-range moment method was applied by Gross, Jackson, and Ziering [7]. The modified moment method was applied by Lees [10]. The iteration method was applied by Willis [11]. The discrete ordinate method was investigated by Broadwell [32] and by Hamel and Wackman [33] for the linearized Boltzmann equation with the hard sphere model, and by Huang and Giddens [21] for the linearized Boltzmann equation with the BGK model. The results based on these methods are summarized and compared in detail by Huang and Giddens [21]. It was concluded that the discrete ordinate method with the new quadrature proposed by Huang and Giddens [30] gives accurate results over a much wider range of Knudsen numbers than any of the other analytic methods. This is due to the fact that general solutions are

readily obtained for arbitrary orders of approximation in the discrete ordinate method. This feature does not appear to occur with the other analytic methods.

For very high plate velocities or strongly varying temperatures, however, the condition of linearity is not applicable. The non-linear Couette flow problem has been solved by Anderson [14], whose numerical technique utilized the Willis iteration scheme [11] on the Boltzmann-Bhatnagar-Gross-Krook equation (or the BBGK equation). It has also been solved by Macomber [15], who applied the velocity moment method to the BBGK equation. The results of the present method will be compared with the results of Anderson and of Macomber in order to check not only the accuracy of the solution, but also the applicability of the method.

Formulation of the Problem

The geometry of this problem is shown in Figure 1. A monatomic gas with no internal degrees of freedom is confined between two parallel plates, y=0 and y=d. The plate y=0 is at rest and is maintained at a constant temperature T_1; the plate y=d is translating in its own plane with a constant velocity W and is maintained at a constant temperature T_2. The problem is steady and one-dimensional in the sense that the velocity distribution function $f(y;\bar{v})$ describing the state of the system depends only on y. The Bhatnagar-Gross-Krook model was chosen for the collision integral in the interest of simplicity and convenience of comparing solutions with results of other methods; however, the method could, in principle, be applied to other models. The one-dimensional, non-linear steady BBGK equation for this case is

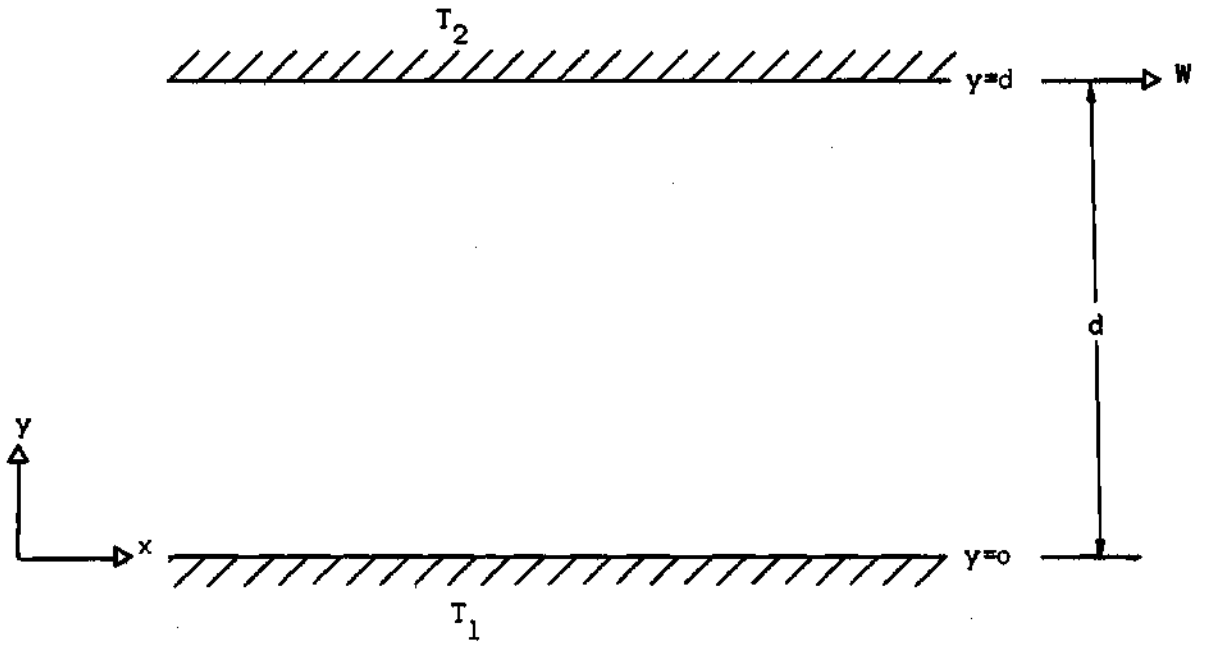

Figure 1. Geometry and Coordinate System for the Couette Flow Problem.

$$v_y \frac{\partial f}{\partial y} = \nu(F - f) \tag{1}$$

and

$$F = n\left(\frac{1}{2\pi RT}\right)^{3/2} e^{-\frac{1}{2RT}(\bar{v} - \bar{u})^2} \tag{2}$$

where $f=f(y;\bar{v})$ is the velocity distribution function which depends on the y-coordinate and molecular velocity $\bar{v}(v_x,v_y,v_z)$, ν is the collision frequency which is generally a function of the law of force between molecules, R is the gas constant for the particular gas, equal to the Boltzmann constant k divided by the molecular mass m, n is the gas particle density, T is the gas temperature, and $\bar{u}$ is the flow velocity.

Equation (1) is one-dimensional in physical space but is three-dimensional in velocity space. As it stands, f is a function of four arguments $(y;v_x,v_y,v_z)$, which renders numerical computations virtually impossible on present day computers because of the excessive storage capacity required. For problems of one-(space) dimension, however, van Kampen [34] points out that a system of reduced distribution functions may be defined which reduces the three-(velocity) dimensional BBGK equation, Equation (1), to a set of coupled simultaneous one-(velocity) dimensional BBGK equations. The reduced distribution functions have only two arguments $(y;v_y)$, which greatly reduces computer storage requirements. Accordingly, the following functions are defined

$$g(y;v_y) = \int_{-\infty}^{\infty}\int_{-\infty}^{\infty} f(y;\bar{v})dv_x dv_z \tag{3a}$$

$$h(y;v_y) = \int_{-\infty}^{\infty}\int_{-\infty}^{\infty} (v_x^2 + v_z^2) f(y;\bar{v}) dv_x dv_z \tag{3b}$$

$$j(y;v_y) = \int_{-\infty}^{\infty}\int_{-\infty}^{\infty} v_x f(y;\bar{v}) dv_x dv_z \tag{3c}$$

Multiplying Equation (1) by the weighting functions 1, $v_x^2 + v_z^2$, and v_x respectively, and integrating over $dv_x dv_z$ remove the v_x and v_z dependence from Equation (1) and allow the application of Equations (3). The resulting set of one-dimensional equations becomes

$$v_y \frac{\partial g}{\partial y} = \nu(G - g) \tag{4a}$$

$$v_y \frac{\partial h}{\partial y} = \nu(H - h) \tag{4b}$$

$$v_y \frac{\partial j}{\partial y} = \nu(J - j) \tag{4c}$$

where

$$G = \frac{n}{(2\pi RT)^{1/2}} e^{-\frac{v_y^2}{2RT}} \tag{5a}$$

$$H = 2RTG + u_x^2 G \tag{5b}$$

$$J = u_x G \tag{5c}$$

The macroscopic moments are

$$n = \int_{-\infty}^{\infty} g dv_y \tag{6a}$$

$$nu_x = \int_{-\infty}^{\infty} j dv_y \tag{6b}$$

$$3nRT = \int_{-\infty}^{\infty} h dv_y + \int_{-\infty}^{\infty} v_y^2 g dv_y - nu_x^2 \tag{6c}$$

and

$$p = \frac{1}{3}(p_{xx} + p_{yy} + p_{zz}) = nkT \tag{6d}$$

It is convenient to define a non-dimensional variable $\tau(y)$, which is similar to the classical Howarth-Dorodnitsyn variable of boundary layer theory [35]

$$\tau(y) = \frac{Kn}{V_1} \int_o^y \nu(y')dy' \tag{7}$$

where the global Knudsen number is defined as

$$Kn = \frac{V_1}{\int_o^d \nu(y')dy'} \tag{8}$$

and*

$$V_1 = \sqrt{RT_1} \tag{9}$$

The definitions of dimensionless variables are also introduced as follows

*This form of characteristic velocity is chosen here to be consistent with the solutions of Anderson and of Macomber.

$$\hat{v} = \frac{v}{V_1} \quad , \qquad \hat{u} = \frac{u}{V_1} \quad , \qquad \hat{W} = \frac{W}{V_1} \quad ,$$

$$\hat{n} = \frac{n}{n_1} \quad , \qquad \hat{T} = \frac{T}{T_1} \quad , \qquad \hat{p} = \frac{p}{mn_1V_1^2} \quad ,$$

$$\hat{g} = \frac{V_1}{n_1} g \quad , \qquad \hat{h} = \frac{1}{n_1V_1} h \quad , \qquad \hat{j} = \frac{1}{n_1} j \quad ,$$

$$\hat{G} = \frac{V_1}{n_1} G \quad , \qquad \hat{H} = \frac{1}{n_1V_1} H \quad , \qquad \hat{J} = \frac{1}{n_1} J \quad .$$

where the subscript "1" specifies the flow condition at the lower plate.

After the process of nondimensionalization of Equations (4) through (5), the discrete ordinate method outlined in Chapter I is applied. This technique consists of approximating the integration over velocity space of the distribution function by the equally spaced quadrature. This requires approximating the velocity dependence of the distribution function by a set of functions, each evaluated at appropriate discrete points in velocity space. The number of discrete points which is taken depends on the degree of approximation which is desired. Equations (4a) through (4c) are solved simultaneously as an approximation to the true distribution function for these discrete velocity points. Therefore, the distribution functions which are obtained are continuous in space but are point functions in velocity space. Since the macroscopic properties of interest are all formed by taking velocity moments of the same distribution function, these moment integrations can be evaluated using the same quadrature by which the distribution function is originally solved. This approach results in an extremely convenient form for calculation and is particularly suited for work

with high-speed computing machines.

Nondimensionalizing Equations (4a) through (4c) and expressing them at the discrete points in velocity space as required in the discrete ordinate method gives (see Reference [29])

$$Kn\ \hat{v}_\sigma \frac{d\hat{g}_\sigma}{d\tau} = (\hat{G}_\sigma - \hat{g}_\sigma) \tag{10a}$$

$$Kn\ \hat{v}_\sigma \frac{d\hat{h}_\sigma}{d\tau} = (\hat{H}_\sigma - \hat{h}_\sigma) \tag{10b}$$

$$Kn\ \hat{v}_\sigma \frac{d\hat{j}_\sigma}{d\tau} = (\hat{J}_\sigma - \hat{j}_\sigma) \tag{10c}$$

and

$$\hat{G}_\sigma = \frac{\hat{n}\hat{T}^{-\frac{1}{2}}}{\sqrt{2\pi}} e^{-\frac{1}{2\hat{T}}\hat{v}_\sigma^2} \tag{11a}$$

$$\hat{H}_\sigma = (2\hat{T} + \hat{u}_x^2)\hat{G}_\sigma \tag{11b}$$

$$\hat{J}_\sigma = \hat{u}_x \hat{G}_\sigma \tag{11c}$$

where $\hat{g}_\sigma$, $\hat{h}_\sigma$, $\hat{j}_\sigma$, $\hat{G}_\sigma$, $\hat{H}_\sigma$, and $\hat{J}_\sigma$ represent $\hat{g}$, $\hat{h}$, $\hat{j}$, $\hat{G}$, $\hat{H}$, and $\hat{J}$ evaluated at the discrete velocity points $\hat{v}_\sigma(\sigma = -n,\ldots,-1,1,\ldots n)$, respectively. The discrete points are defined in Appendix A.

In order to specify the interaction of the molecules with the surface boundaries, it is assumed that molecules which strike a plate are subsequently emitted with a Maxwellian velocity distribution characterized by the plate temperature and velocity. Since it is important to distinguish between molecules which are traveling toward a plate and those moving away

from it within a distance of the order of several mean free paths from the plate regardless of the Knudsen number, it is convenient to define the half-range distribution function as follows

$$\hat{f}^{+}(\hat{y};\hat{v}_y) = 0 \quad , \qquad \text{for} \quad \hat{v}_y < 0$$

$$\hat{f}^{-}(\hat{y};\hat{v}_y) = 0 \quad , \qquad \text{for} \quad \hat{v}_y > 0$$

The normalized boundary conditions (for 2n discrete velocity points) can then be written as follows

$$\hat{g}_\sigma^{+}(\tau = 0) = \frac{1}{\sqrt{2\pi}} e^{-\hat{v}_\sigma^2/2} \qquad , \text{for } \hat{v}_\sigma > 0 \quad (12a)$$

$$\hat{g}_\sigma^{-}(\tau = 1) = \frac{\hat{n}_2}{\sqrt{2\pi\hat{T}_2}} e^{-\frac{1}{2\hat{T}_2}\hat{v}_\sigma^2} \qquad , \text{for } \hat{v}_\sigma < 0 \quad (12b)$$

$$\hat{h}_\sigma^{+}(\tau = 0) = \frac{1}{\sqrt{2\pi}} e^{-\hat{v}_\sigma^2/2} \qquad , \text{for } \hat{v}_\sigma > 0 \quad (12c)$$

$$\hat{h}_\sigma^{-}(\tau = 1) = \frac{\hat{n}_2 \hat{T}_2^{1/2}}{\sqrt{2\pi}} e^{-\frac{1}{2\hat{T}_2}\hat{v}_\sigma^2} + \frac{\hat{n}_2 \hat{W}^2}{\sqrt{2\pi\hat{T}_2}} e^{-\frac{1}{2\hat{T}_2}\hat{v}_\sigma^2} \qquad , \text{for } \hat{v}_\sigma < 0 \quad (12d)$$

$$\hat{j}_\sigma^{+}(\tau = 0) = 0 \qquad , \text{for } \hat{v}_\sigma > 0 \quad (12e)$$

$$\hat{j}_\sigma^-(\tau = 1) = \frac{\hat{n}_2 \hat{W}}{\sqrt{2\pi \hat{T}_2}} e^{-\frac{1}{2\hat{T}_2} \hat{v}_\sigma^2} \quad , \text{ for } \hat{v}_\sigma < 0 \qquad (12f)$$

Another condition to determine the parameter $\hat{n}_2$ is that the net mass flux normal to the plates be zero at the plates, i.e.

$$\int_o^\infty \hat{v}_y \hat{g}^+(\hat{v}_y) d\hat{v}_y - \int_o^{-\infty} \hat{v}_y \hat{g}^-(\hat{v}_y) d\hat{v}_y = 0 \qquad (13)$$

In order to apply the discrete ordinate method, the integrals above are expressed as finite sums according to the formulation defined in Appendix A and in Reference [29], i.e.,

$$\int_o^\infty [\hat{v}_y \hat{g}^+(\hat{v}_y) e^{\frac{1}{2\hat{T}} \hat{v}_y^2}] e^{-\frac{1}{2\hat{T}} \hat{v}_y^2} d\hat{v}_y$$

$$= \sum_{\sigma=1}^{n} k_\sigma [\hat{v}_\sigma \hat{g}^+(\hat{v}_\sigma) e^{\frac{1}{2\hat{T}} \hat{v}_\sigma^2}] \qquad (14)$$

where k_σ is the weighting coefficient for the velocity component $\hat{v}_\sigma$.

Equation (13) then becomes

$$- \sum_{\sigma=-1}^{-n} k_\sigma \hat{v}_\sigma \hat{g}_\sigma^-(\hat{v}_\sigma) e^{\frac{1}{2\hat{T}} \hat{v}_\sigma^2} + \sum_{\sigma=1}^{n} k_\sigma \hat{v}_\sigma \hat{g}_\sigma^+(\hat{v}_\sigma) e^{\frac{1}{2\hat{T}} \hat{v}_\sigma^2} = 0 \qquad (15)$$

The moments defined in Equations (6) are integrated as illustrated in Equation (14) using the quadrature presented in Appendix A.

Thus, the problem leads to solving Equations (10a) through (10c)

subject to the boundary conditions in Equations (12) and (15).

Computational Procedures

It is very important to note that the most significant advantage which is gained by applying the present method to Equations (4a) through (5c) is that the functions $\hat{g}_\sigma$, $\hat{h}_\sigma$, $\hat{j}_\sigma$, $\hat{G}_\sigma$, $\hat{H}_\sigma$, and $\hat{J}_\sigma$ no longer depend on the velocity component $\hat{v}_y$. This is to say that the system of non-linear, first order partial differential equations in Equation (4) has been transformed to a system of non-linear, first order ordinary differential equations in Equation (10). The resulting set of equations can be solved by incorporating a finite difference technique coupled with an iterative scheme.

Consider the following finite difference grid formulation:

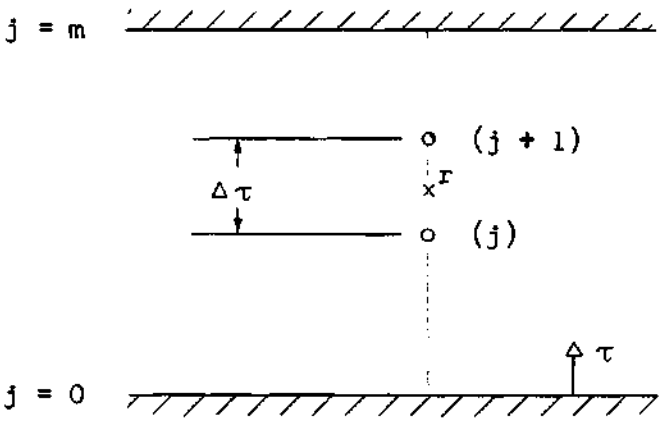

The finite difference derivatives are written about point "r" [36]. Other quantities in Equation (10) are averaged at point r, i.e.,

$$\hat{g}_\sigma|_r = \frac{1}{2}[\hat{g}_\sigma(j+1) + \hat{g}_\sigma(j)] \tag{16}$$

Since the problem exhibits a "two stream" character (one molecular

stream coming toward the wall and another molecular stream going away from the wall) with discontinuities at the walls, the difference equation must be rearranged for each part of the solution. Starting from the lower wall with the known values of $\hat{g}_\sigma^+(\tau = 0)$ from Equation (12a), the difference form of Equation (10)is applied as follows

$$\hat{g}_\sigma^+(j) = \left[\frac{\hat{G}_\sigma^+(j-1) + \hat{G}_\sigma^+(j)}{2} - \left(\frac{1}{2} - \frac{Kn\hat{v}_\sigma}{\Delta\tau}\right)\hat{g}_\sigma^+(j-1)\right] \Big/ \left(\frac{1}{2} + \frac{Kn\hat{v}_\sigma}{\Delta\tau}\right) \tag{17}$$

The $\hat{h}_\sigma^+$ and $\hat{j}_\sigma^+$ equations are similarly transformed.

The resulting values of $\hat{g}_\sigma^+(\tau = 1)$ obtained from the solution of Equation (17) are integrated to apply the no normal mass flux boundary condition, Equation (16). This yields $\hat{n}_2$, which, in turn, generates values of $\hat{g}_\sigma^-(\tau = 1)$, Equation (12b). Starting with these values of $\hat{g}_\sigma^-(\tau = 1)$, Equation (17) is rearranged and applied in the following form marching from the upper plate to the lower plate:

$$\hat{g}_\sigma^-(j) = \left[\frac{\hat{G}_\sigma^-(j+1) + \hat{G}_\sigma^-(j)}{2} - \left(\frac{1}{2} + \frac{Kn\hat{v}_\sigma}{\Delta\tau}\right)\hat{g}_\sigma^-(j+1)\right] \Big/ \left(\frac{1}{2} - \frac{Kn\hat{v}_\sigma}{\Delta\tau}\right) \tag{18}$$

The $\hat{h}_\sigma^-$ and $\hat{j}_\sigma^-$ equations are similarly transformed.

The equilibrium distribution function values, $\hat{G}_\sigma^\pm$, $\hat{H}_\sigma^\pm$, and $\hat{J}_\sigma^\pm$, are determined from the moments of the previous iterate. The zeroeth iterate is the free molecular solution. This yields a system of 6n non-linear algebraic equations in 6n unknowns ($\hat{g}_\sigma$, $\hat{h}_\sigma$, and $\hat{j}_\sigma$, $\sigma = -n,\ldots,-1,1,\ldots n$)

which is solved by the method of successive approximations.

This scheme forms an implicit finite difference procedure which converges very well for the range of Knudsen numbers, $0.001 \leq Kn \leq 100$. Due to the presence of Kn in Equation (10), the following procedure is used: First, the free molecular values of $\hat{n}$, $\hat{u}_x$, and $\hat{T}$ are assigned as the zeroeth iterates to functions $\hat{G}_\sigma$, $\hat{H}_\sigma$, and $\hat{J}_\sigma$ in Equation (11), and Equation (10) is solved for Kn=100 by iteration. Once convergence is obtained for Kn=100, the newly calculated values of $\hat{n}$, $\hat{u}$, and $\hat{T}$ (Kn=100) are used as the zeroeth iterates to solve Equation (10) for Kn=10. This same process is repeatedly applied to Equation (10) to solve for successively smaller Knudsen number cases, i.e., Kn=1, 0.1, 0.01, 0.001, etc. In this way,* the results for the transition, slip, and continuum flow regimes can be obtained most efficiently. Convergence is assumed to have occurred when the difference in successive iterates of the macroscopic variables is $\leq 10^{-4}$. This normally requires two iterations for a Knudsen number of 100 and as many as 20 iterations for a Knudsen number of 0.001.

Results

A Burroughs B-5500 digital computer was used for the computations. The "odd" equally spaced quadrature with n=8 was used. Figures 2 through 15 present typical results of these computations (100 space steps across the channel were taken). Convergence of the solution to a unique set of values was checked by running cases with 50 space steps across the channel and n=6. A case with n=14 and 100 space steps was also run and yielded the same solution. Results presented in Figures 2 through 7 are in excellent

*This scheme was also used by Macomber [15].

agreement with Anderson's numerically exact results [14]. Since the calculated curves fall on top of Anderson's curves, Anderson's results are not shown in the figures. In these figures Macomber's results [15] are also compared. In Figures 2 through 6 Macomber's results are shown for cases Kn=10 and 0.5, and in Figure 7 Macomber's result is shown only for Kn = 0.5.

Although one normally associates linear velocity profiles with the Couette flow problem, DeGroff [37] has shown that by merely introducing a temperature dependence to the viscosity, the velocity profiles for continuum Couette flow are curved, and in fact, exhibit an inflection point at the centerline when $\hat{T}_1=\hat{T}_2$. The present solutions are presented as functions of the reduced coordinate τ. It is interesting to note that the continuum solution in the τ coordinate system yields a linear velocity profile regardless of the temperature-viscosity relationship. The present results for Kn=0.001 have attained the continuum characteristic of zero slip velocity at the plates, but even for this low Knudsen number, a global pressure gradient exists and the velocity profiles are not linear.

The effect of temperature ratio is evident in Figure 2. For large Knudsen numbers, the velocity profiles for various $\hat{T}_2$ are of essentially the same shape, differing primarily in slip at the wall. In this limit of near-free molecular flow, the solutions are essentially superpositions of wall conditions, and the dependence of $\hat{n}_2/\hat{n}_1$ on $\hat{T}_2$ (and weakly on $\hat{W}$) accounts for the change in slip. As the Knudsen number decreases, the coupling becomes more local and differential effects of local rather than global Knudsen number become apparent.

The non-linear kinetic theory phenomena are evident in the density profiles, Figures 5, 6, 8, and 12, which do not vary inversely with the

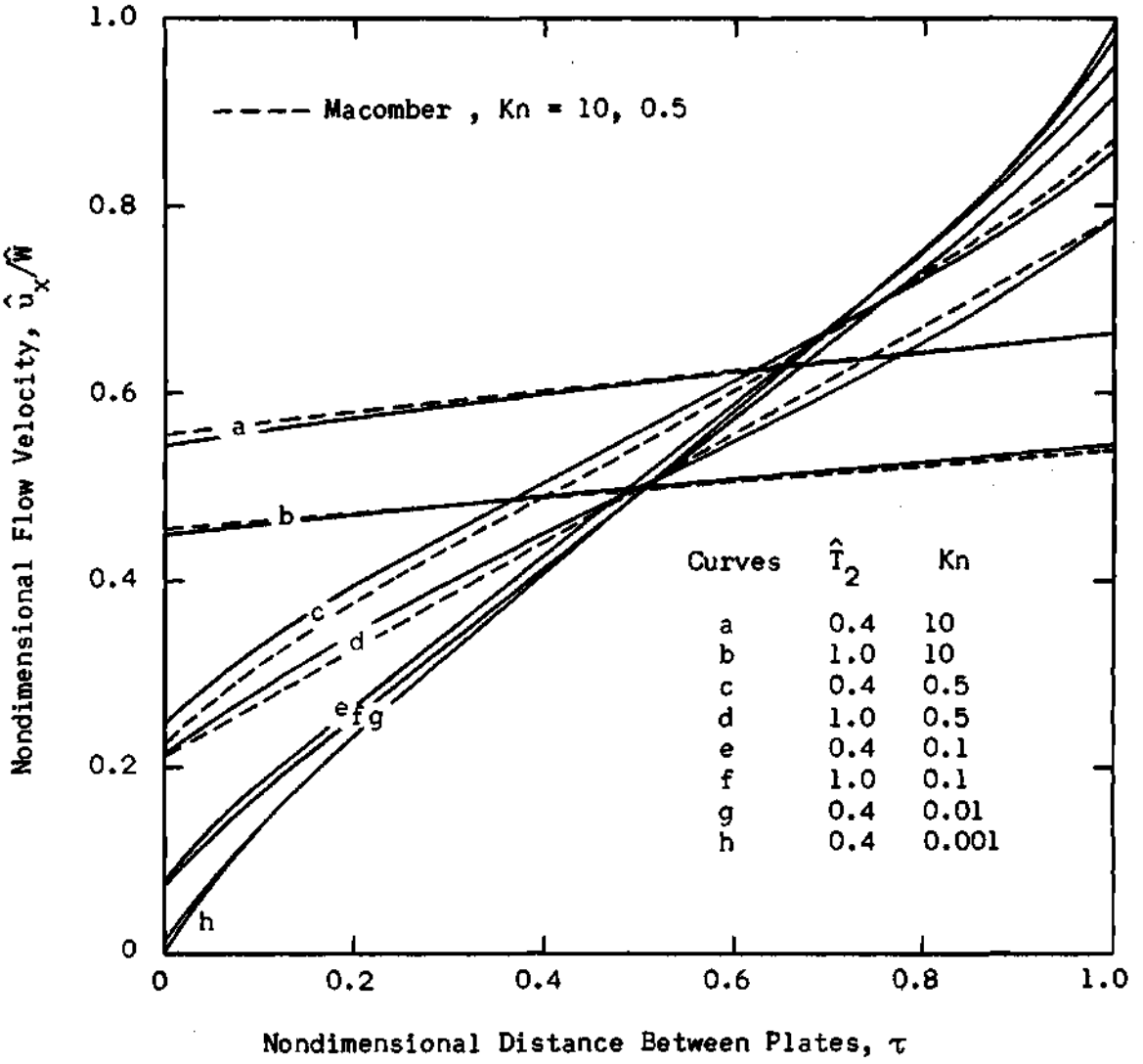

Figure 2. Couette Flow Velocity Profiles for $\hat{W} = 1$.

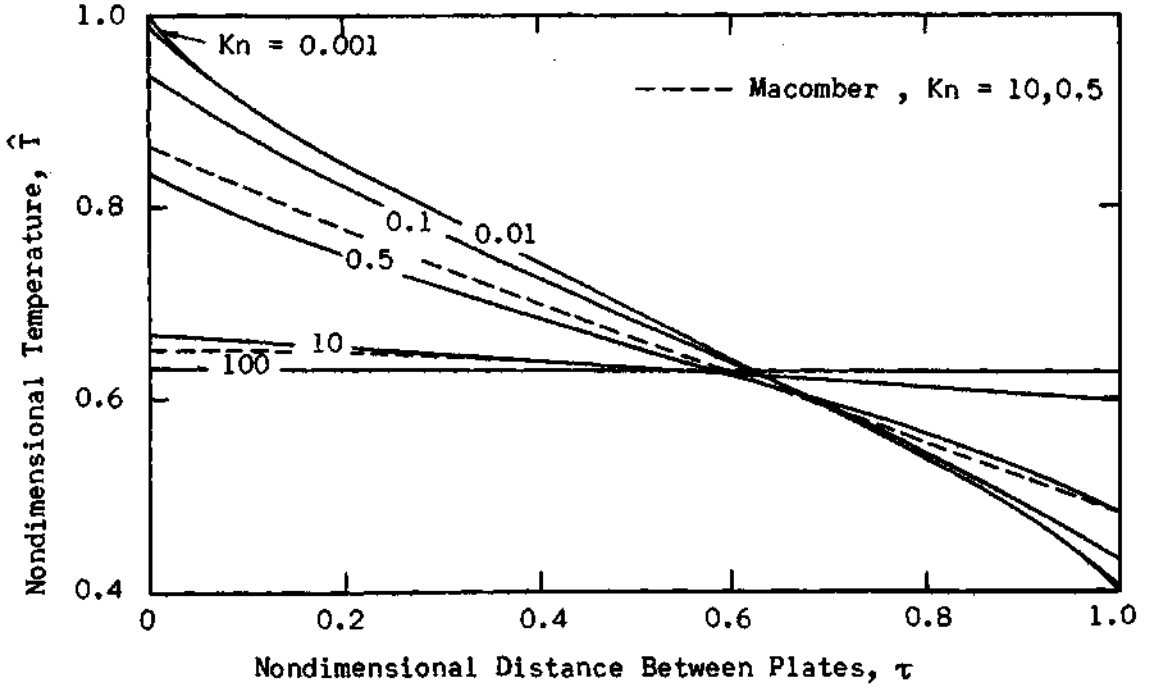

Figure 3. Couette Flow Temperature Profiles for $\hat{W} = 0$, $\hat{T}_2 = 0.4$.

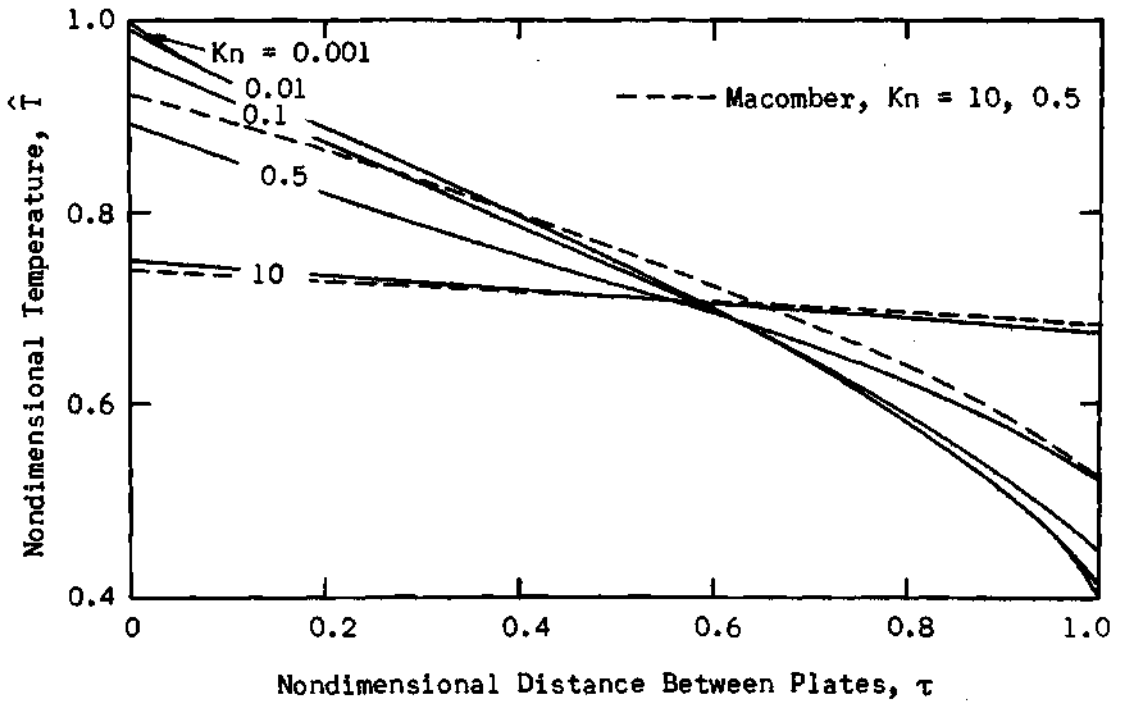

Figure 4. Couette Flow Temperature Profiles for $\hat{W} = 1$, $\hat{T}_2 = 0.4$.

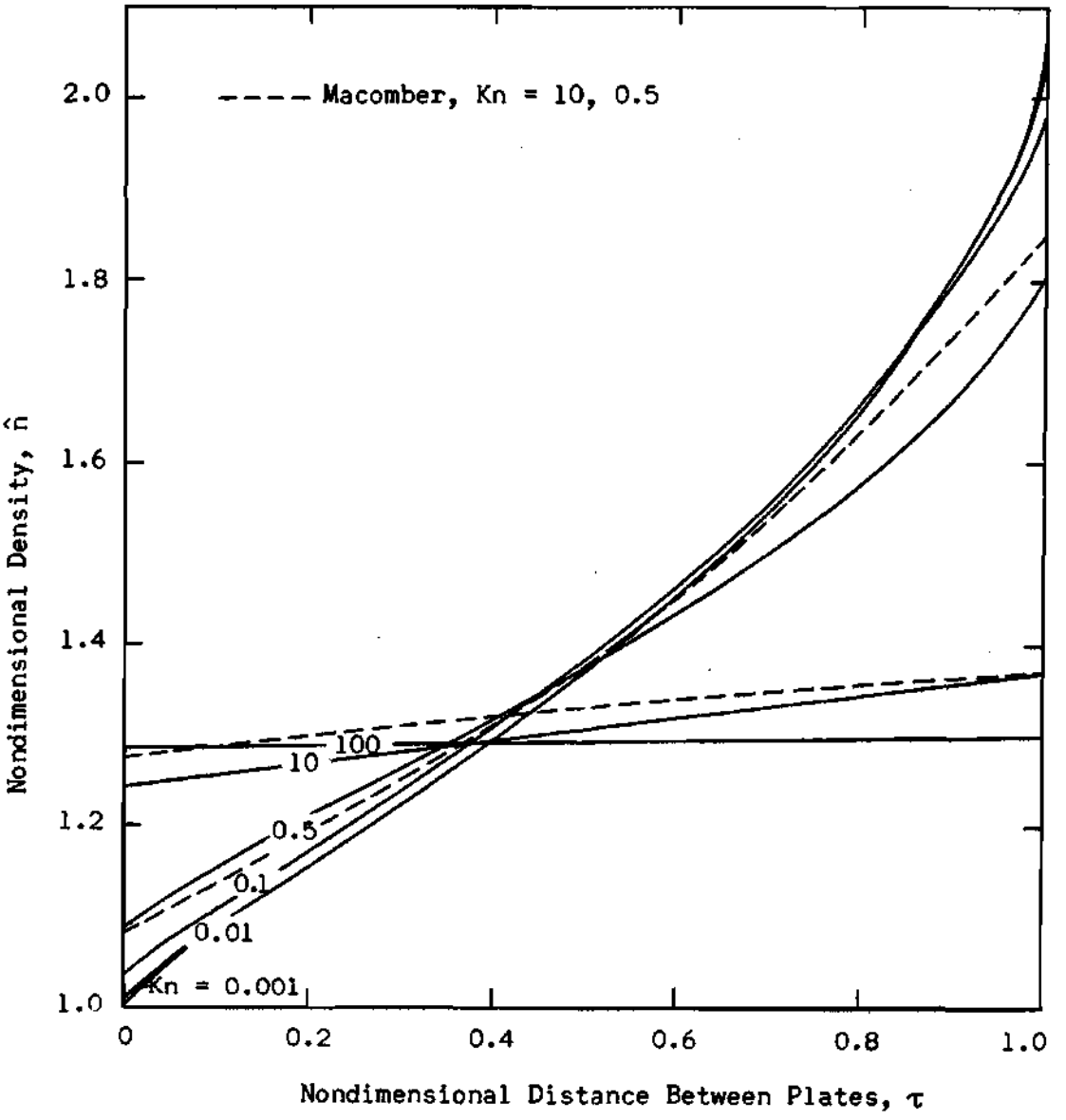

Figure 5. Couette Flow Density Profiles for $\hat{W} = 0$, $\hat{T}_2 = 0.4$.

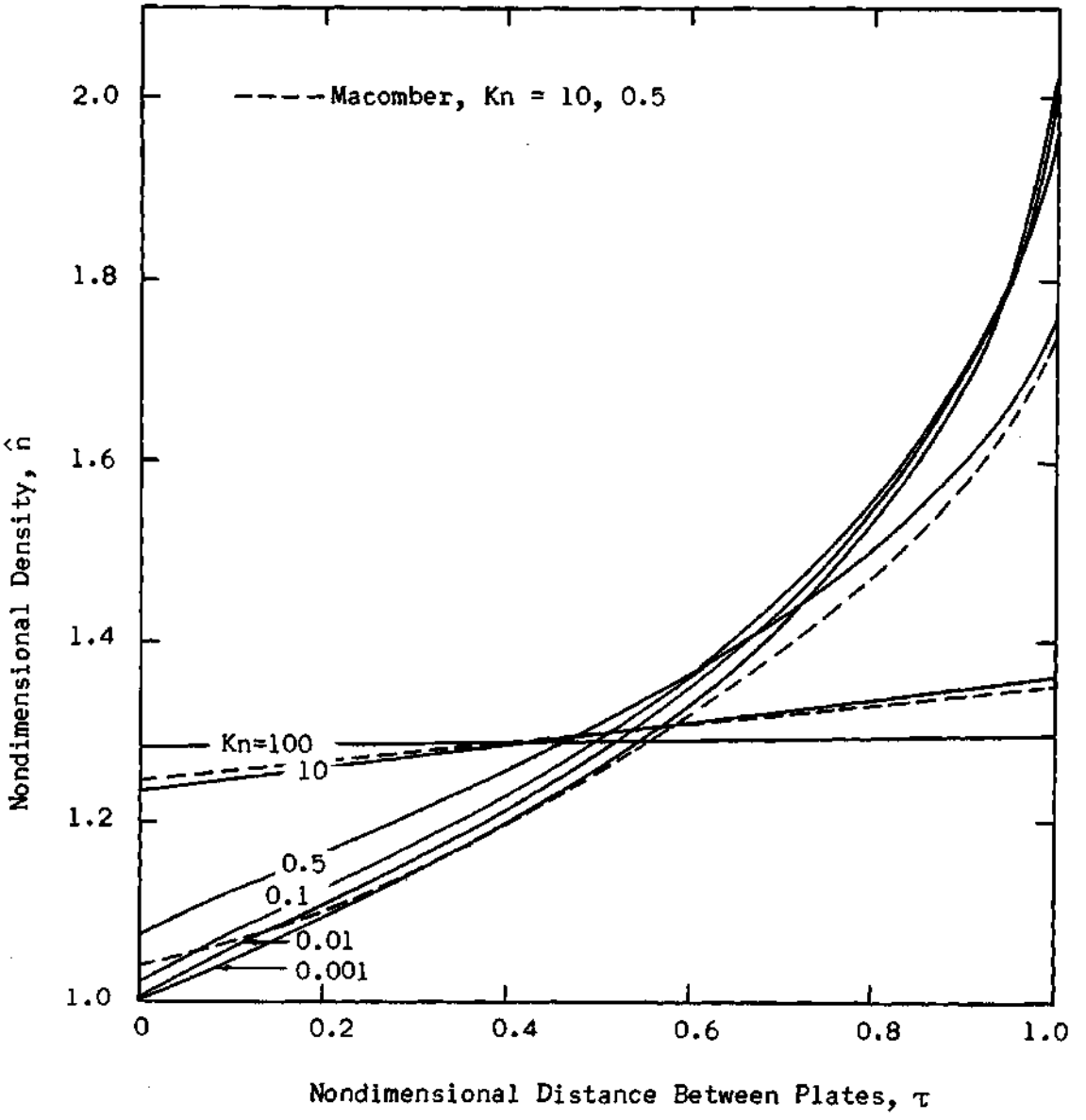

Figure 6. Couette Flow Density Profiles for $\hat{W} = 1$, $\hat{T}_2 = 0.4$.

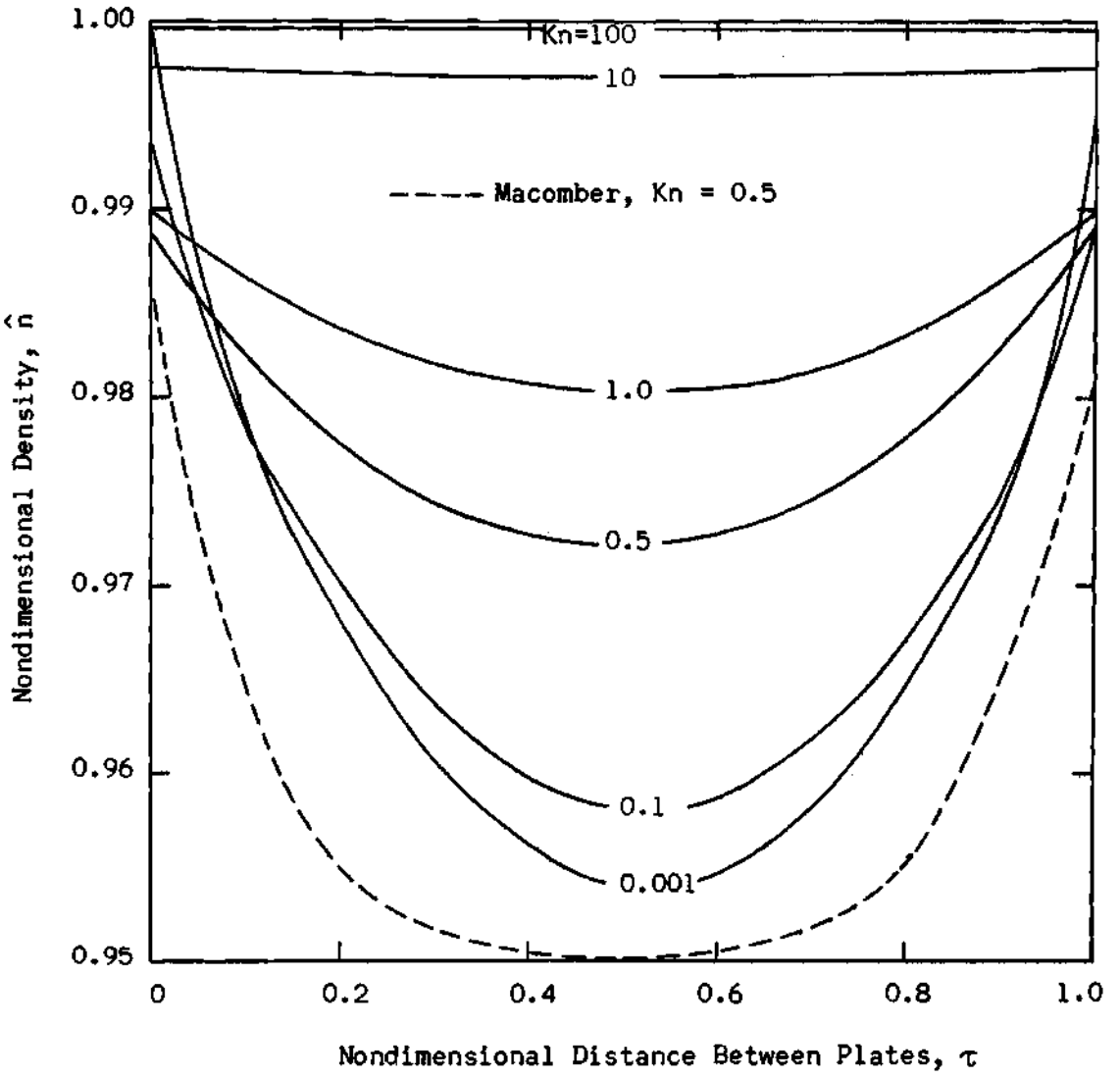

Figure 7. Couette Flow Density Profiles for $\hat{W} = 1$, $\hat{T}_2 = 1$.

temperature profiles as would be expected from continuum theory where the pressure $p \sim nT \cong$ constant. While the reduced coordinate used in plotting these curves may exaggerate the effect somewhat, a global pressure gradient and local Knudsen layers appear whenever there are temperature and/or density gradients.

Figures 8 through 15 report calculated results for W=3. In these computations the "odd" equally spaced quadrature with n=8 and n=14 was used, and 100 steps across the channel were taken. The error of the n=8 solutions as compared to n=14 solutions seems to be about 7 per cent for the low Knudsen number solutions of $\hat{W}$=3, $\hat{T}_2$=1 and as high as 30 per cent for $\hat{W}$=3, $\hat{T}_2$=0.4. However, for high Knudsen numbers, the error is only 1 per cent when $\hat{T}_2$=1, but grows to 20 per cent when $\hat{T}_2$=0.4 (see Figure 12, Kn=100). The error exhibited by the n=8 solution can be attributed to the fact that such a low order approximation (n=8) cannot be expected to yield very accurate results for such high plate velocities and temperature ratios.

An anomaly appearing in the $\hat{W}$=3, $\hat{T}_2$=1 case, Figures 8 through 11, is the relative position of the Kn=10 and Kn=100 solutions. For instance, in Figure 8, one would expect the Kn=100 density profile to lie above the Kn=10 density profile based on results exhibited by the lower plate velocity cases. This error, which is only of the order of 2 per cent, can easily be attributed to the finite difference formulation because, for high Knudsen numbers, the derivatives are nearly zero and, by difference formulation, are represented by the difference in two values of distribution function which may differ only in the fifth or sixth decimal. The finite difference scheme cannot be expected to generate distribution functions accurate to so many decimal places. The resulting error is small for

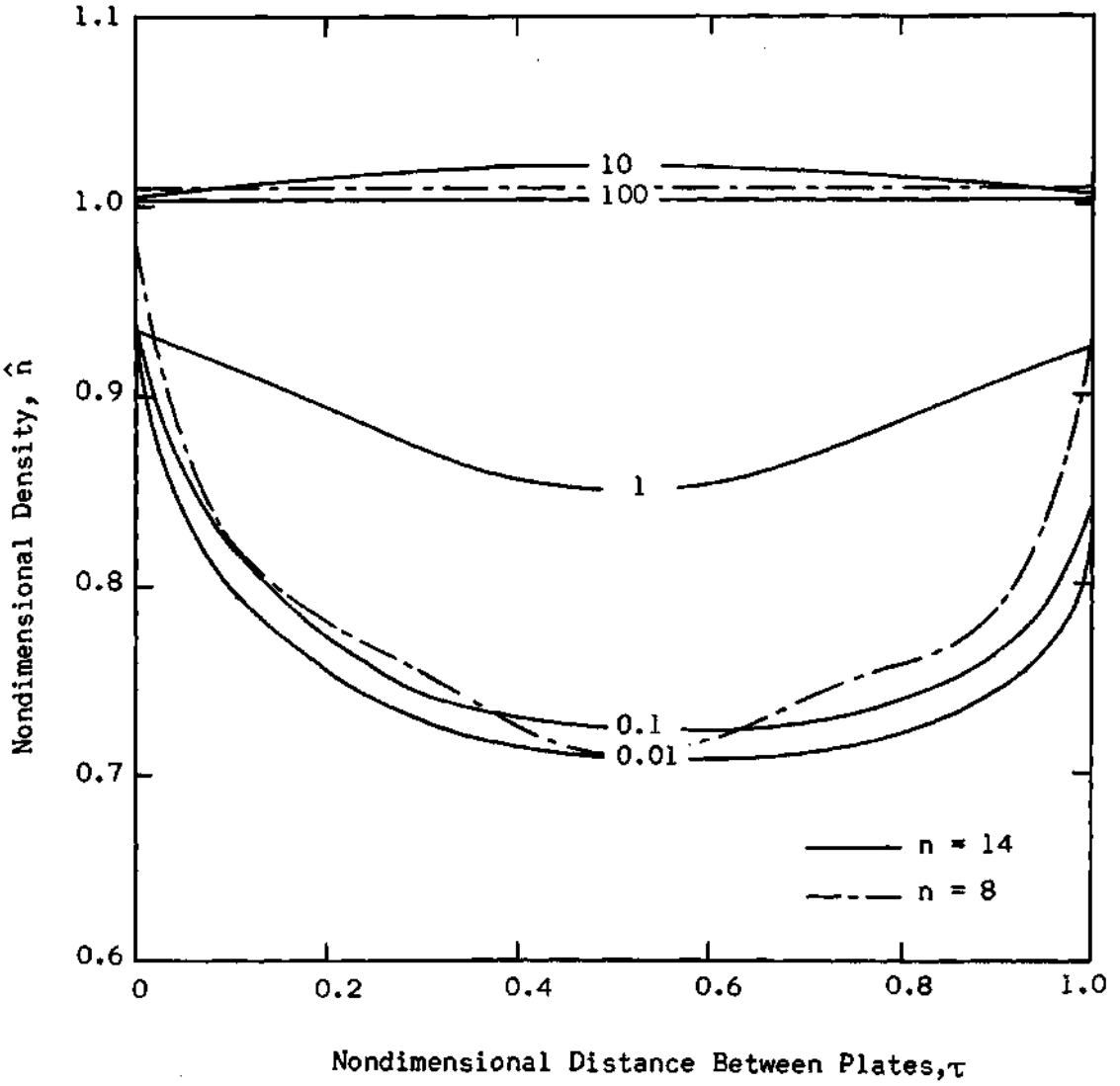

Figure 8. Couette Flow Density Profiles for $\hat{W} = 3$, $\hat{T}_2 = 1$.

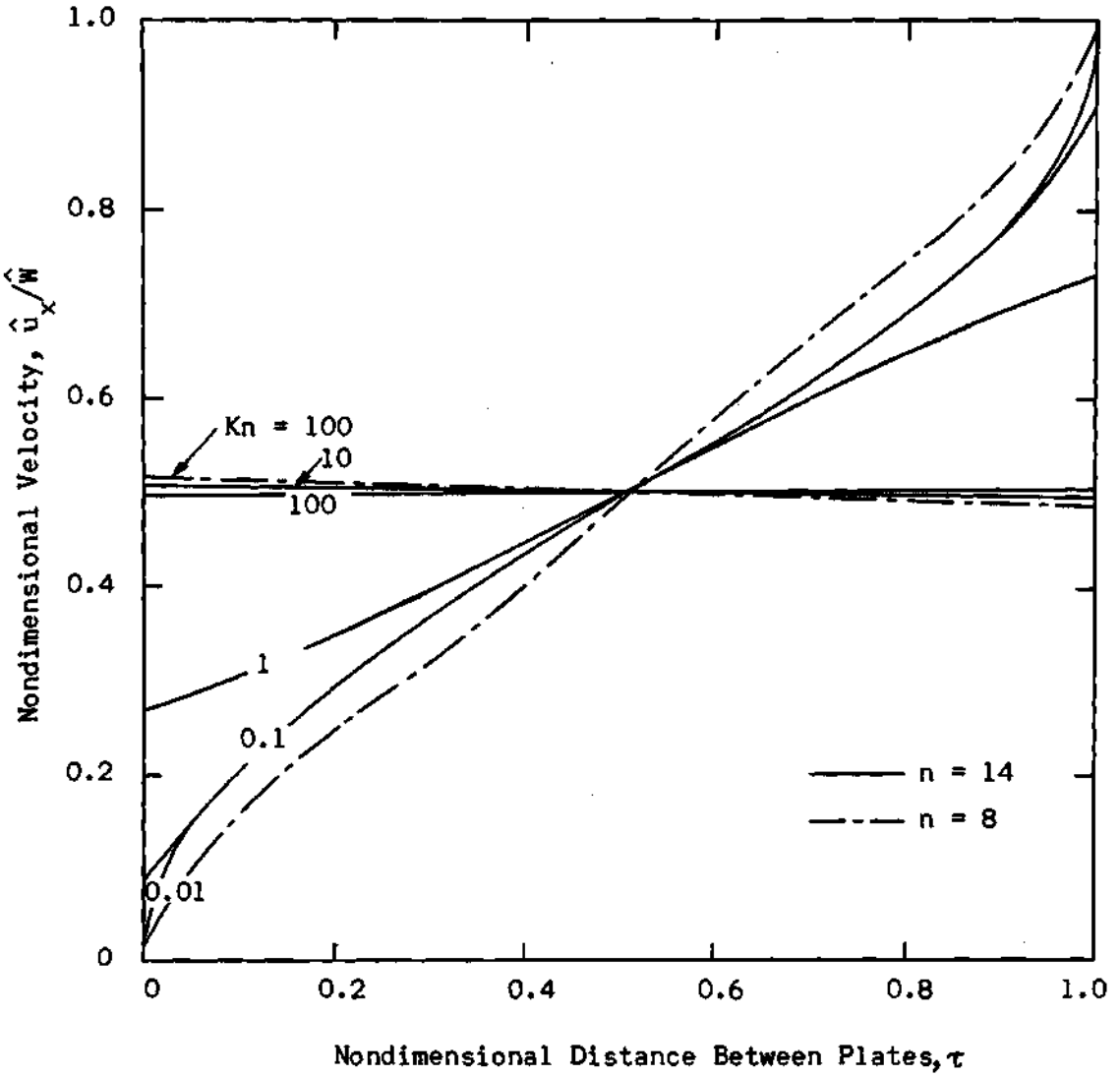

Figure 9. Couette Flow Velocity Profiles for $\hat{W} = 3$, $\hat{T}_2 = 1$.

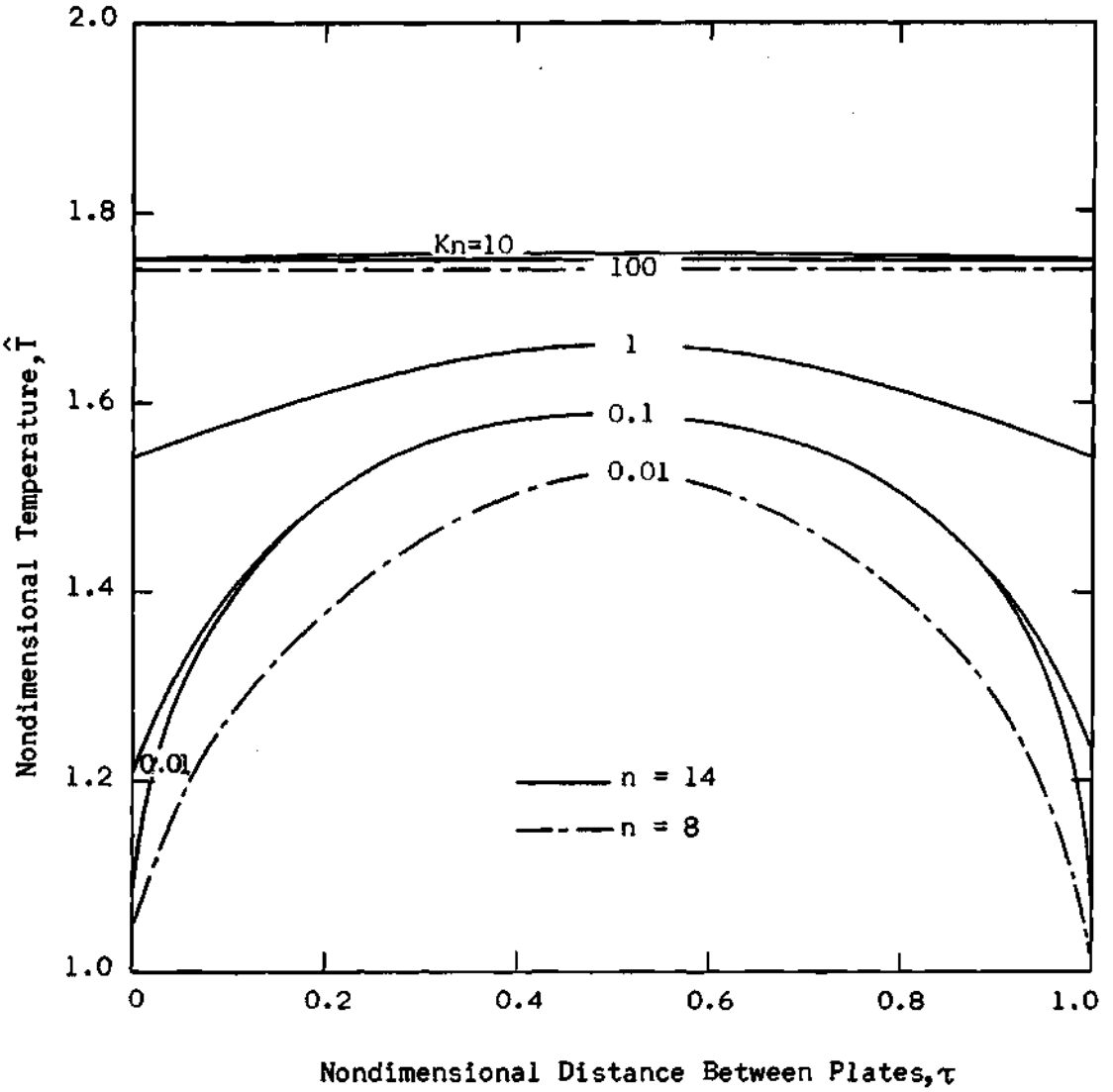

Figure 10. Couette Flow Temperature Profiles for $\hat{W} = 3$, $\hat{T}_2 = 1$.

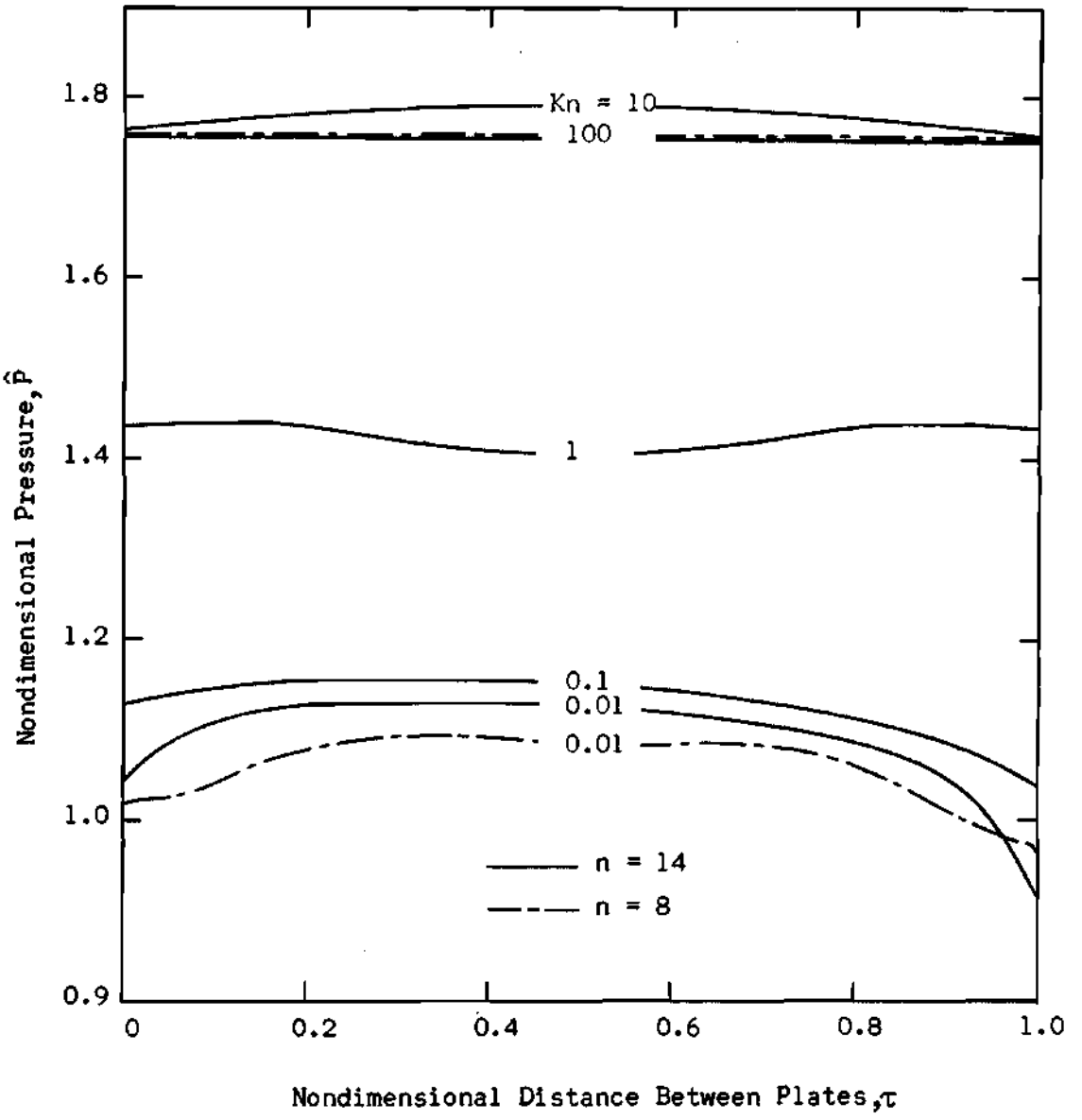

Figure 11. Couette Flow Pressure Profiles for $\hat{W} = 3$, $\hat{T}_2 = 1$.

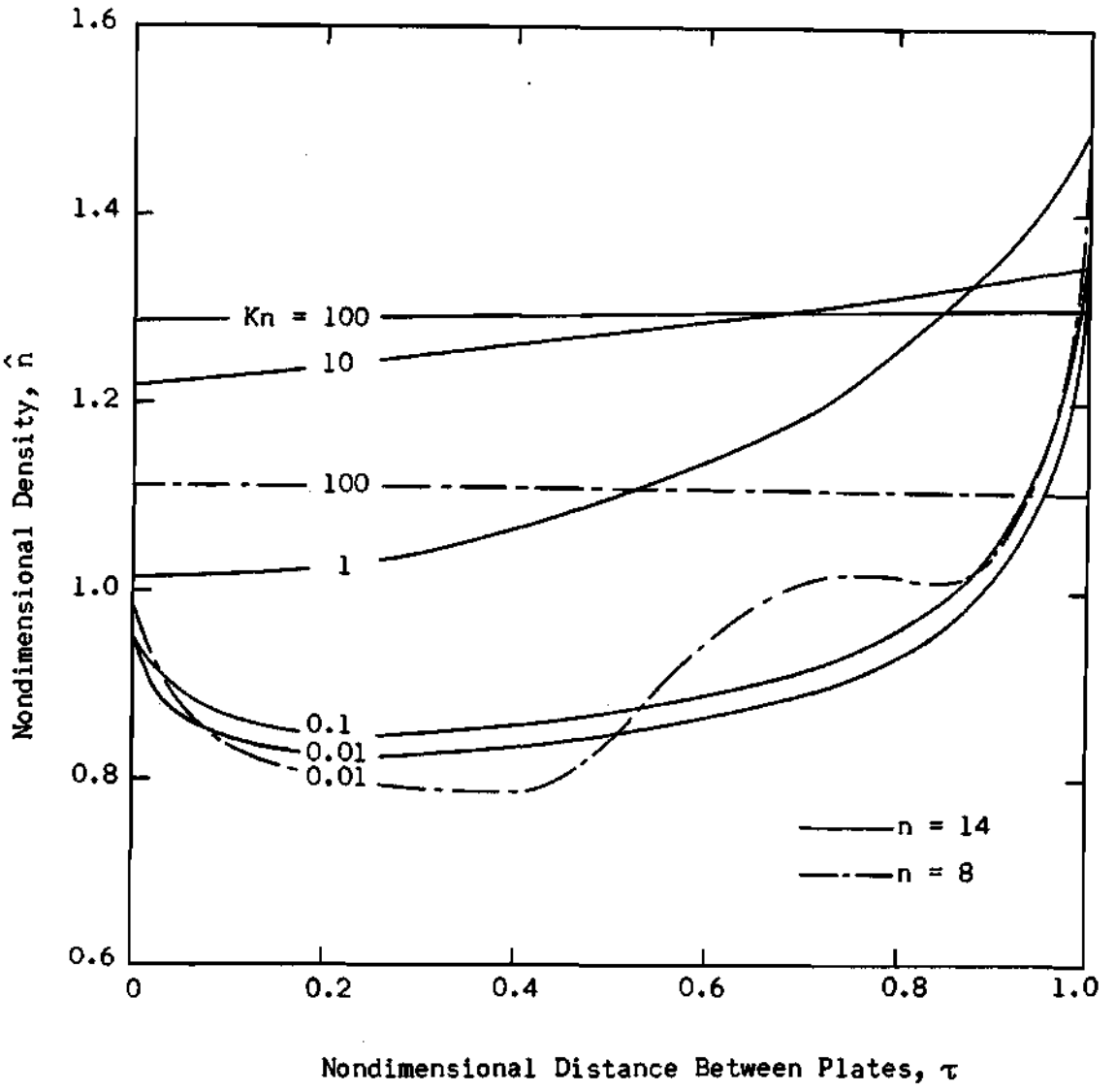

Figure 12. Couette Flow Density Profiles for $\hat{W} = 3$, $\hat{T}_2 = 0.4$.

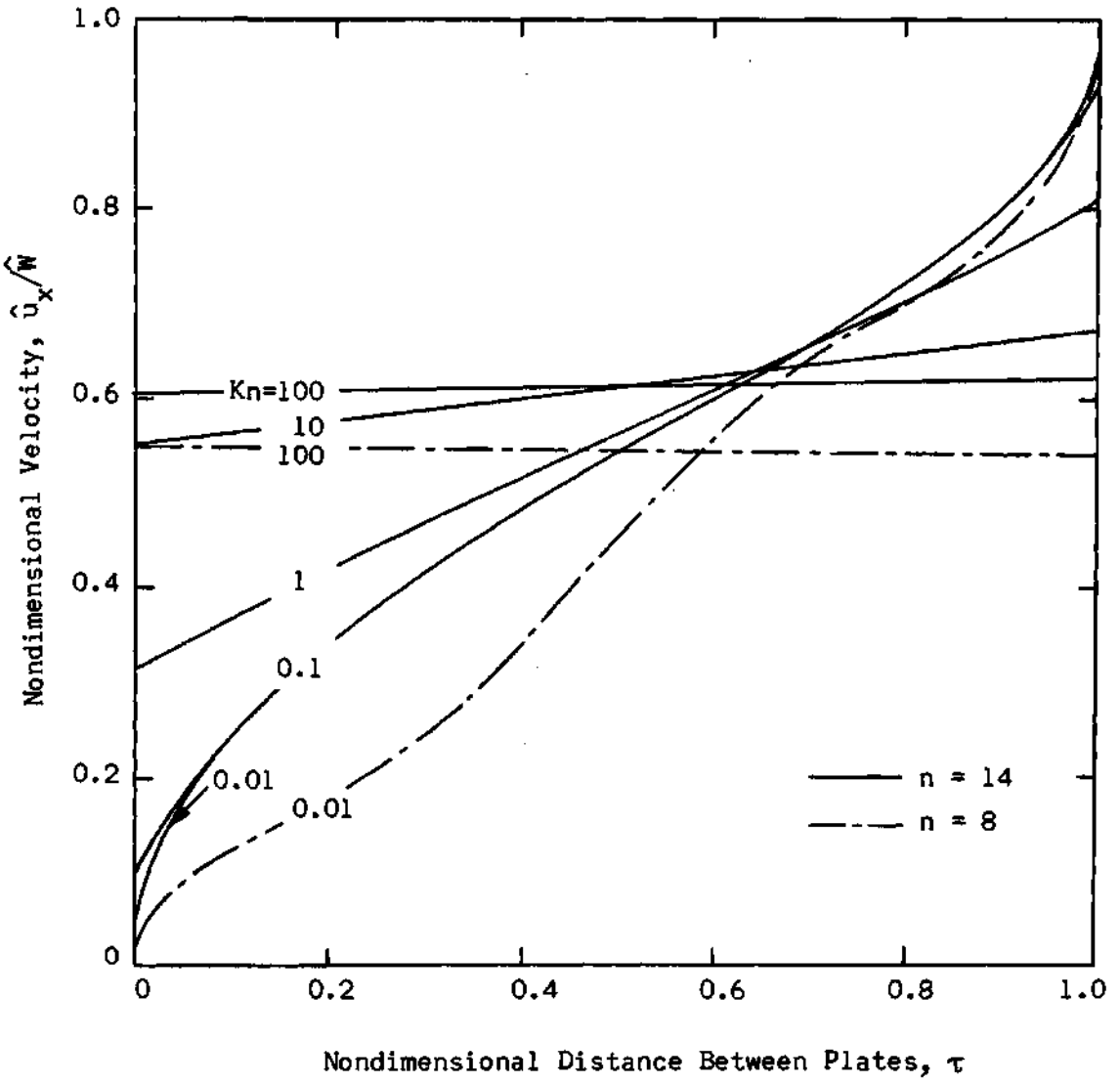

Figure 13. Couette Flow Velocity Profiles for $\hat{W} = 3$, $\hat{T}_2 = 0.4$.

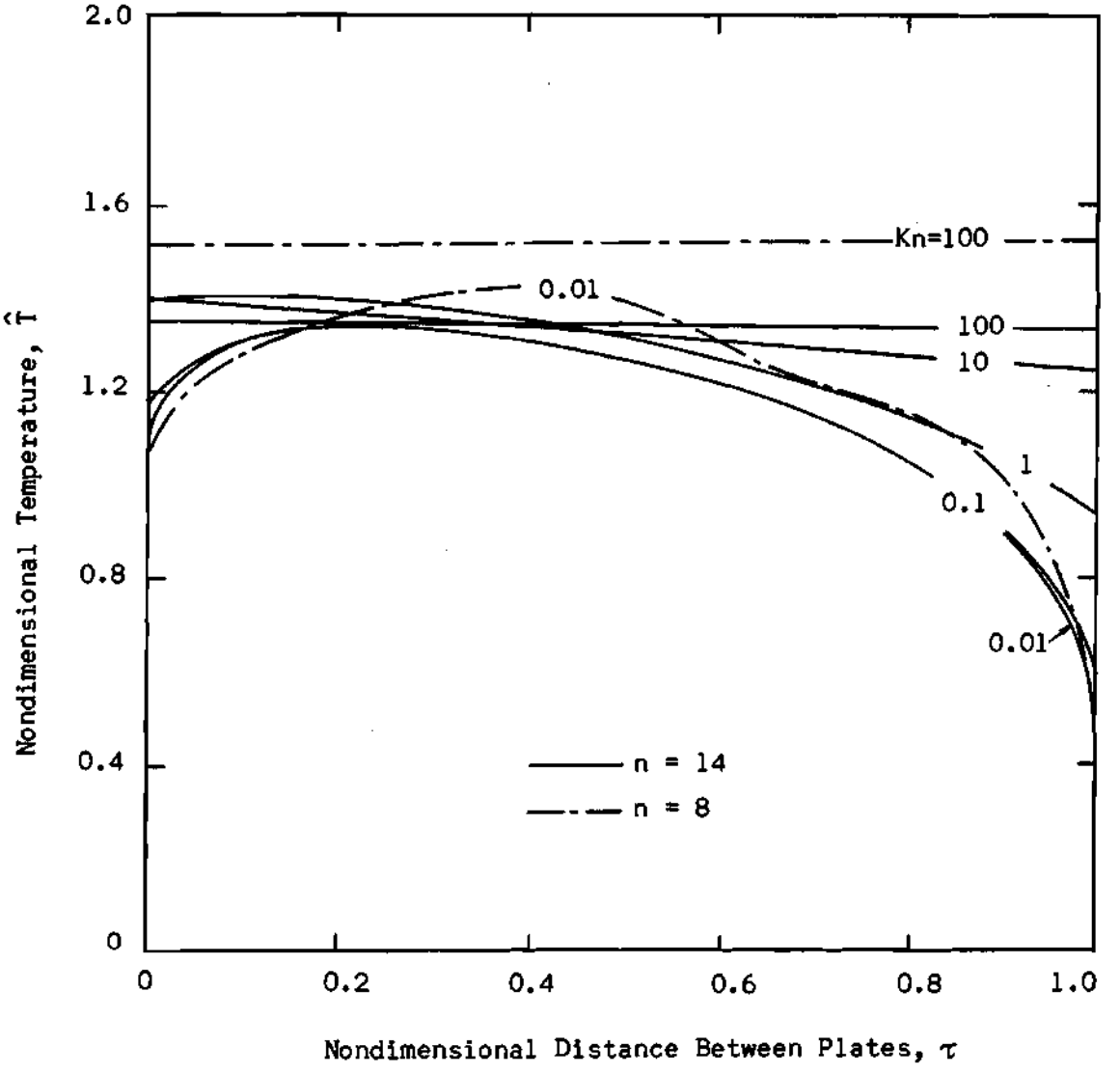

Figure 14. Couette Flow Temperature Profiles for $\hat{W} = 3$, $\hat{T}_2 = 0.4$.

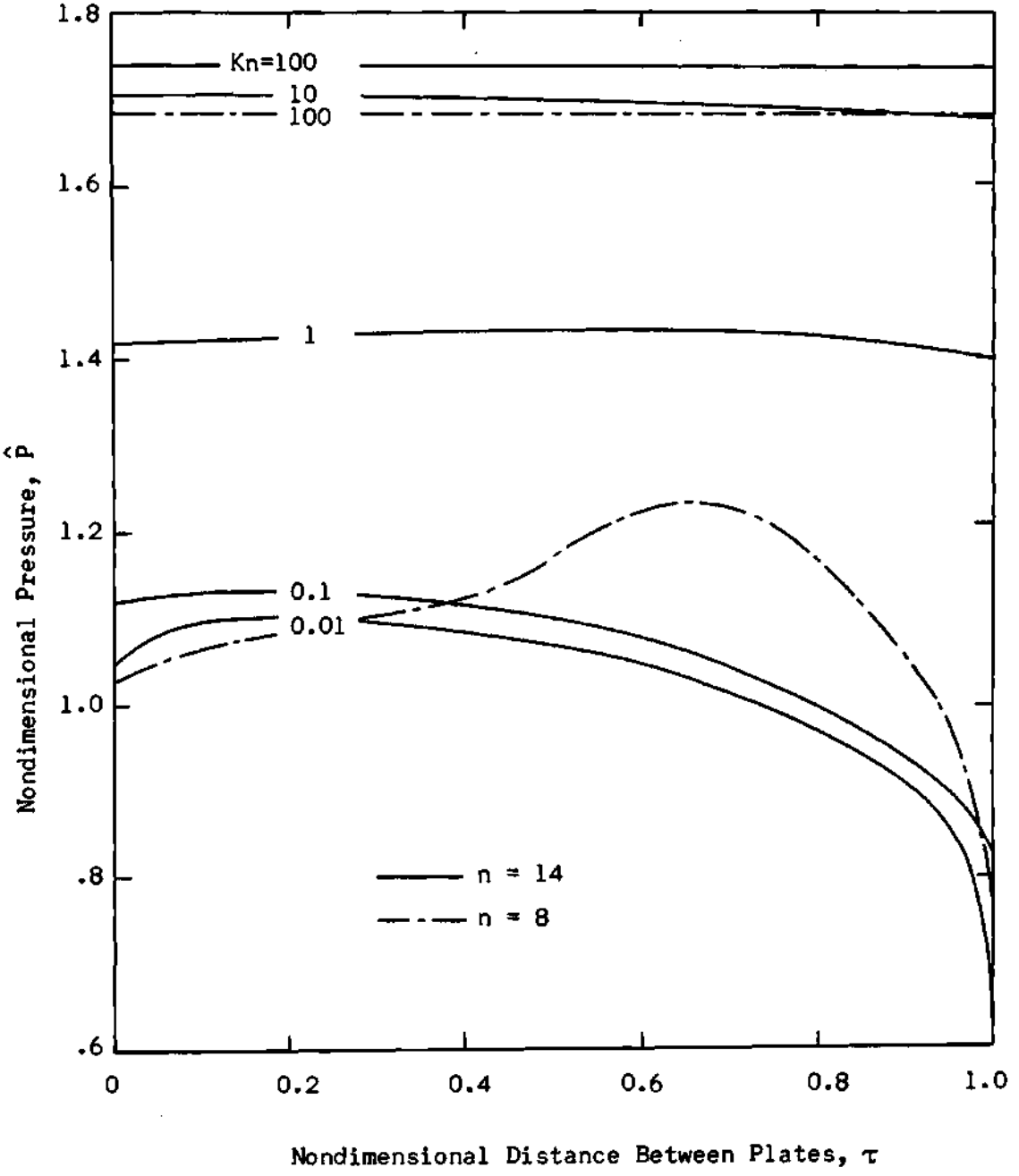

Figure 15. Couette Flow Pressure Profiles for $\hat{W} = 3$, $\hat{T}_2 = 0.4$.

the present cases, and, since the discrete ordinate method is an "approximate" method, the error due to the difference equations is within a reasonable limit.

The usefulness of the solutions of the Couette flow problem using the BBGK equation lies primarily in their role as calibrations for the application of the method of discrete ordinates to non-linear problems.

In regard to the applicability of the present method, there are two points which are worthy of note. First, the proposed discrete ordinate method is capable of obtaining accurate solutions from large Knudsen numbers (the free molecular and the near-free molecular flow regime) all the way to small Knudsen numbers (the slip and continuum flow regime). This can be seen from Figures 2 through 7 in which numerical results are presented from Kn=100, 10 to Kn=0.01 and 0.001. The solutions for Kn=0.001 exhibit clearly the continuum case. It should be noted that the numerical scheme used by Anderson [14] cannot be applied to calculate cases with Knudsen numbers $Kn < 0.1$. Second, the proposed discrete ordinate method is also capable of obtaining good solutions from small Mach numbers (subsonic flow) to large Mach numbers (supersonic or hypersonic flow). Although no standard solutions are available for comparisons for the $\hat{W}$=3 case, it is felt that the solutions presented in Figures 8 through 15 are quite reasonable. It is believed that higher order approximations ($n > 8$) should be used for $\hat{W} \geq 3$ cases.

In conclusion, the application of the proposed discrete ordinate method to the non-linear Couette flow with heat transfer has yielded excellent results with a very reasonable computing time,* leading the author

*The computer time needed for each iteration (using a Burroughs B-5500 computer) is approximately 20 seconds ($n=8$, $\Delta\tau = 1/100$).

to believe that it is a very powerful tool for boundary value problems in non-linear rarefied gasdynamics.

CHAPTER III

THE LEADING EDGE PROBLEM

Background of the Problem

One of the most difficult, yet practical, problems of viscous aerodynamics is the study of the phenomena occuring near the sharp leading edge of a flat plat which is aligned with a high speed gas stream. When the leading edge is mathematically sharp, and when the gas is rarefied, a flat plate generates a wide spectrum of flow regimes. These range from a near-free molecular region near the leading edge to the continuum picture of a classical boundary layer far down the plate. The viscous flow regimes can be defined physically by a model proposed by Pan and Probstein [38] and exhibited in Figure 16. Although the limits of each of the various flow regimes are defined somewhat arbitrarily, it has been demonstrated by Talbot [39] that the initial departure of the interaction theories from experimental results could be correlated by the rarefaction parameter, $\bar{V}_{\infty,x} = M_\infty \sqrt{C/Re}_x$. A more specific interrelation with this parameter is defined in later sections. However, an approximate relationship of $\bar{V}_{\infty,x}$ to the flow regimes is depicted in Figure 16. The position down the plate, x, and the local Reynold's number, Re_x, are also presented in accordance with the free stream properties of the present solution and their relationship to $\bar{V}_{\infty,x}$.

At the leading edge, the details of the flow must be considered from a kinetic theory viewpoint. This "kinetic" region is where the flow exhibits near-free molecular behavior, that is, molecule-surface collisions dominate

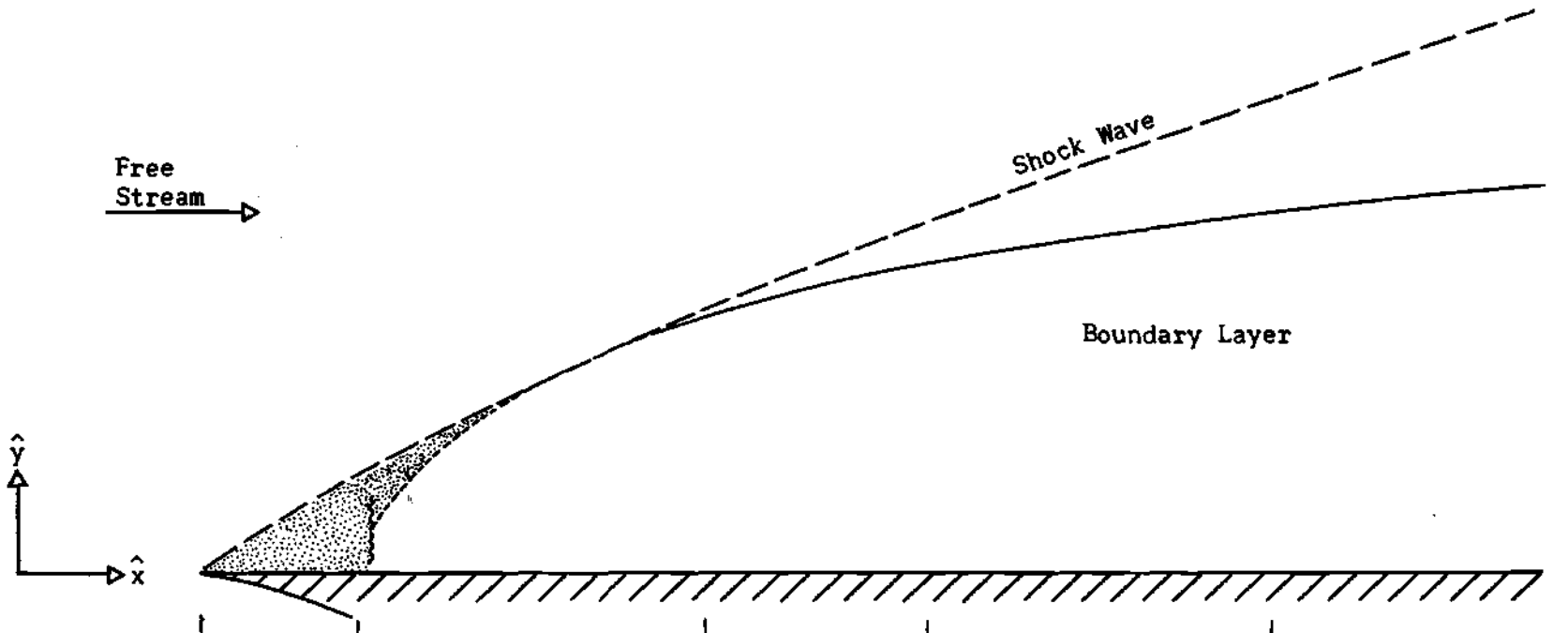

$\hat{x}$	0	10	20	30	40	50	60	70
$\bar{V}_{x,\infty}(M_\infty=1.5)$	∞	0.301	0.213	0.174	0.151	0.134	0.123	0.114
$Re_x(M_\infty=1.5)$	0	24.7	49.4	74.2	98.9	123.6	148.3	173.1

Figure 16. Schematic Flow Field for the Sharp Leading Edge Problem.

the flow description, with slip velocity and temperature jump effects being most pronounced. The "kinetic" region will extend downstream into a "transition" region where both molecule-molecule and molecule-surface collisions are equally important. The beginning of the continuum regime is signalled by the "merged" region where the shock wave and viscous boundary layer are merged. Farther downstream the shock wave emerges from the boundary layer and the "strong interaction" region begins, eventually decaying into a "weak interaction" region where the shock wave has decayed to a Mach line. Here the classical boundary layer situation is attained.

Various aspects of this problem have been studied for many years. Most of the theoretical investigations have been with the classical boundary layer equations and Navier-Stokes equations, which are valid in the "interaction" regions, and the investigations have attempted to extrapolate their results into the "merged" layer and "transition" region. The kinetic theory approach is to start at the leading edge and proceed downstream. The ultimate objective, of course, is to connect these two efforts in a meaningful way in the "transition" and "merged" regions.

The literature on this problem is quite extensive and only some most crucial and well-known papers will be cited. Excellent critiques have been presented by Moulic [40] and by Potter [41]. The most important contributions are presented according to their method of approach and region of applicability.

Weak and Strong Interaction Experiment

The pioneering effort to obtain experimental results for the interaction regimes was offered by Becker [42] when he drew interest to the leading edge problem by publishing data showing the surface pressure strongly

rising above the predictions of theory. Several later experimental efforts in the interaction regimes have followed Becker's initial work and are summarized comprehensively by Moulic [40] and by Hayes and Probstein [43].

Merged Layer and Transition Region Experiment

In order to achieve sufficiently large Knudsen number and sufficiently small Reynold's number results, several experimental investigations have been undertaken using rarefied test facilities and/or hypersonic test streams.

Early measurements by Schaaf, et.al. [44] showed significant departures from strong interaction theories for an adiabatic flat plate in the range $3 < M_\infty < 6$. The results were attributed to slip effects. Laurmann [45] performed similar experiments and showed the lack of a clearly defined shock wave near the leading edge. Moulic [40] obtained skin friction data for the same cases and corrected some of Schaaf's earlier pressure results.

Nagamatsu, et.al. [46,47] obtained surface pressure and heat transfer data at large Mach numbers, $7 < M_\infty < 26$, for a cold plate.

Recently, Becker and Boylan [48] obtained pressure data and wall slip velocity measurements for the merged and transition flow regimes with Mach numbers, $4 < M_\infty < 10$. They used a cold plate with T_w/T_o of about 0.2. The wall slip and pressure measurements are used for comparison later.

McCroskey [49] has achieved results similar to those of Becker and Boylan for $M_\infty = 24.5$. The works of Nagamatsu, Becker and Boylan, and McCroskey exhibit plateaus of maximum heat transfer and pressure near the leading edge.

Significant departures from strong interaction theories are obvious

in all these merged layer experiments, but an assessment of the pressure data and shock wave shapes shows considerable disagreement. For that matter, even the various strong interaction pressure data vary considerably in magnitude.

Kinetic Region Experiment

The first experimental results extending upstream of the transition regime were presented by Vidal and Wittliff [50]. They measured surface pressure and heat transfer on a cold flat plate with Mach number $13 < M_\infty < 25$ for all regions from weak interaction to the kinetic regime, and concluded that the governing parameter was $\bar{V}_{\infty,x}$. They also established the departure from strong interaction theory to begin when $\bar{V}_{\infty,x} \gtrsim 0.1$ or 0.2. Later Wallace and Burke [51] presented cold wall data for skin friction and heat transfer for a flat plate under conditions similar to those of Vidal and Wittliff. In addition it should be noted that Wallace and Burke were the first to contribute local skin friction information very near the leading edge of a sharp flat plate. The results of these two groups confirmed Nagamatsu's observation of plateaus in surface quantities near the leading edge, although the pressure data were substantially lower near the leading edge.

Chuan and Waiter [52] have also reported kinetic region surface pressure distributions on an adiatic flat plate for Mach numbers $6 < M_\infty < 8$. Their surface measurements did not reveal the pressure plateau noted on the other experimental studies, but they did conclude that very near the leading edge the measured flow field properties and surface pressures are not predicted by continuum theories.

Experimental results for both the transition and kinetic regimes,

$\bar{V}_{\infty,x} > 0.3$, are seen to be quite limited and results for $\bar{V}_{\infty,x} > 1$ are, to date, non-existent. This lack of information can be attributed to the extreme difficulty of placing measuring devices in regions whose physical length is of the order of a mean free path. Certainly, accurate measurements under these conditions are extremely difficult to obtain, and considerable question exists as to the interpretation of schlieren photographs, corrections to pressure measurements, the significance of non-uniform flow, and the effects of flow angularity. At best, the available experiments have lacked sufficient detail to construct an accurate model of the flow field or to closely examine the theoretical models.

Weak and Strong Interaction Theory

The basic idea of the viscous "interaction" studies is that the boundary layer has a significant displacement thickness which forms an effective body, and thereby produces a shock wave. The shock is curved, and decays from a strong shock in the strong interaction regime to a weak shock in the weak interaction regime. Pioneering theoretical work by Lees and Probstein [53] in the weak interaction regime was followed by numerous weak and strong interaction theories that are summarized by Hayes and Probstein [43]. The fundamental parameters in these regimes are the viscous interaction parameter or rarefaction parameter, $\bar{V}_{\infty,x} = M_\infty \sqrt{C/Re_x}$, and the hypersonic interaction parameter, $\bar{X}_{\infty,x} = M_\infty^3 \sqrt{C/Re_x}$. There is reasonable agreement between experimental surface quantities and the "interaction" theory predictions.

Merged Layer and Transition Region Theory

The entrance into the merged region is marked by significant influence of slip velocity and temperature jump effects in the flow field.

Aroesty [54] has demonstrated that surface velocity slip and surface temperature jump alone cannot explain the surface pressure and heat transfer behavior that has been observed. On the other hand, Nagamatsu, et.al. [46] have proposed that the slip velocity influences the entire flow field. On the basis of schlieren observations, they conclude that when the shock wave forms, it is merged with the boundary layer. They further claim that the shock wave angle does not reach a maximum until the end of the slip regions.

Laurmann [55] recently applied the Oseen linearization to the Navier-Stokes equations in the limit of hypersonic flow, thereby neglecting the non-linear features of the problem and viscous dissipation effects. His solution exhibits general features of the weak interaction model for large Reynolds numbers. At the leading edge there is free molecular flow with perfect slip, and the solution consists of a viscous layer whose displacement thickness is proportional to x^2 initially, and to $x^{1/2}$ as x increases. This reverse curvature is similar to the prediction of the Nagamatsu model.

Other studies of the merged layer are based on order of magnitude estimates and non-dimensional groupings of the Navier-Stokes equations. A comprehensive study of this model has been presented by Pan and Probstein [38]. Starting with the Navier-Stokes equations and the assumption of a thin shock layer, they find first order effects arising from velocity slip and temperature jump at the surface, from shock wave thickness and curvature, from transport effects behind the shock, and from normal pressure gradients. They also assume similar velocity and temperature profiles. Their theory, however, does not yield good solutions in the transition and kinetic regions.

Using a formulation based on the tangent wedge approximation for

the inviscid flow field and the assumption of "similar" solutions of the compressible boundary layer equations, Li and Nagamatsu [56] obtained skin friction and heat transfer results for various wall temperature values. The significant contribution of their efforts was to present a modified Reynold's analogy applicable to non-insulated flat plates. Although their heat transfer and skin friction expressions are strictly valid only in the interaction regimes, it is interesting to note that the ratio of the two, or Reynold's analogy, is not so restricted. It is thus conceivable that their Reynold's analogy can be extended into the merged layer since continuum mechanics still dominate the flow and thus the qualitative behavior of the interrelation between these two transport properties should remain constant - at least to first order. Their results will be used for comparison later.

Garvine [57] recently applied an order of magnitude analysis and concluded that the most crucial element in the problem is the streamwise variation of the flow field profiles. As a result, the governing equations cannot be solved without an accurate knowledge of the initial flow conditions at the upstream edge of the continuum regimes. This indicates that the local similarity assumption of Pan and Probstein can not be valid in the transition regime.

Using a similar analysis involving the ordinary flat plate boundary layer equations, Oguchi [58] applied special boundary conditions that depend on the position of the shock wave. Anomalous results in skin friction and heat transfer motivated Oguchi in his second paper [59] to include velocity slip and temperature jump at the wall. These effects lowered the pressure and produced a shock wave with reverse curvature. However, as pointed

out by Garvine [57], both analyses were done incorrectly and the results are open to question.

Very recently, Butler [60], using the Los Alamos computer facilities, obtained a numerical solution of the Navier-Stokes equations for the interaction and merged layer regimes of a flat plate at Mach number, M=10. His results do not exhibit a pressure plateau near the leading edge. He does, however, present some interesting comparisons of the slip and no-slip models.

Kinetic Region Theory

All of the flow models discussed so far have been based on concepts of continuum fluid dynamics. However, it is well known that the continuum assumptions are no longer valid as the Knudsen number becomes very large, i.e., very near the leading edge. In this region only a kinetic theory solution can adequately describe the events occuring there. A common assumption is that the flow at the leading edge is free molecular. Thus, only random motion of the molecules brings them to the plate. The first few collisions between streaming and emitted particles drastically alter this situation. In the near-free molecular region, Charwat [61] proposed a first collision and a second collision near-free molecular model. His analysis considers the interdiffusion of molecules from the surface with streaming molecules of the free stream and then analyzes the scattering of successive "groups" of molecules. An ensuing momentum transport due to these first collisions is used to predict the qualitative behavior of the surface pressure. His analysis is based on a near-Newtonian flow, $M_\infty \to \infty$, a very cold wall, $T_w \ll T_\infty$, and the neglect of any upstream effects, thus beginning with a true free molecular solution at x=0. His results predict a pressure

plateau beginning downstream of the leading edge. Using a similar first collision theory based on a somewhat less rigorous approach, Kogan [62] suggests that even very close to the leading edge no true free molecular flow region will exist. He bases his discussion on the fact that molecules scattered upstream cannot be entirely neglected. Recently Bird [63] substantiated the statement by Kogan based on his computer experiments. Using Monte-Carlo techniques to study a flow field consisting of rigid-sphere molecules governed by an assumed form of the probability distribution e(x), Bird showed that the influence of the reflected molecules is actually felt in the order of a mean free path upstream of the leading edge. Because of limited computer storage his analysis was limited to a finite length plate, ten mean free paths long, and to a small number of collisions with the plate (on the order of 1000 surface collisions). His solution predicts, contrary to experimental evidence, that even at the leading edge the pressure is rising and no pressure plateau exists.

The first collison theories of Charwat and Kogan, in spite of their restrictions, yield a physically meaningful picture of the qualitative behavior of the phenomena in the kinetic region. Charwat states that he views his theory as a subtle form of dimensional analysis rather than a quantitative theory. Bird's approach, on the other hand, should be more quantitative than the first collision theories, but, because of the limitations of the method used, his solution cannot be considered very accurate.

It should be mentioned that the kinetic theory approach to this problem is still in its infancy, and there is a need for a solution of the Boltzmann equation which will have the ability to span the entire

spectrum from free molecular to continuum flow. There is to date no solution of the two-(space) dimensional Boltzmann equation, or its substitute equations, in their entirety which have accomplished this study.

It seems appropriate here to clarify the purpose of this chapter. The purpose of this chapter is to demonstrate that the present discrete ordinate method can make the previously unapproachable two-(space) dimensional problem accessible to solution and thus present a meaningful study of the phenomena occuring in the leading edge problem for the flow regimes from near free molecule flow to the weak interaction region. Primary emphasis is placed on the merged, transition, and kinetic regions ($\bar{V}_{\infty,x} > 0.15$) but the solution is extended downstream to show the development of the continuum regime.

Formulation of the Problem

The geometry of the leading edge problem is shown in Figure 16. A semi-infinite flat plate is submerged at zero angle of attack in a supersonic rarefied gas stream. M_∞ is the free stream Mach number of the gas with density n_∞ and temperature T_∞. The plate is at temperature T_w. The problem is two-dimensional in physical space in that the distribution function, $f(x, y; \bar{v}, t)$ describing the state of the system depends on x and y. The Boltzmann equation with the BGK model is chosen as the governing equation, and for this case is

$$v_x \frac{\partial f}{\partial x} + v_y \frac{\partial f}{\partial y} = \nu(x,y)(F - f) \qquad (1)$$

where

$$F = n\left(\frac{1}{2\pi RT}\right)^{3/2} e^{-\frac{1}{2RT}(\bar{v} - \bar{u})^2} \tag{2}$$

In order to reduce computer storage requirements, reduced distribution functions are conveniently defined, analogous to the reductions in the Couette flow equations of Chapter II. The reduced distribution functions are

$$g(x, y; v_x, v_y) = \int_{-\infty}^{\infty} f(x, y; \bar{v})dv_z \tag{3-a}$$

$$h(x, y; v_x, v_y) = \int_{-\infty}^{\infty} v_z^2 f(x, y; \bar{v})dv_z \tag{3-b}$$

Thus, integrating out the v_z dependence in Equation (1) by using Equations (3), the single three-dimensional BBGK equation (1) reduces to the following two simultaneous two-dimensional equations

$$v_x \frac{\partial g}{\partial x} + v_y \frac{\partial g}{\partial y} = \nu(x, y)(G - g) \tag{4-a}$$

$$v_x \frac{\partial h}{\partial x} + v_y \frac{\partial h}{\partial y} = \nu(x, y)(H - h) \tag{4-b}$$

where

$$G = \frac{n}{2\pi RT} e^{-\frac{1}{2RT}[(v_x - u_x)^2 + (v_y - u_y)^2]} \tag{5-a}$$

$$H = RTG \tag{5-b}$$

the moments are found as follows

$$n = \int_{-\infty}^{\infty}\int_{-\infty}^{\infty} g dv_x dv_y \tag{6-a}$$

$$nu_x = \int_{-\infty}^{\infty}\int_{-\infty}^{\infty} v_x g dv_x dv_y \tag{6-b}$$

$$nu_y = \int_{-\infty}^{\infty}\int_{-\infty}^{\infty} v_y g dv_x dv_y \tag{6-c}$$

$$\frac{3}{2} nRT = \frac{1}{2}\int_{-\infty}^{\infty}\int_{-\infty}^{\infty} h dv_x dv_y + \frac{1}{2}\int_{-\infty}^{\infty}\int_{-\infty}^{\infty} [(v_x - u_x)^2 + (v_y - u_y)^2] g dv_x dv_y \tag{6-d}$$

$$\tau_{xy} = -m\int_{-\infty}^{\infty}\int_{-\infty}^{\infty} v_x v_y g dv_x dv_y + mnu_x u_y \tag{6-e}$$

$$q_y = \frac{m}{2}\int_{-\infty}^{\infty}\int_{-\infty}^{\infty} v_y v_x^2 g dv_x dv_y - mu_x \int_{-\infty}^{\infty}\int_{-\infty}^{\infty} v_x v_y g dv_x dv_y + \frac{m}{2}\int_{-\infty}^{\infty}\int_{-\infty}^{\infty} v_y^3 g dv_x dv_y - mu_y \int_{-\infty}^{\infty}\int_{-\infty}^{\infty} v_y^2 g dv_x dv_y + \frac{m}{2}\int_{-\infty}^{\infty}\int_{-\infty}^{\infty} v_y h dv_x dv_y - \frac{3}{2} nRTu_y + \frac{mnu_y}{2}(u_y^2 + u_x^2) \tag{6-f}$$

$$p = mnRT \tag{6-g}$$

where τ_{xy} is the shear stress in the x-y plane and q_y is the heat flux normal to the plate.

The collision frequency, $\nu(x,y)$, is taken to be of the form [64]

$$\nu = \frac{nkT}{\mu} \tag{7}$$

where the viscosity, μ, is assumed to have a temperature dependence

$$\frac{\mu}{\mu_\infty} = \left(\frac{T}{T_\infty}\right)^S \tag{8}$$

where S is a constant for a given gas [1]. The viscosity, μ, is related to the free stream mean free path by the relation [1]

$$\lambda_\infty = \frac{16}{5} \frac{\mu_\infty}{mn_\infty \sqrt{2\pi RT_\infty}} \tag{9}$$

Combining Equations (7) through (9) gives

$$\nu = \frac{16}{5} \frac{nRT}{n_\infty \lambda_\infty \sqrt{2\pi RT_\infty}} \left(\frac{T}{T_\infty}\right)^{-S} \tag{10}$$

A characteristic velocity is defined as

$$V_\infty = \sqrt{2RT_\infty} \tag{11}$$

The definitions of dimensionless variables are introduced as follows

$$\hat{u}_x = u_x/V_\infty, \qquad \hat{u}_y = u_y/V_\infty , \qquad \hat{v}_i = v_i/V_\infty , \qquad \hat{n} = n/n_\infty ,$$

$$\hat{T} = T/T_\infty , \qquad \hat{p} = p/p_\infty , \qquad \hat{\tau}_{xy} = \tau_{xy}/mn_\infty u_{x_\infty}^2 ,$$

$$\hat{q}_y = q_y/c_p T_\infty mn_\infty u_{x_\infty} , \qquad \hat{x} = x/\lambda_\infty , \qquad \hat{y} = y/\lambda_\infty ,$$

$$\hat{g} = gV_\infty^2/n_\infty , \qquad \hat{h} = h/n_\infty , \qquad \hat{\nu} = \nu\lambda_\infty/V_\infty ,$$

$$\hat{G} = GV_\infty^2/n_\infty , \qquad \hat{H} = H/n_\infty .$$

After the process of nondimensionalization of Equations (4) and (5) is accomplished, the discrete ordinate method outlined in the previous chapters is applied. The application of the method reduces the set of governing integro-differential equations, Equations (4), to a set of partial differential equations.

The resulting differential equations are

$$\hat{v}_\sigma \frac{\partial \hat{g}}{\partial \hat{x}}_{\sigma,\delta} + \hat{v}_\delta \frac{\partial \hat{g}}{\partial \hat{y}}_{\sigma,\delta} = \hat{\nu}(\hat{G}_{\sigma,\delta} - \hat{g}_{\sigma,\delta}) \tag{12-a}$$

$$\hat{v}_\sigma \frac{\partial \hat{h}}{\partial \hat{x}}_{\sigma,\delta} + \hat{v}_\delta \frac{\partial \hat{h}}{\partial \hat{y}}_{\sigma,\delta} = \hat{\nu}(\hat{H}_{\sigma,\delta} - \hat{h}_{\sigma,\delta}) \tag{12-b}$$

where

$$\hat{G}_{\sigma,\delta} = \frac{\hat{n}}{\pi\hat{T}} e^{-[(\hat{v}_\sigma - \hat{u}_x)^2 + (\hat{v}_\delta - \hat{u}_y)^2]/\hat{T}} \tag{13-a}$$

$$\hat{H}_{\sigma,\delta} = \frac{\hat{T}\hat{G}}{2}_{\sigma,\delta} \tag{13-b}$$

and

$$\hat{\nu} = \frac{8}{5\sqrt{\pi}} \hat{n}\hat{T}^{(1-S)} \tag{14}$$

where $\hat{g}_{\sigma,\delta}$, $\hat{h}_{\sigma,\delta}$, $\hat{G}_{\sigma,\delta}$, and $\hat{H}_{\sigma,\delta}$ represent $\hat{g}$, $\hat{h}$, $\hat{G}$, and $\hat{H}$ evaluated at the discrete velocity point $(\hat{v}_\sigma, \hat{v}_\delta)$ (σ=-n,...,-1,1,...,n, δ=-n,...,-1, 1,...,n), respectively.

Introducing the transformation

$$\hat{\eta} = 1 - e^{-a\hat{y}} \tag{15}$$

into Equations (12) then gives

$$\hat{v}_\sigma \frac{\partial \hat{g}}{\partial \hat{x}}_{\sigma,\delta} + \hat{v}_\delta a(1 - \hat{\eta}) \frac{\partial \hat{g}}{\partial \hat{\eta}}_{\sigma,\delta} = \hat{v}(\hat{G}_{\sigma,\delta} - \hat{g}_{\sigma,\delta}) \tag{16}$$

$$\sigma = -n,\ldots,-1,1,\ldots n$$

$$\delta = -n,\ldots,-1,1,\ldots n$$

and a similar equation for $\hat{h}_{\sigma,\delta}$. This transformation not only maps the infinite $\hat{y}$ region into a unit region ($0 \leq \hat{\eta} \leq 1$) but it also does so in an efficient manner. That is, if the region $0 \leq \hat{\eta} \leq 1$ is divided into m equal steps for the purpose of applying a finite difference scheme, the points in actual physical space are quite close together in the region near the plate where gradients are largest and are spaced farther apart in regions away from the surface where there is little change in flow properties.

In order to specify the interaction of the molecules with the surface of the plate, it is assumed that molecules which strike the surface are subsequently emitted with a Maxwellian velocity distribution characterized by the plate temperature, $\hat{T}_w$, and zero net tangential velocity. The two-stream concept introduced earlier is applied here also by defining the half-range distribution functions

$$\hat{f}^+(\hat{x}, \hat{\eta}; \hat{v}_x, \hat{v}_y) = 0 \quad , \qquad \text{for } \hat{v}_y < 0$$

$$\hat{f}^-(\hat{x}, \hat{\eta}; \hat{v}_x, \hat{v}_y) = 0 \quad , \qquad \text{for } \hat{v}_y > 0$$

The non-dimensionalized boundary conditions (for 2n x 2n discrete velocity points) can then be written

$$\hat{g}^{\pm}(\hat{x} < 0,\ \hat{\eta};\ \hat{v}_\sigma,\ \hat{v}_\delta) = \frac{1}{\pi}\, e^{-[(\hat{v}_\sigma - \hat{u}_{x_\infty})^2 + \hat{v}_\delta^2]} \tag{17-a}$$

$$\hat{h}^{\pm}(\hat{x} < 0,\ \hat{\eta};\ \hat{v}_\sigma,\ \hat{v}_\delta) = \frac{1}{2\pi}\, e^{-[(\hat{v}_\sigma - \hat{u}_{x_\infty})^2 + \hat{v}_\delta^2]} \tag{17-b}$$

$$\hat{g}^{\pm}(\hat{x},\ \hat{\eta}=1;\ \hat{v}_\sigma,\ \hat{v}_\delta) = \frac{1}{\pi}\, e^{-[(\hat{v}_\sigma - \hat{u}_{x_\infty})^2 + \hat{v}_\delta^2]} \tag{17-c}$$

$$\hat{h}^{\pm}(\hat{x},\ \hat{\eta}=1;\ \hat{v}_\sigma,\ \hat{v}_\delta) = \frac{1}{2\pi}\, e^{-[(\hat{v}_\sigma - \hat{u}_{x_\infty})^2 + \hat{v}_\delta^2]} \tag{17-d}$$

$$\hat{g}^{+}(\hat{x} > 0,\ \hat{\eta}=0;\ \hat{v}_\sigma,\ \hat{v}_\delta) = \frac{\hat{n}_w}{\pi \hat{T}_w}\, e^{-[(\hat{v}_\sigma - \hat{u}_{x_{\hat{\eta}=0}})^2 + \hat{v}_\delta^2]/\hat{T}_w} \tag{17-e}$$

$$\hat{h}^{+}(\hat{x} > 0,\ \hat{\eta}=0;\ \hat{v}_\sigma, \hat{v}_\delta) = \frac{\hat{n}_w}{2\pi}\, e^{-[(\hat{v}_\sigma - \hat{u}_{x_{\hat{\eta}=0}})^2 + \hat{v}_\delta^2]/\hat{T}_w} \tag{17-f}$$

The density of the molecules diffusing from the plate, $\hat{n}_w$, is not known a priori and may be found by applying the condition of zero mass flux normal to the plate at the surface. In discrete ordinate form, this condition yields the relation (see Chapter II, Equation (14))

$$-\sum_{\sigma=-n}^{n} \sum_{\delta=-n}^{-1} k_\sigma k_\delta \hat{v}_\delta \hat{g}^{-}_{\sigma,\delta}\, e^{(\hat{v}_\sigma^2 + \hat{v}_\delta^2)/\hat{T}} \quad + \tag{18}$$

$$\sum_{\sigma=-n}^{n} \sum_{\delta=1}^{n} k_\sigma k_\delta \hat{v}_\delta \hat{g}^{+}_{\sigma,\delta} e^{(\hat{v}_\sigma^2+\hat{v}_\delta^2)/\hat{T}} = 0$$

where k_σ and k_δ are the quadrature weighting coefficients for velocity components $\hat{v}_\sigma$ and $\hat{v}_\delta$, respectively (see Appendix A).

Thus, the problem reduces to solving Equations (16) subject to conditions (17). This yields 2n x 2n equations with 2n x 2n discrete unknowns.

Computational Procedure

As discussed in Chapters I and II, the application of the discrete ordinate technique removes the microscopic velocity dependence from the reduced distribution functions. Accordingly, the functions, $\hat{g}_{\sigma,\delta}$, $\hat{h}_{\sigma,\delta}$, $\hat{G}_{\sigma,\delta}$, and $\hat{H}_{\sigma,\delta}$ in Equations (16) are independent of the velocity variables $\hat{v}_\sigma$ and $\hat{v}_\delta$. Therefore, Equations (16) can be solved by incorporating a finite difference technique in physical space coupled with an iterative scheme.

The finite difference scheme used for the Couette flow problem was modified for application to a two-(space) dimensional problem. However, attempts to use this scheme on the leading edge problem proved to be penalizing in computer time. To alleviate the computer time problem, a much simpler finite difference scheme was devised which resulted in a very rapidly converging formulation, with time required for each iteration kept to within a workable limit. The difference derivatives are written as differences from point (i, j) with other quantities evaluated at point (i, j) in the grid formulation below

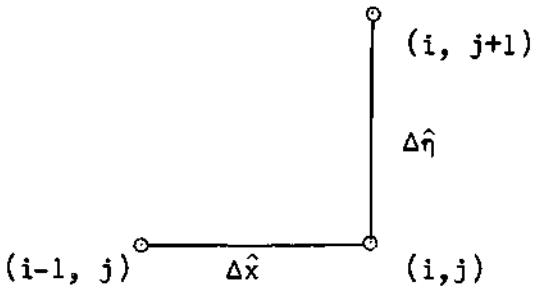

The difference form of Equation (16) becomes

$$\hat{v}_\sigma\left[\frac{\hat{g}_{\sigma,\delta}(i,j) - \hat{g}_{\sigma,\delta}(i-1,j)}{\Delta\hat{x}}\right] + \hat{v}_\delta a(1-\hat{\eta}_j)\left[\frac{\hat{g}_{\sigma,\delta}(i,j+1) - \hat{g}_{\sigma,\delta}(i,j)}{\Delta\hat{\eta}}\right]$$

$$= \hat{v}(i,j)[\hat{G}_{\sigma,\delta}(i,j) - \hat{g}_{\sigma,\delta}(i,j)] \qquad (19)$$

Equation (19) is rearranged and used to solve for $\hat{g}^-_{\sigma,\delta}$ as a backward difference equation as follows

$$\hat{g}^-_{\sigma,\delta}(i,j) = \Big[\frac{\hat{v}_\sigma}{\Delta\hat{x}}\,\hat{g}^-_{\sigma,\delta}(i-1,j) - \frac{\hat{v}_\delta a}{\Delta\hat{\eta}}(1-\hat{\eta}_j)\hat{g}^-_{\sigma,\delta}(i,j+1) \qquad (20)$$

$$+ \hat{v}(i,j)\hat{G}^-_{\sigma,\delta}(i,j)\Big]$$

$$\Big/\left[\frac{\hat{v}_\sigma}{\Delta\hat{x}} - \frac{\hat{v}_\delta a}{\Delta\hat{\eta}}(1-\hat{\eta}_j) + \hat{v}(i,j)\right]$$

To be consistent with the backward differencing scheme, the derivatives are written in the direction of flow of the molecules. Appropriately, then, the grid formulation for the $\hat{g}^+_{\sigma,\delta}$ molecules is taken to be as illustrated below

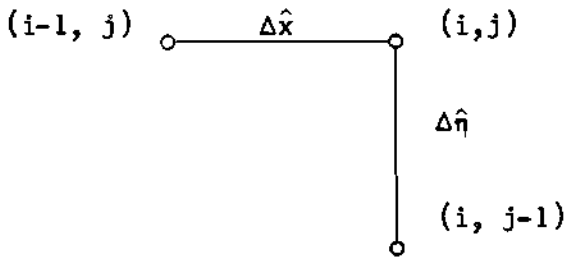

Accordingly, the difference form of Equation (16) becomes

$$\hat{v}_\sigma\left[\frac{\hat{g}_{\sigma,\delta}(i,j) - \hat{g}_{\sigma,\delta}(i-1,j)}{\Delta\hat{x}}\right] + \hat{v}_\delta a(1-\hat{\eta}_j)\left[\frac{\hat{g}_{\sigma,\delta}(i,j) - \hat{g}_{\sigma,\delta}(i,j-1)}{\Delta\hat{\eta}}\right]$$

$$= \hat{v}(i,j)[\hat{G}_{\sigma,\delta}(i,j) - \hat{g}_{\sigma,\delta}(i,j)] \qquad (21)$$

Equation (21) is rearranged and used to solve for $\hat{g}^{+}_{\sigma,\delta}$ as follows

$$\hat{g}^{+}_{\sigma,\delta}(i,j) = \Big[\frac{\hat{v}_\sigma}{\Delta\hat{x}}\,\hat{g}^{+}_{\sigma,\delta}(i-1,j) + \frac{\hat{v}_\delta a}{\Delta\hat{\eta}}\,(1-\hat{\eta}_j)\hat{g}^{+}_{\sigma,\delta}(i,j-1) + \hat{v}(i,j)\hat{G}^{+}_{\sigma,\delta}(i,j)\Big] \Big/ \Big[\frac{\hat{v}_\sigma}{\Delta\hat{x}} + \frac{\hat{v}_\delta a}{\Delta\hat{\eta}}\,(1-\hat{\eta}_j) + \hat{v}(i,j)\Big] \qquad (22)$$

The $\hat{h}^{\pm}_{\sigma,\delta}$ equations are similarly reduced.

Freestream conditions are assigned to the column of grid points just ahead of the leading edge and to the grid points at $\hat{\eta}=1$. Equation (20) is used to solve $\hat{g}^{-}_{\sigma,\delta}(i,j)$ for $i > 0$ and $0 \leq j < m$. The resulting values of $\hat{g}^{-}_{\sigma,\delta}(i,j=0)$ are integrated to apply the condition of no normal mass flux at $\hat{\eta}=0$, Equation (18). This yields $\hat{n}_w$, which in turn generates values of

$\hat{g}^{+}_{\sigma,\delta}(i,j=0)$, Equation (17-e). Starting with these values of $\hat{g}^{+}_{\sigma,\delta}(i,j=0)$, Equation (22) is used to generate $\hat{g}^{+}_{\sigma,\delta}(i,j)$ for $0 < j < m$. The $\hat{h}^{\pm}_{\sigma,\delta}$ equation is similarly solved.

The equilibrium distribution function values, $\hat{G}^{\pm}_{\sigma,\delta}$ and $\hat{H}^{\pm}_{\sigma,\delta}$, are all determined from moments of the previous iterate. The zeroeth iterate at $\hat{x}$ station i is the station i-1 solution. This yields a system of 2n x 2n nonlinear algebraic equations with 2n x 2n unknowns ($\hat{g}_{\sigma,\delta}$ and $\hat{h}_{\sigma,\delta}$, $\sigma = -n,\ldots,-1,1,\ldots,n$, $\delta = -n,\ldots,-1,1,\ldots,n$) which is solved by the method of successive approximations. Convergence is assumed to have occurred when the difference between successive iterates at a particular $\hat{x}$ station is $\leq 10^{-4}$. Normally three iterations are required.

A Burroughs B-5500 digital computer was used for the calculations. The "odd" equally spaced quadrature with $n = 4$ was used for both the $\hat{v}_x$ and $\hat{v}_y$ integrations. The grid size in the physical $\hat{\eta}$ space was taken to be $\Delta\hat{\eta} = 0.033$ (30 space steps), and the grid size in the $\hat{x}$ space was chosen to be $\Delta\hat{x} = 2$ for $-2 \leq \hat{x} \leq 50$ ($Re_x < 125$) and $\Delta\hat{x} = 10$ thereafter. The resulting required computer storage was 25,000 words for the distribution function alone (storing values at two $\hat{x}$ stations). This requirement, along with the rest of the computer program, presses the entire B-5500 storage capability. Because of this storage problem, no smaller grid size could be applied and no larger order of quadrature could be used. Therefore, convergence was checked by comparing the difference of successive iterates and by showing the Gauss-Seidel eigenvalue, $\lambda_{G.S.}$, to be less than one, a necessary and sufficient condition for convergence [65]. The approximate value for $\lambda_{G.S.}$ was found to be ≤ 0.2 (See Appendix B).

The constant "a" in Equation (15) serves as a "stretching factor"

and was chosen to be a = 0.01.

The viscosity-temperature exponent in Equation (8) was taken to be S = 0.816, which is the value for Argon, a monatomic gas, and thus representative of the BBGK equation.

The Chapman-Rubesin constant, C, used only in the calculation of the plotting parameter, $\overline{V}_{\infty,x}$, was chosen to be unity.

The free stream Mach number was chosen to be $M_\infty = 1.5$ in order to achieve reasonable accuracy with the n = 4 quadrature. All the flow phenomena of interest in the leading edge problem are exhibited at this Mach number.

Results

As the distribution function was determined at successive stations down the plate, all macroscopic moments of interest were obtained by applying the same quadrature used to solve the governing equations. The density, tangential velocity, normal velocity, temperature, pressure, shear stress, and normal heat flux were all computed according to Equations (6). A complete presentation of all the macroscopic and microscopic phenomena of interest occurring in the leading edge problem for $M_\infty = 1.5$ is offered in the following sections.

Density Profiles

The density profiles at several $\hat{x}$ stations for $\hat{T}_w = 1.0$ are illustrated in Figure 17. An inspection of the various density profiles reveals the distinctive characteristics pertaining to each of the various flow regimes. At $\hat{x} = 0$ the results of near-free molecular phenomena are identified by an initial deflection of molecules away from the plate. By the time transition occurs, i.e., $0 \leq \hat{x} \leq 10$, the density profile assumes a new

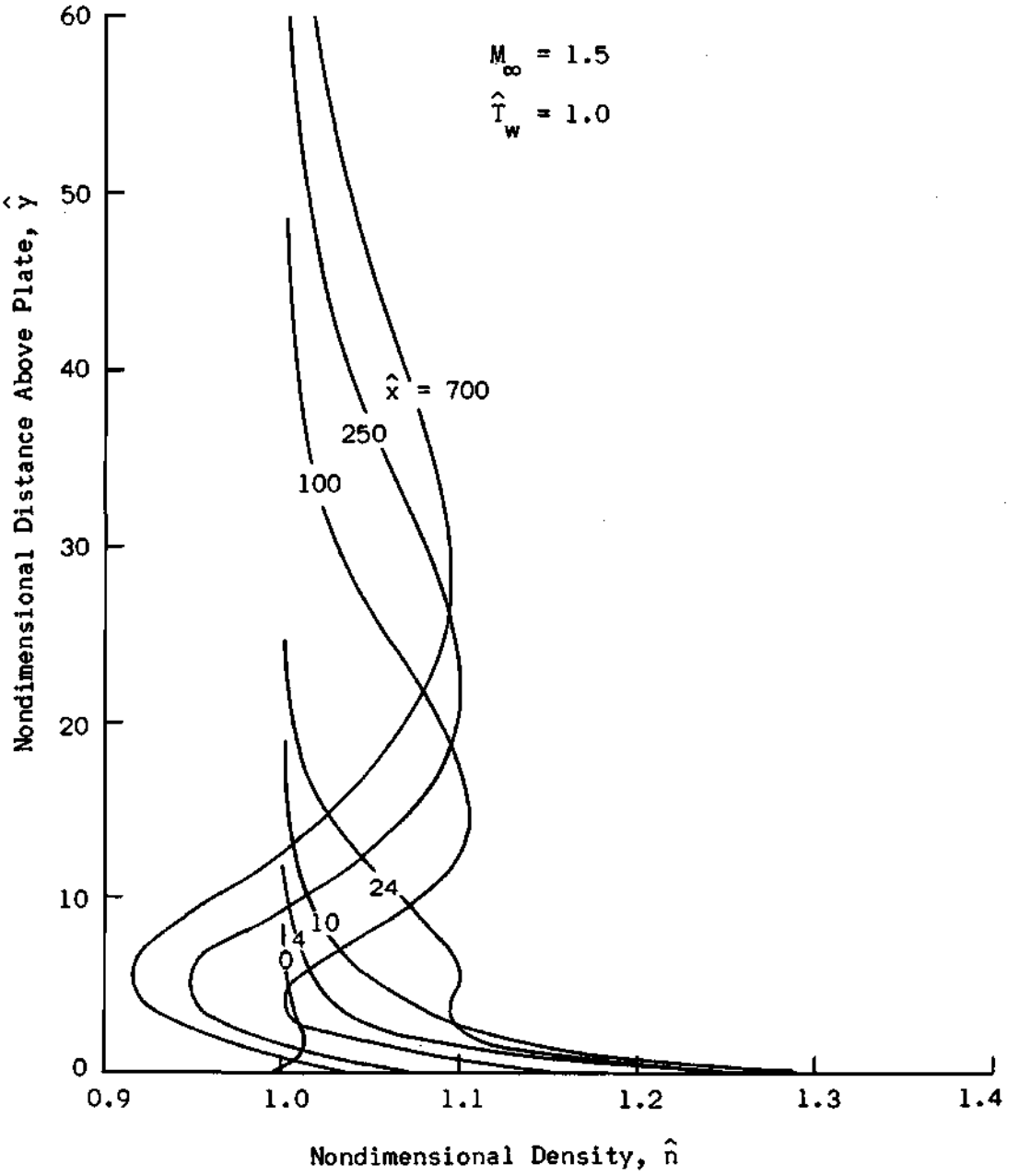

Figure 17. Flat Plate Density Profiles for $\hat{T}_w = 1.0$.

character. By definition, the transition regime is where surface-molecule and molecule-molecule collisions become equally important. This is demonstrated by the fact that the gas has tried to adjust itself to the wall velocity and temperature. This sudden recovery is felt only very near the surface because of the still limited molecule-molecule communication. This adjustment causes the density profile to change slope within a few mean free paths of the wall (see Figure 17, $\hat{x} = 4$ and $\hat{x} = 10$). When the gas has traveled farther down the plate, a change from "transition" to "merged" character becomes evident. By this time the molecule-molecule collisions have begun to dominate the flow description, and the effects of the wall are perturbed into the free stream in the form of a shock wave. The density profile at $\hat{x} = 24$ clearly exhibits the initial formation of the shock wave which eventually emerges from the boundary layer as a well-defined shock structure profile for larger $\hat{x}$. The density profiles for $\hat{x} = 100$, 250, and 700 demonstrate the final formation of similar profiles which are normally associated with classical continuum boundary layer theory.

The density profiles for $\hat{T}_w = 1.5$ are presented in Figure 18. The effect of the hot wall on the density is felt strongly within the boundary layer where the profiles vary significantly from those for the cold wall solution, $\hat{T}_w = 1$, in Figure 17. It is interesting to note, however, that the shock wave portion of the profiles is not significantly influenced by the plate temperature.

The solution of the shock structure profiles from the Navier-Stokes equations by Gilbarg and Paolucci [66] and from the BBGK equation by Liepmann, et.al. [64] predict a shock thickness on the order of ten mean paths for a free stream Mach number, $M_\infty = 1.5$. Their results also show

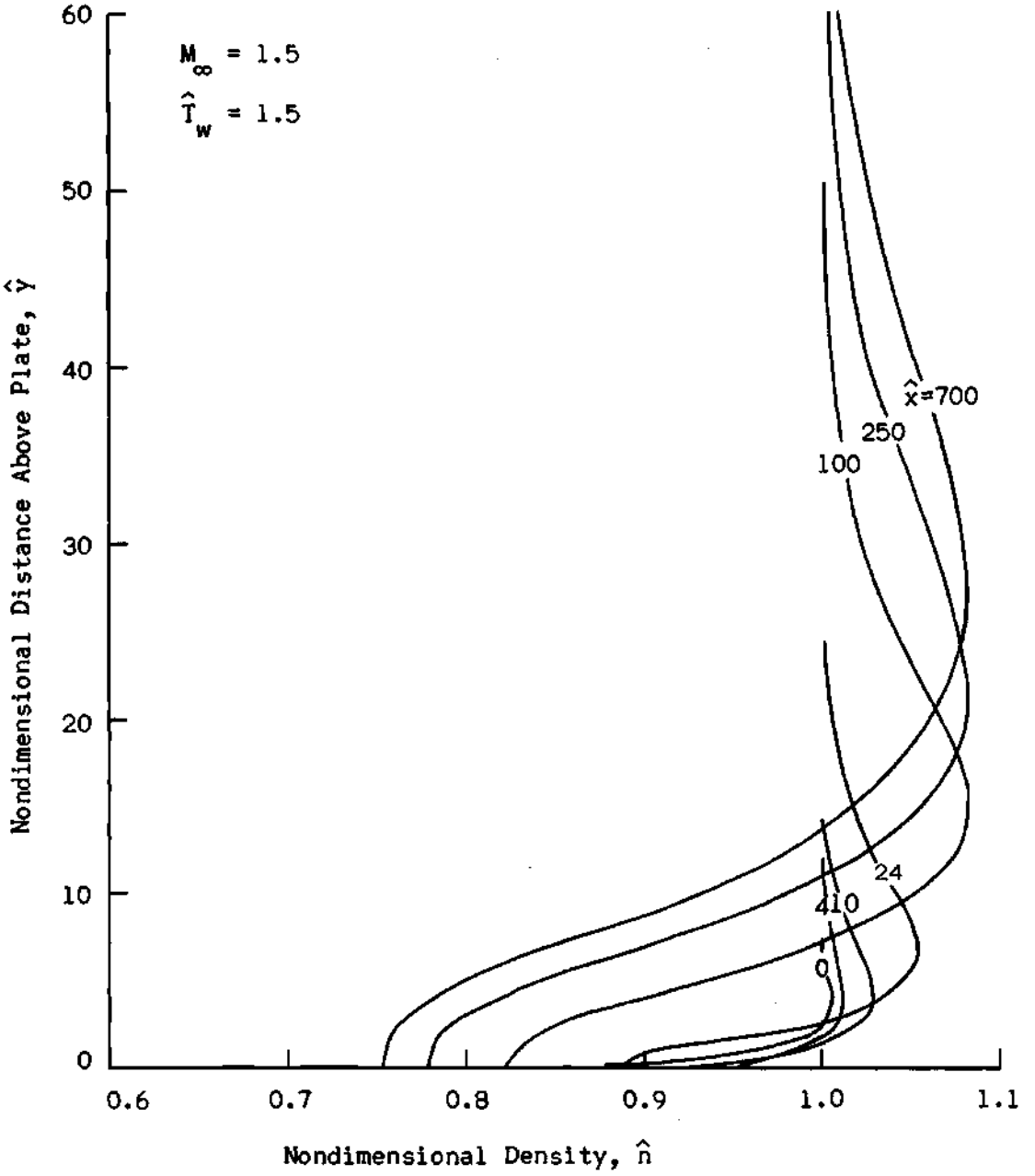

Figure 18. Flat Plate Density Profiles for $\hat{T}_w$ = 1.5.

the shock becoming thicker as the shock wave gets weaker. This agrees well with the present solution as can be seen from the density profiles, Figures 17 and 18.

Tangential Velocity Profiles

Figure 19 illustrates the variation of the tangential velocity profiles along the plate. The velocity profiles are much as would be expected. For $\hat{x} = 0$ the boundary layer is very thin and slip at the wall is very pronounced. A very rapid recovery of the velocity slip at the wall is demonstrated by the $\hat{x} = 4$ and 10 profiles with the slip becoming negligible for $\hat{x} \geq 100$. A more detailed discussion of the velocity slip decay is deferred to a later section. Also obvious in Figure 19 is the steady growth of the boundary layer thickness while the tangential velocity profiles remain similar.

The tangential velocity profiles for $\hat{T}_w = 1.5$ are presented in Figure 20. These profiles are essentially the same as the cold wall results in Figure 19, differing primarily in slip at the wall. A more complete discussion of the wall temperature effects on the slip velocity is deferred to a later section.

Normal Velocity Profiles

Figure 21 illustrates the variation of the normal velocity profiles along the plate for $\hat{T}_w = 1.0$. These profiles demonstrate the formation of the shock wave as do the density profiles in Figure 17. At small $\hat{x}$ stations (from $\hat{x} = 0$ to 20), the shock wave is more clearly defined from the normal velocity profiles than it is from the density profiles. This has also been experimentally observed by Laurmann [45]. The strength of the shock wave is seen to grow from the leading edge through the kinetic and transition regimes.

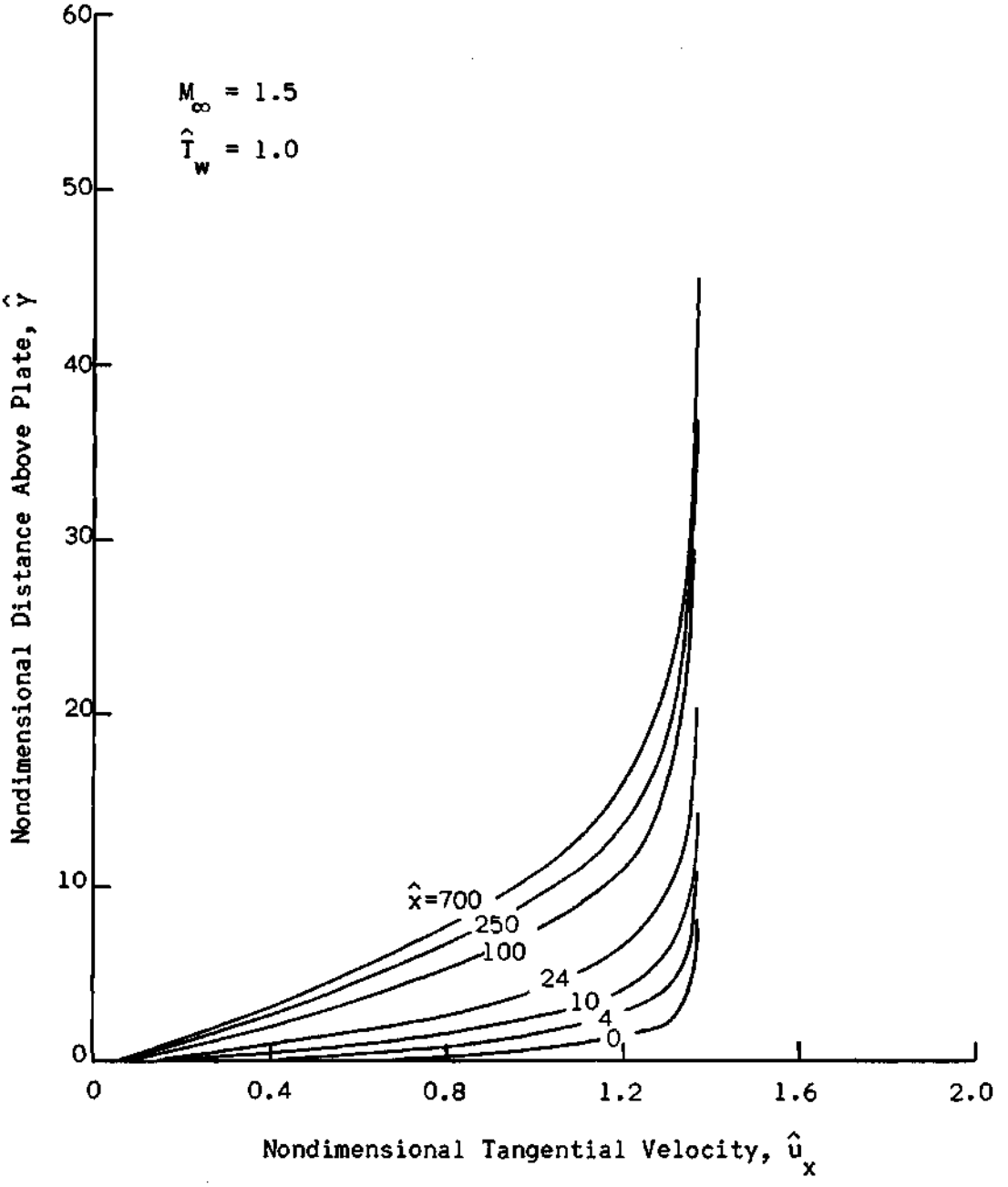

Figure 19. Flat Plate Tangential Velocity Profiles for $\hat{T}_w$ = 1.0.

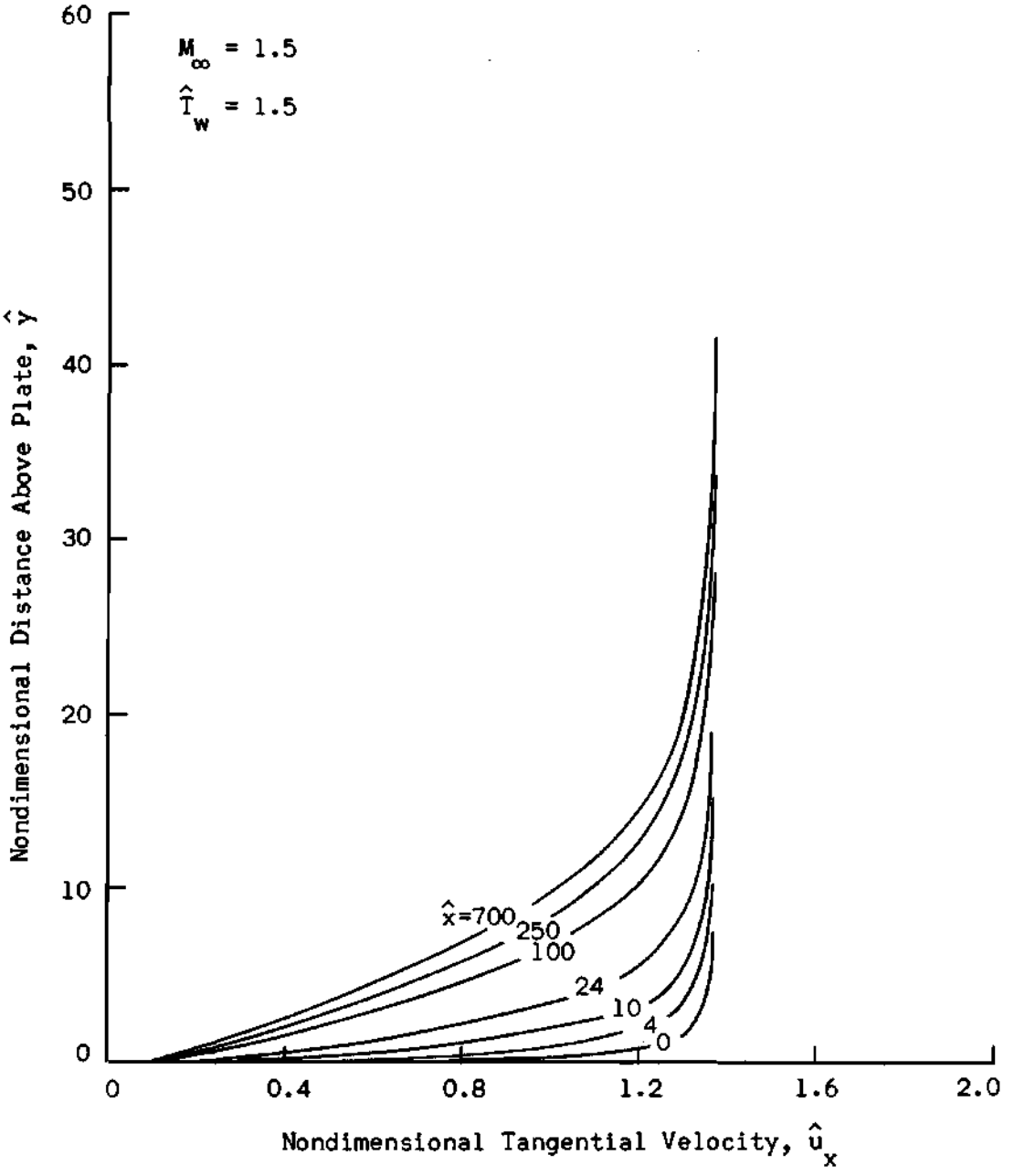

Figure 20. Flat Plate Tangential Velocity Profiles for $\hat{T}_w$ = 1.5.

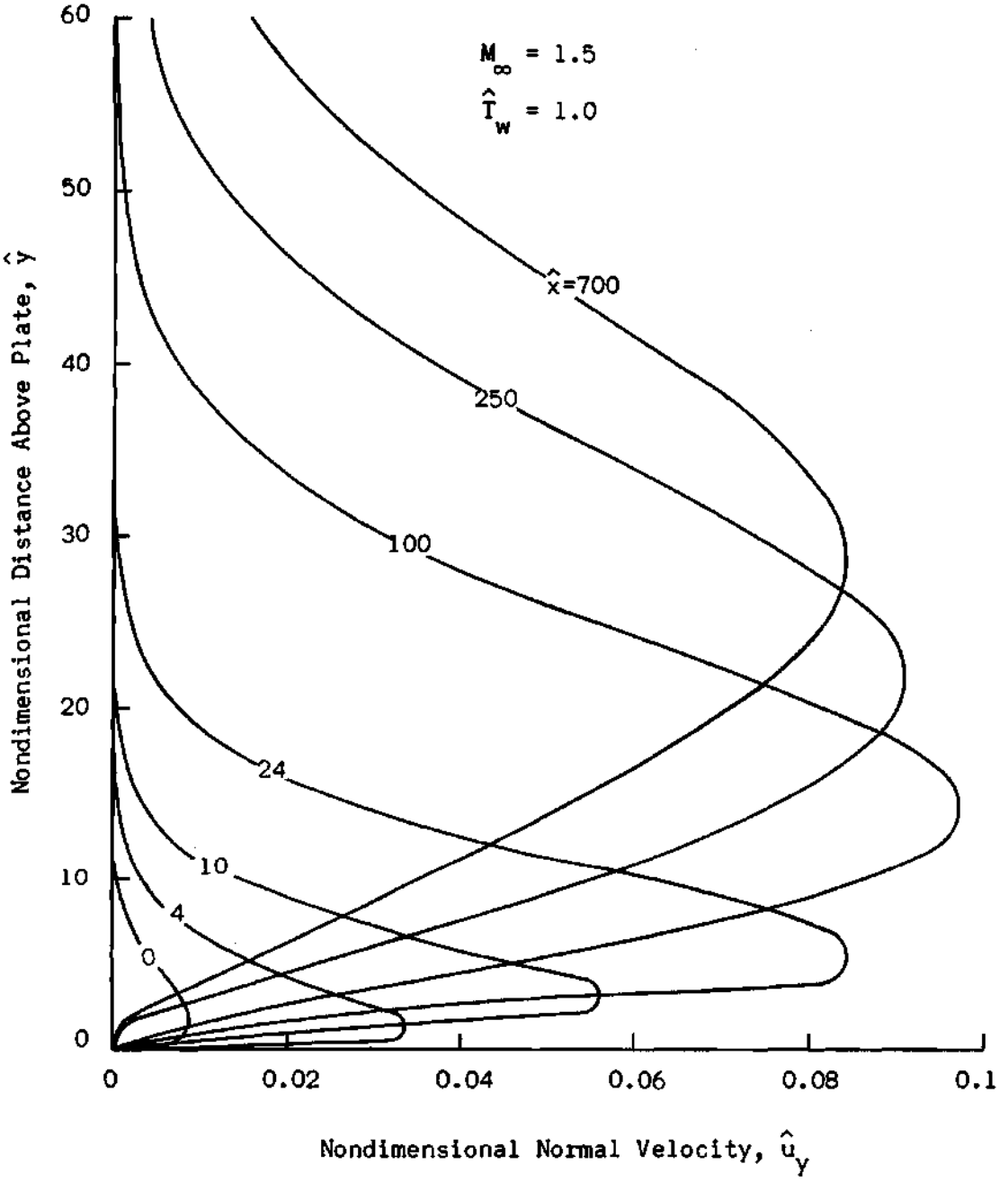

Figure 21. Flat Plate Normal Velocity Profiles for $\hat{T}_w$ = 1.0.

By $\hat{x} = 100$ the influence of continuum mechanics dominates the flow description, as evidenced by the negligible slip at the wall. Accordingly the shock wave has achieved maximum strength. For $\hat{x} > 100$ the shock wave remains fairly constant in strength as it propagates outward from the plate.

The normal velocity profiles for $\hat{T}_w = 1.5$ are presented in Figure 22. These solutions also exhibit the characteristics described above.

Temperature Profiles

The character of the temperature profiles for $\hat{T}_w = 1.0$ is demonstrated in Figure 23. These profiles also indicate the various flow regimes described above. At $\hat{x} = 0$ the effect of wall temperature is propagated into the free stream in the same manner as is the wall velocity. This is as expected because the gas temperature there is strongly influenced by the kinetic energy loss of the free stream due to decreased tangential velocity. The effect of the wall temperature is not yet strongly felt because of the negligible molecule-molecule communication. However, as molecule-molecule collisions become more numerous the gas adjacent to the wall begins to adjust itself to the wall conditions. This is illustrated by the $\hat{x} = 4$ and $\hat{x} = 10$ temperature profiles. Farther down the plate ($\hat{x} \geq 100$) the temperature profiles assume a distinct cold wall boundary layer character with the shock wave emerging into the free stream.

The temperature profiles for $\hat{T}_w = 1.5$ are presented in Figure 24. As is the case with the density profiles in Figures 17 and 18, the effect of increased wall temperature is felt strongly within the boundary layer but does not significantly affect the upper portion of the temperature profiles.

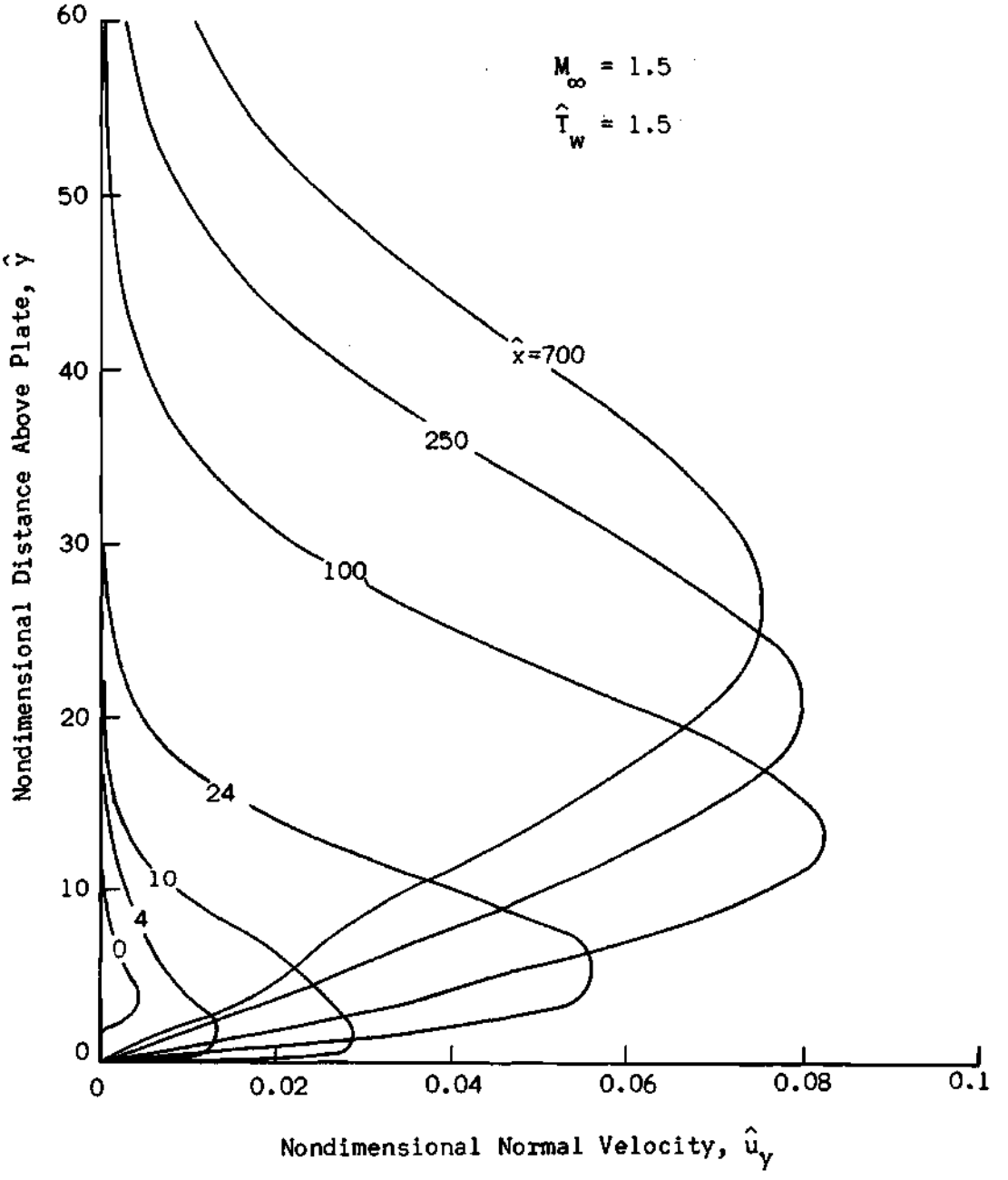

Figure 22. Flat Plate Normal Velocity Profiles for $\hat{T}_w$ = 1.5.

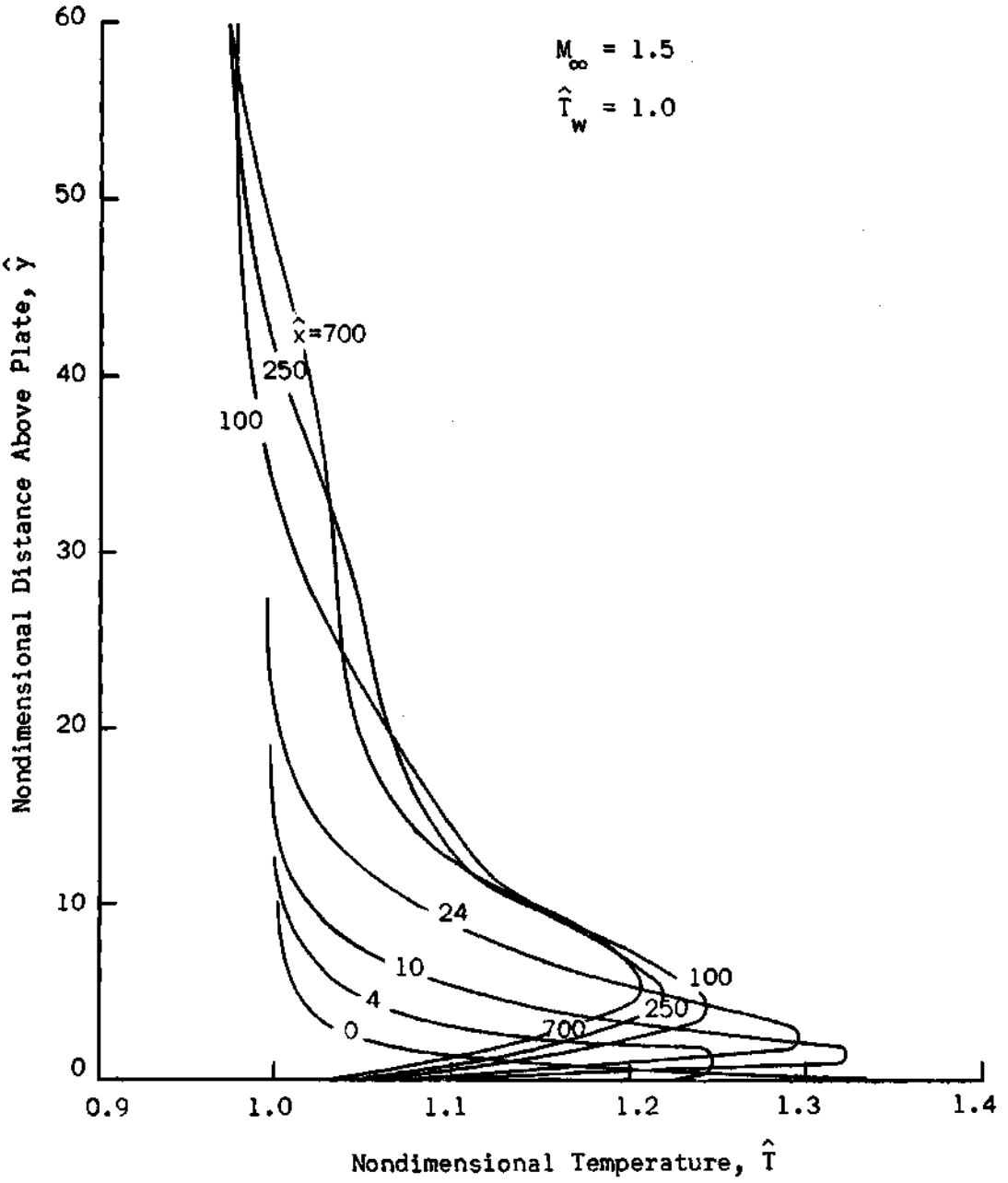

Figure 23. Flat Plate Temperature Profiles for $\hat{T}_w$ = 1.0.

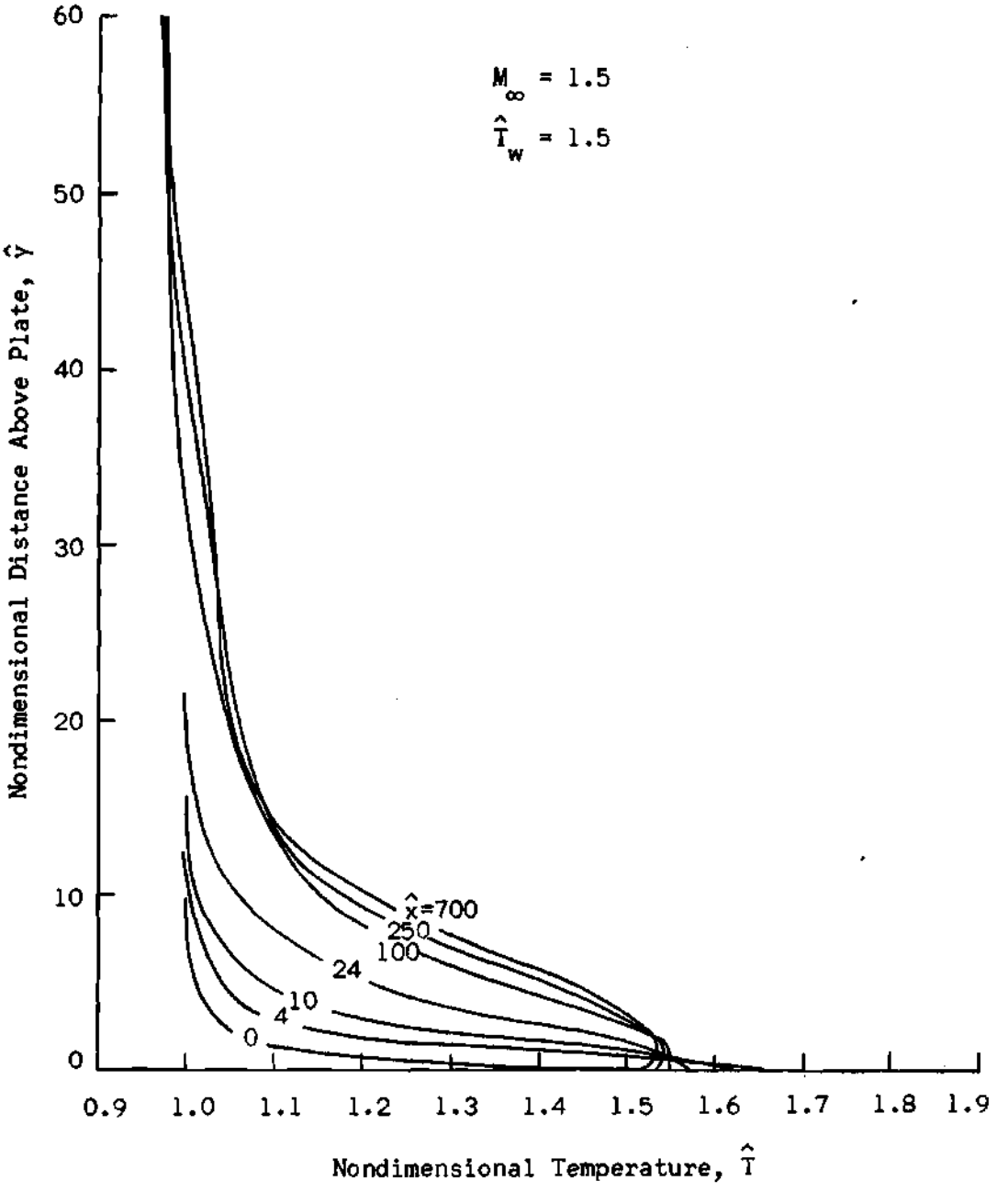

Figure 24. Flat Plate Temperature Profiles for $\hat{T}_w$ = 1.5.

Pressure Profiles

Figure 25 illustrates the associated pressure profiles for $\hat{T}_w = 1.0$. These pressure profiles exhibit the formation of an initial pressure pulse and its subsequent decay to a near-constant boundary layer pressure profile associated with classical boundary layer theory.

The pressure profiles for $\hat{T}_w = 1.5$ are presented in Figure 26. It is interesting to note that even though the density and temperature profiles within the boundary layer are significantly influenced by different wall temperatures, the pressure is not appreciably altered.

Shock Front Position

The position of the shock front as a function of distance from the leading edge is presented in Figure 27. The shock front position was taken to be the outermost disturbance exhibited by the normal velocity data. This corresponds to the normal velocity having decayed to slightly less than one per cent of its maximum value.* The shock angle approaches an almost constant value after about twenty mean free paths from the leading edge. The classical solution for the Mach line of a flow with $M_\infty = 1.5$ is $\alpha = \sin^{-1}\left(\frac{1}{M_\infty}\right) = 41.8°$. The present solution yields a shock wave angle close to 38° for large $\hat{x}$. The trend of the present results agrees with

*This definition of the shock front is consistant with Butler's interpretation of his numerical data [60]. The "maximum-slope" definition of the shock center used by several authors is not a suitable choice of reference, as pointed out by Liepmann, et.al. [63]. They demonstrate that the shock wave profile is not symmetrical and that the upstream, or low-density, side of the shock wave profile is elongated, thus causing the true shock wave "center" to be moved upstream. The location of the shock wave center then becomes arbitrary and somewhat misleading. A more suitable indication of the position of the shock front is to predict the extension of its influence as one would predict the edge of the boundary layer. This is the scheme used in the present investigation.

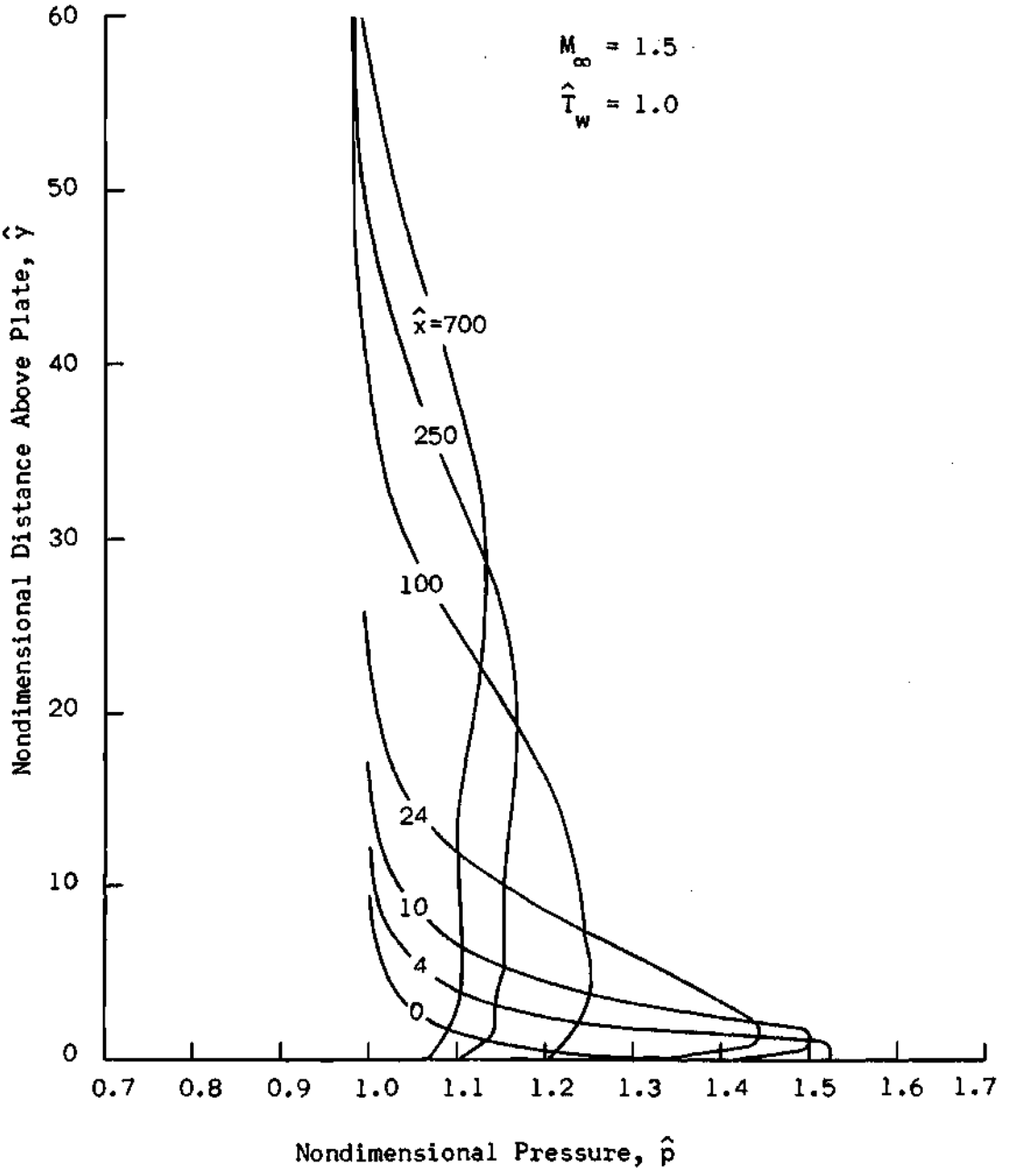

Figure 25. Flat Plate Pressure Profiles for $\hat{T}_w$ = 1.0.

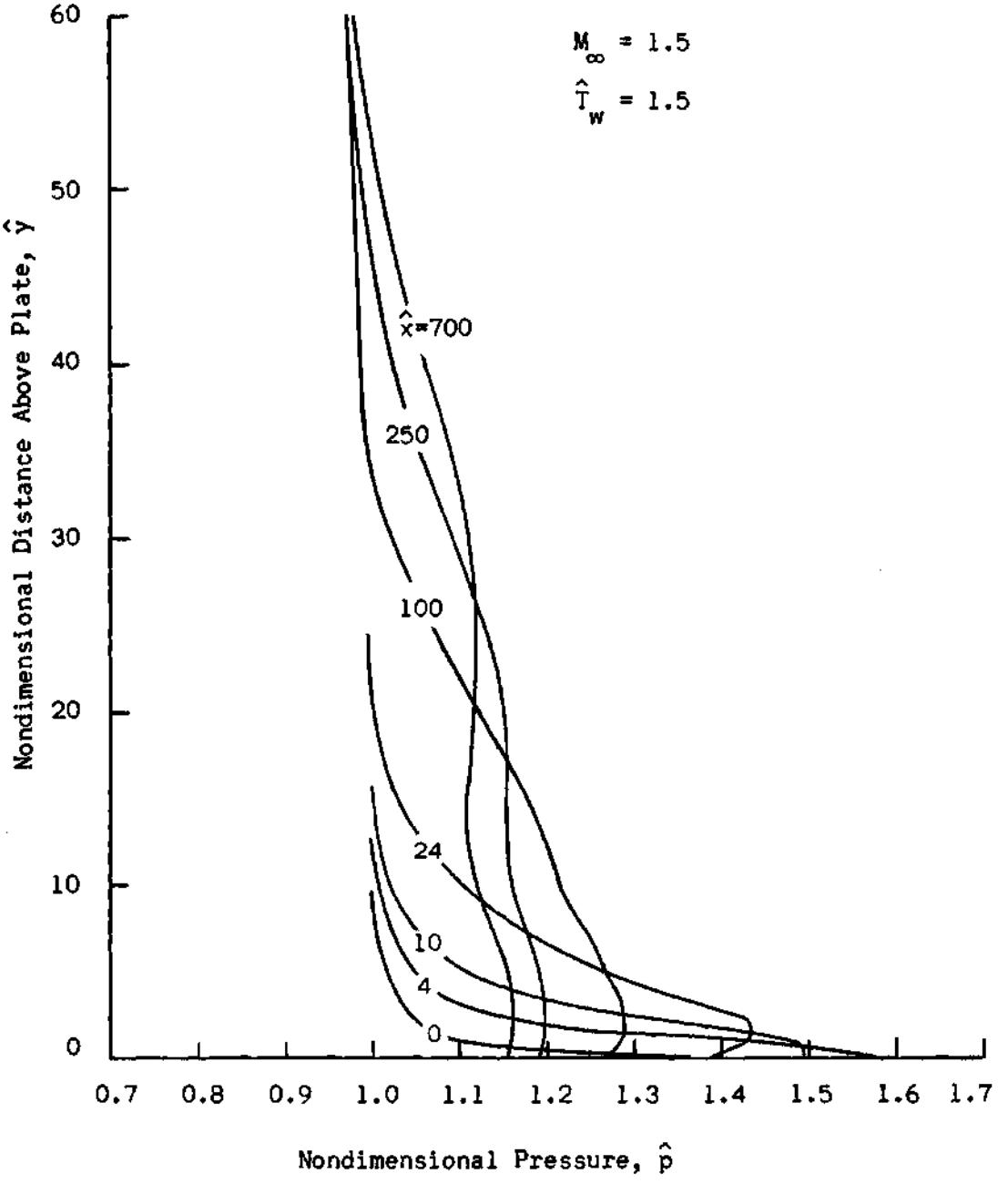

Figure 26. Flat Plate Pressure Profiles for $\hat{T}_w$ = 1.5.

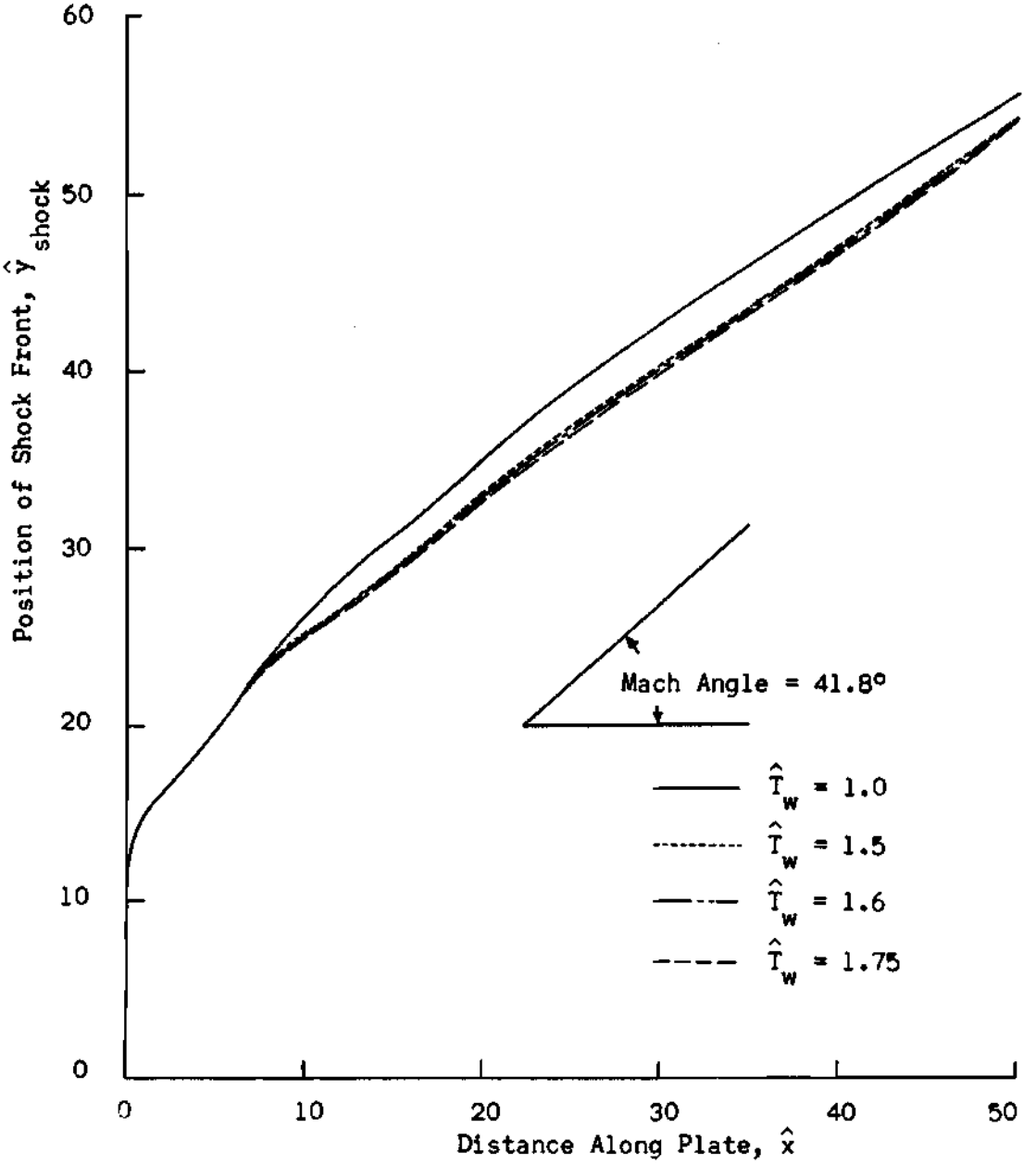

Figure 27. Position of Shock Front.

Butler's numerical solution of the Navier-Stokes equations [60] which shows that by introducing velocity slip and temperature jump at the wall, the shock angle is reduced.

The influence of different wall temperatures on the shock front position is also illustrated in Figure 27. The results indicate that for a hotter plate the increased slip coupled with the other hot plate effects merely causes a very slight downstream shift in the shock position, but does not significantly alter the final shock front angle.

Surface Pressure

Experimental and theoretical studies of surface pressure distributions are numerous in the literature. However, as pointed out by Becker and Boylan [48], there is considerable disagreement between various experimental investigations. In order to achieve experimental results in the transition regime, investigations were limited to $M_\infty > 4$, since the physical length of this region is proportional to the Mach number. No experimental results in the transition regime are available for Mach numbers of the order of the present investigation. Comparisons of the present pressure calculations with recent experimental transition regime results at moderate Mach numbers, $M_\infty = 4.1$, 9.19, and 10.15, by Becker and Boylan [48], and $M_\infty = 5.5$ by Moulic [40] are presented in Figure 28. Also presented is the second order weak interaction theory of Hayes and Probstein [43]

$$C_p = 2\left[\frac{A}{M_\infty^2} \frac{T_w}{T_\infty} + (\gamma-1)B\right]\bar{V}_{\infty,x} + \frac{(\gamma+1)}{2}\left[\frac{A}{M_\infty^2} \frac{T_w}{T_\infty} + (\gamma-1)B\right]^2 M_\infty^2 \bar{V}_{\infty,x}^2 \tag{23}$$

where $A = 0.865$ and $B = 0.166$ for $\gamma = 5/3$ and $Pr = 1$. The interaction

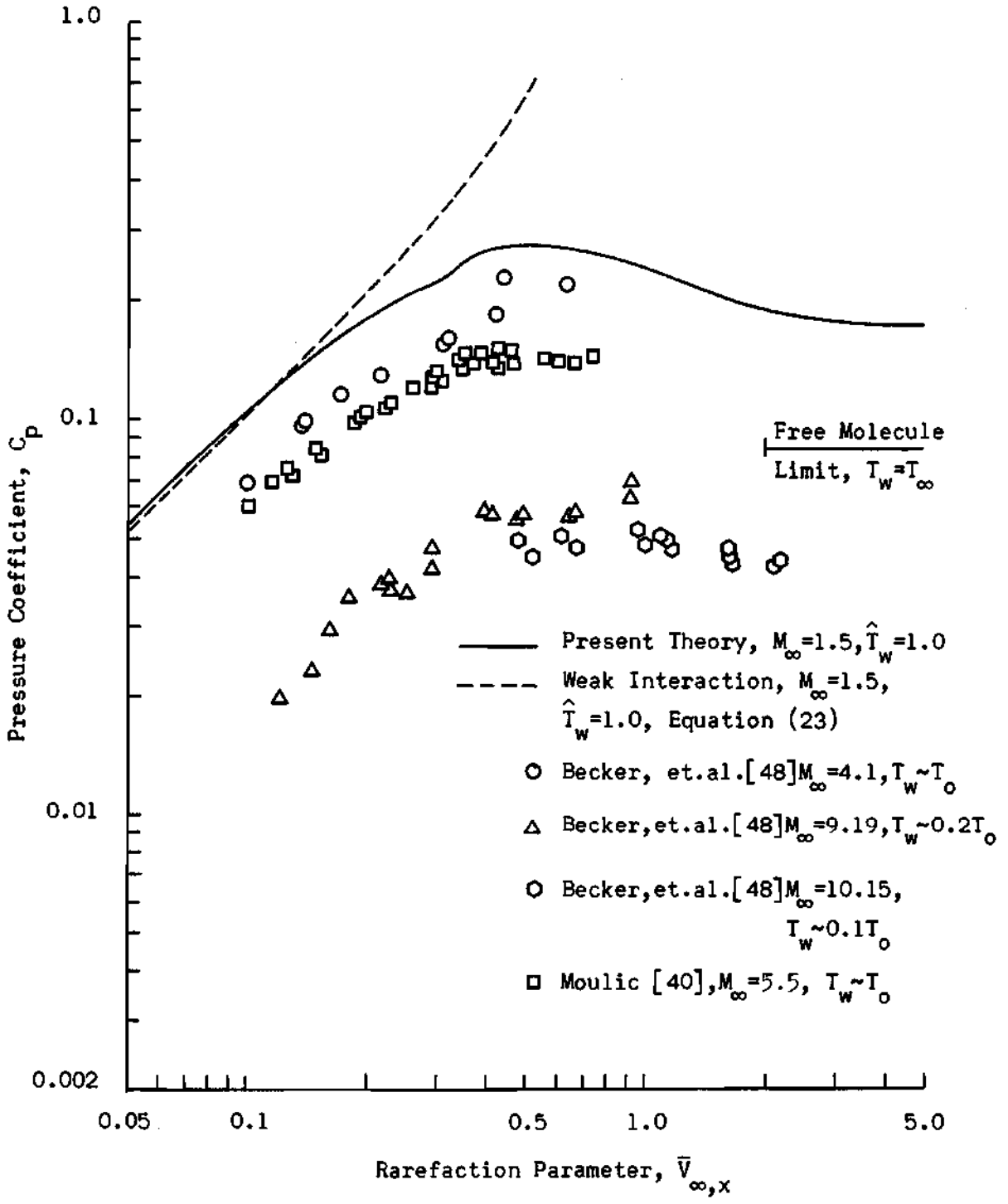

Figure 28. Surface Pressure Coefficient.

theories are considered inadequate for $\bar{V}_{\infty,x} \geq 0.15$ and, in fact, strong interaction effects do not significantly influence the flow description unless $M_\infty \geq 8$ [48]. Thus far, there are no theoretical predictions for pressure variations sufficiently near the leading edge at nominal Mach numbers.

The present results are indeed interesting because of their qualitative agreement with available experimental data at nominal Mach numbers and their excellent agreement for $\bar{V}_{\infty,x} \leq 0.15$ with the weak interaction theory of Hayes and Probstein [43]. The pressure plateau noted by several experimental investigators [47,48,49] is confirmed and, in fact, occurs in the transition range of the rarefaction parameter $0.4 \leq \bar{V}_{\infty,x} \leq 0.6$ as pointed out by Becker and Boylan [48] and by Moulic [40]. An obvious trend exhibited by the pressure coefficient results in Figure 28 is a steady increase in the maximum pressure coefficient as the Mach number decreases.

Also presented in Figure 28 is the free molecular limit for $T_w = T_o$. The present results, although exhibiting a negative pressure gradient in the kinetic region as predicted by the near-free molecular theory of Kogan [62], do not decrease to the free molecular solution at the leading edge. The recent theoretical results of Kogan [62] and of Bird [63] indicate that such a result is reasonable.

The effect of wall temperature on the pressure coefficient is illustrated in Figure 29. The plate temperature values vary from the cold plate configuration, $\hat{T}_w = 1$, to a hot plate configuration, $\hat{T}_w = 1.75$. The change in wall temperature does not alter the characteristic of the pressure distribution and only changes the magnitude of the pressure slightly. This

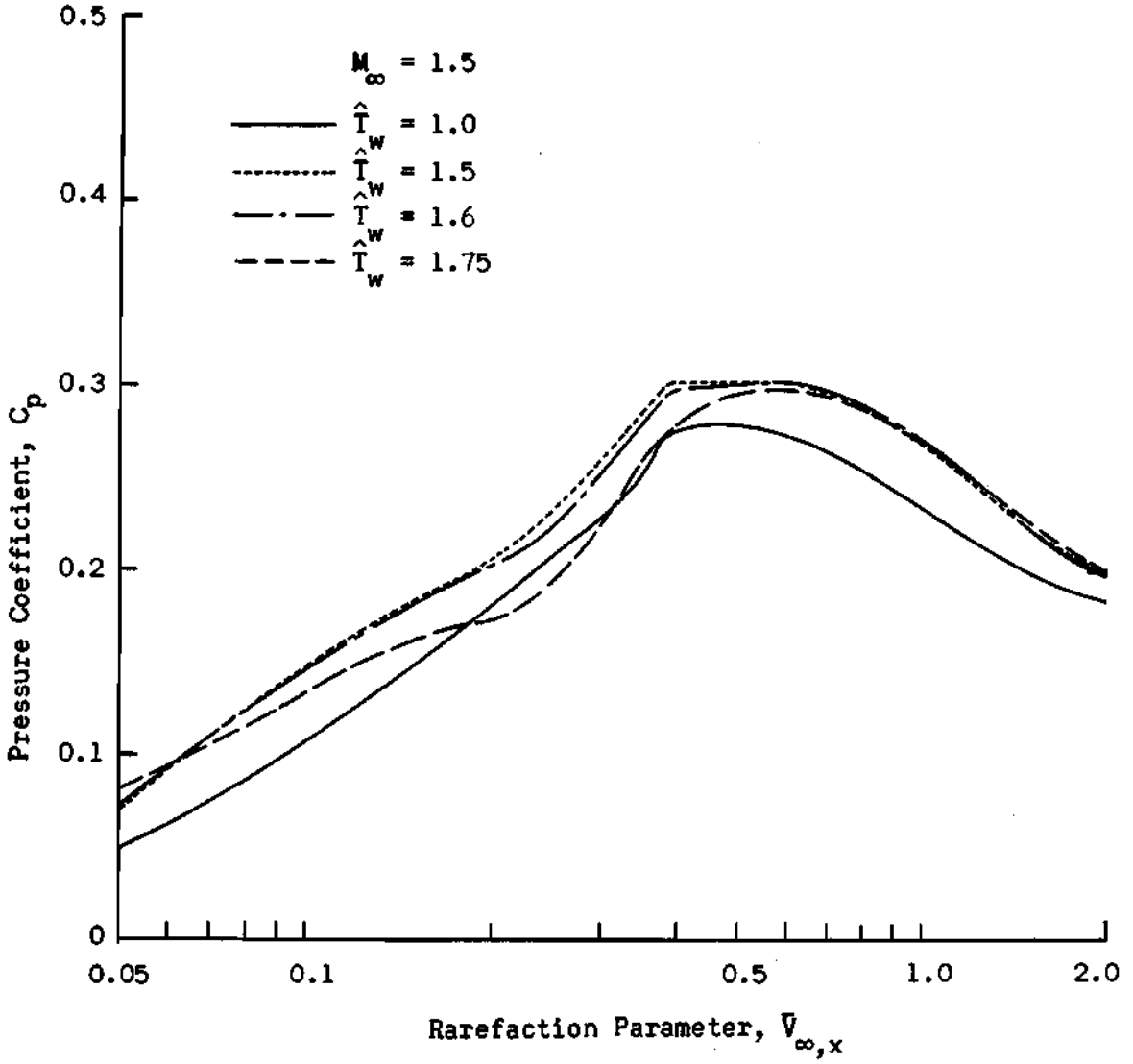

Figure 29. Effect of Plate Temperature on Surface Pressure.

conclusion agrees with Butler's numerical continuum solution [60], although his results do not extend beyond $\bar{V}_{\infty,x} > 0.6$. The fact that the pressure curves do not vary significantly for plate temperatures ranging from cold wall conditions to near-adiabatic conditions supports the comparison in Figure 28 with experimental results at different wall temperatures.

Skin Friction

In seeking an understanding of the complex phenomena occurring between the leading edge and the continuum regime, it is desirable to obtain as many corroborating properties as possible. One of these subjects is the behavior of the wall shear stress which was calculated for the present model from Equation (6-e) and is presented in Figure 30 as a function of the rarefaction parameter, $\bar{V}_{\infty,x}$. The solution is compared to the classical boundary layer theory of Blassius [35],

$$C_f = \frac{0.664}{\sqrt{Re_x}} \quad , \tag{24}$$

and to the free molecular limit as presented by Wallace and Burke [51],

$$C_f = \frac{1}{M_\infty^2} \left(\frac{2}{\pi\gamma} \right)^{1/2} \quad . \tag{25}$$

Also presented in Figure 30 are the experimental results of Wallace and Burke [51] and of Moulic [40].

Although the present solution of the flow field beyond $\hat{x} \gtrsim 100$ ($\bar{V}_{\infty,x} < 0.1$) is not expected to be accurate to more than two decimal places, the shear stress results are seen to be in very good qualitative agreement with the weak interaction solution. Continuing toward the leading edge, an

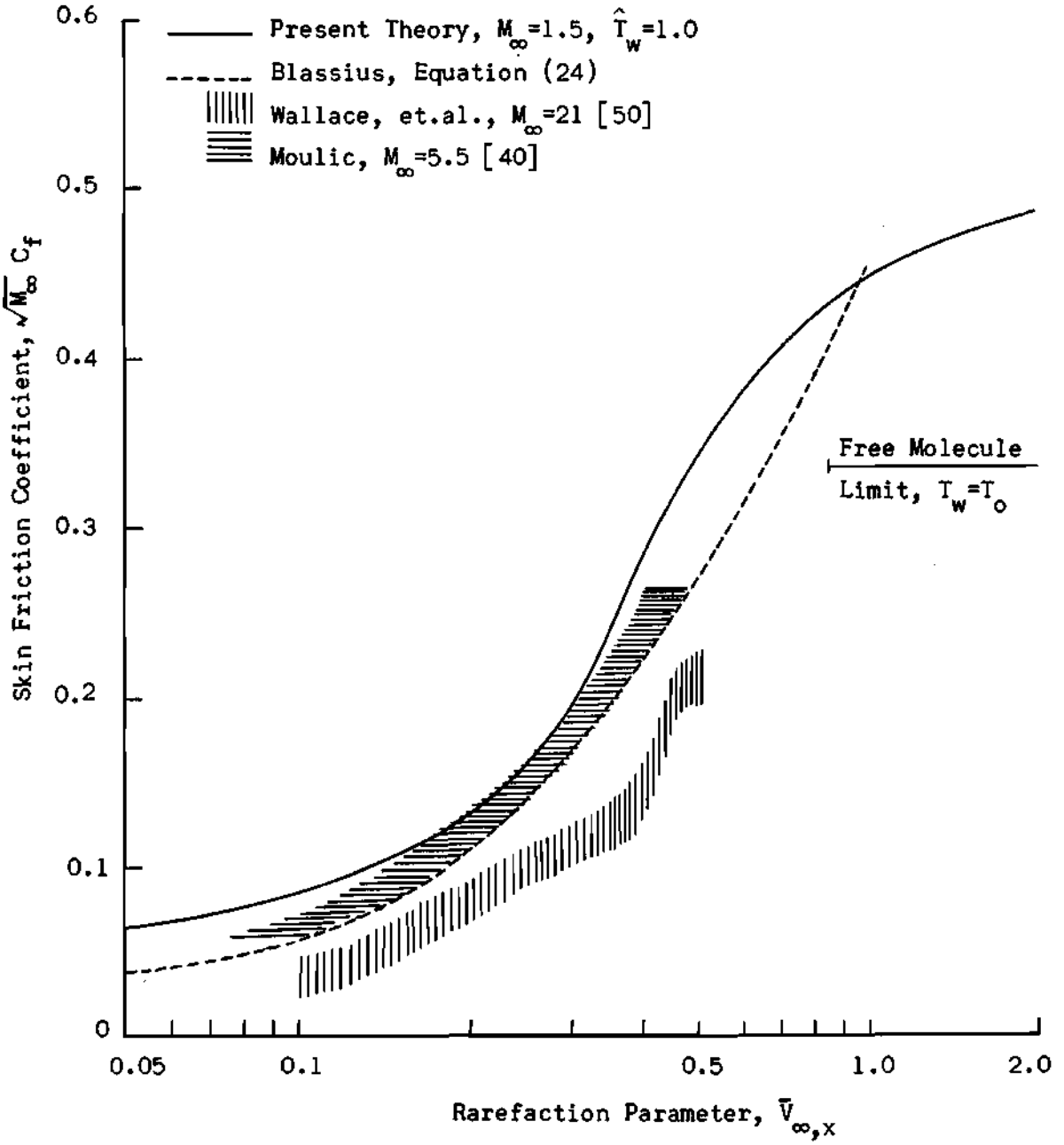

Figure 30. Skin Friction Coefficient.

initial tendency of the shear stress to increase more rapidly is apparent. Finally, as the transition and kinetic regions are traversed, the solution tends toward a near-free molecular value.

This behavior of the shear stress value was, in fact, predicted by Mirels [67] who used the Oseen linearization on the Navier-Stokes equations with a correction for slip, and verified experimentally by Wallace and Burke [51]. The results of Moulic [40] are the only other experimental skin friction data reaching into the transition regime. His results indicate the initial departure from interaction theory but do not attain sufficiently high values of $\bar{V}_{\infty,x}$ to corroborate the beginning of a skin friction plateau as indicated by Wallace and Burke. The present solution does not exhibit a "peak" of maximum skin friction behind the leading edge, but merely a reduction in slope of the skin friction curve as the leading edge is approached.

The effect of different wall temperatures on the surface friction is illustrated in Figure 31. The general character of the skin friction distribution does not change significantly for the temperature range investigated. The weak interaction theory of Li and Nagamatsu [56] predicts an increase in skin friction with increasing plate temperature. For the present case of wall temperature increasing from 1.0 to 1.75, their theory predicts a forty per cent increase in skin friction. The present solution illustrated in Figure 31 exhibits an increase of approximately fifty per cent for $\bar{V}_{\infty,x} < 0.2$ (the interaction regimes). The present solution, however, demonstrates a phenomena previously unattained by other theoretical studies, yet intuitively expected. Namely, the change in character of the skin friction behavior as the kinetic region is entered. Since the kinetic

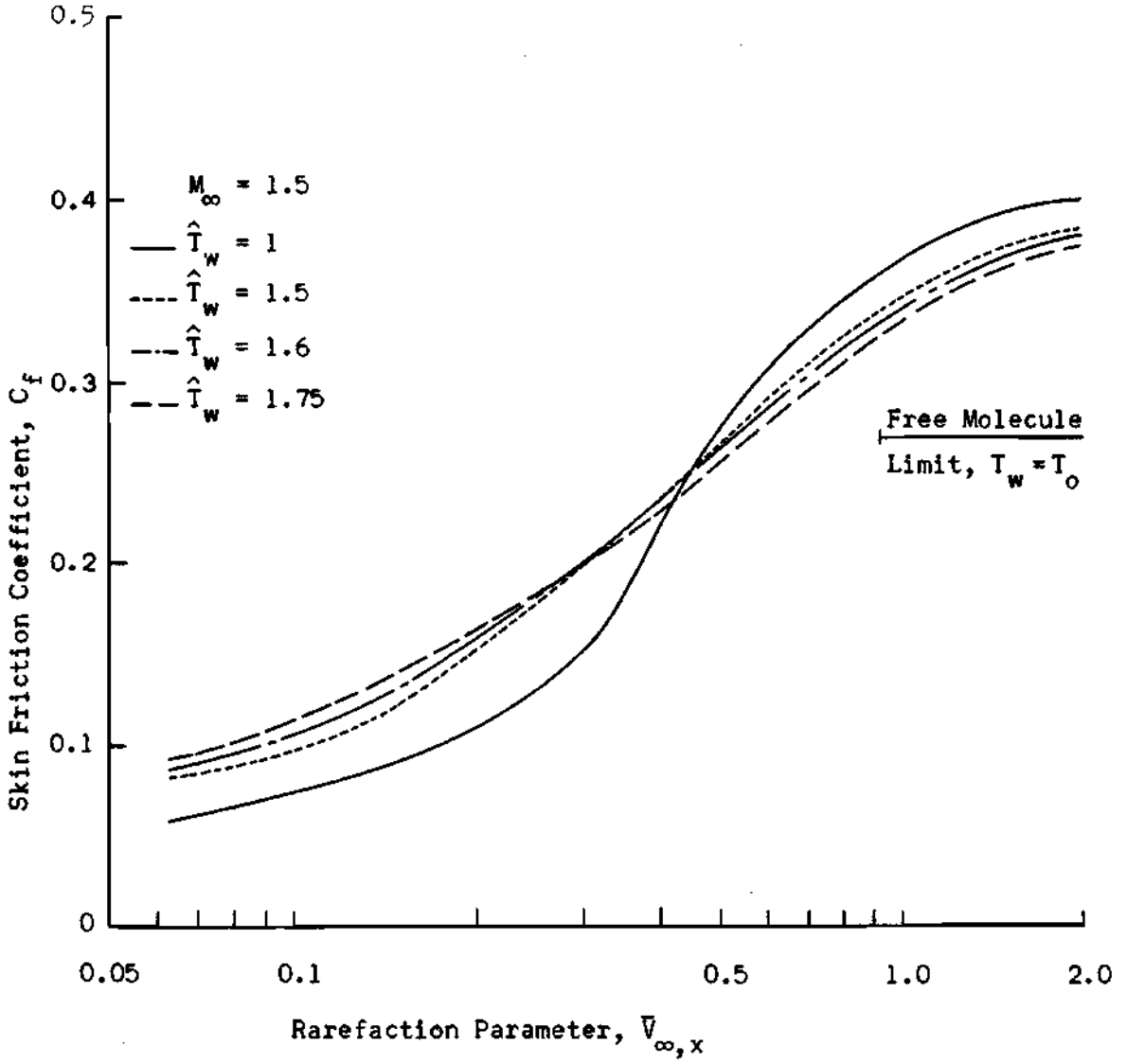

Figure 31. Effect of Plate Temperature on Skin Friction.

region is dominated by slip effects, and since the slip is increased with increasing temperature, one would expect the skin friction to decrease with increasing plate temperature more toward a free molecular value at the leading edge. This phenomenon is exhibited by the present model and perhaps gives a better understanding of the transition regime as well.

Heat Transfer

In order to investigate the heat transfer characteristics of the present theoretical model, a study was made of the temperature profile development and normal heat flux at the plate for several constant wall temperature values. An analysis of these data is used to determine the adiabatic wall temperature associated with the continuum regime.

Figures 32 and 33 illustrate the asymptotic development of the temperature profiles in the gas. The only significant difference in the temperature profiles at $\hat{x} = 100$ and $\hat{x} = 250$ is the growing boundary layer thickness. This then shows the existence of similar profiles in the continuum regime. From continuum analyses, the adiabatic wall condition is obtained when $\left.\frac{dT}{dy}\right|_{y=0} = 0$. Calculations from the data reveal that this condition occurs when $\hat{T}_w \approx 1.62$. Continuum theory predicts an adiabatic wall temperature, $\hat{T}_{aw} = 1.75$ for $M_\infty = 1.5$. The present solution is quite reasonable since the trend of this data indicates an asymptotic approach to a value near the continuum result.

An additional check on the heat transfer characteristics was made by solving the heat flux into the plate from Equation (6-f). These calculations are the least accurate of all the data because they involve integration of a higher order moment. Nevertheless, typical results for the heat transfer coefficient are presented in Figure 34. The solution is

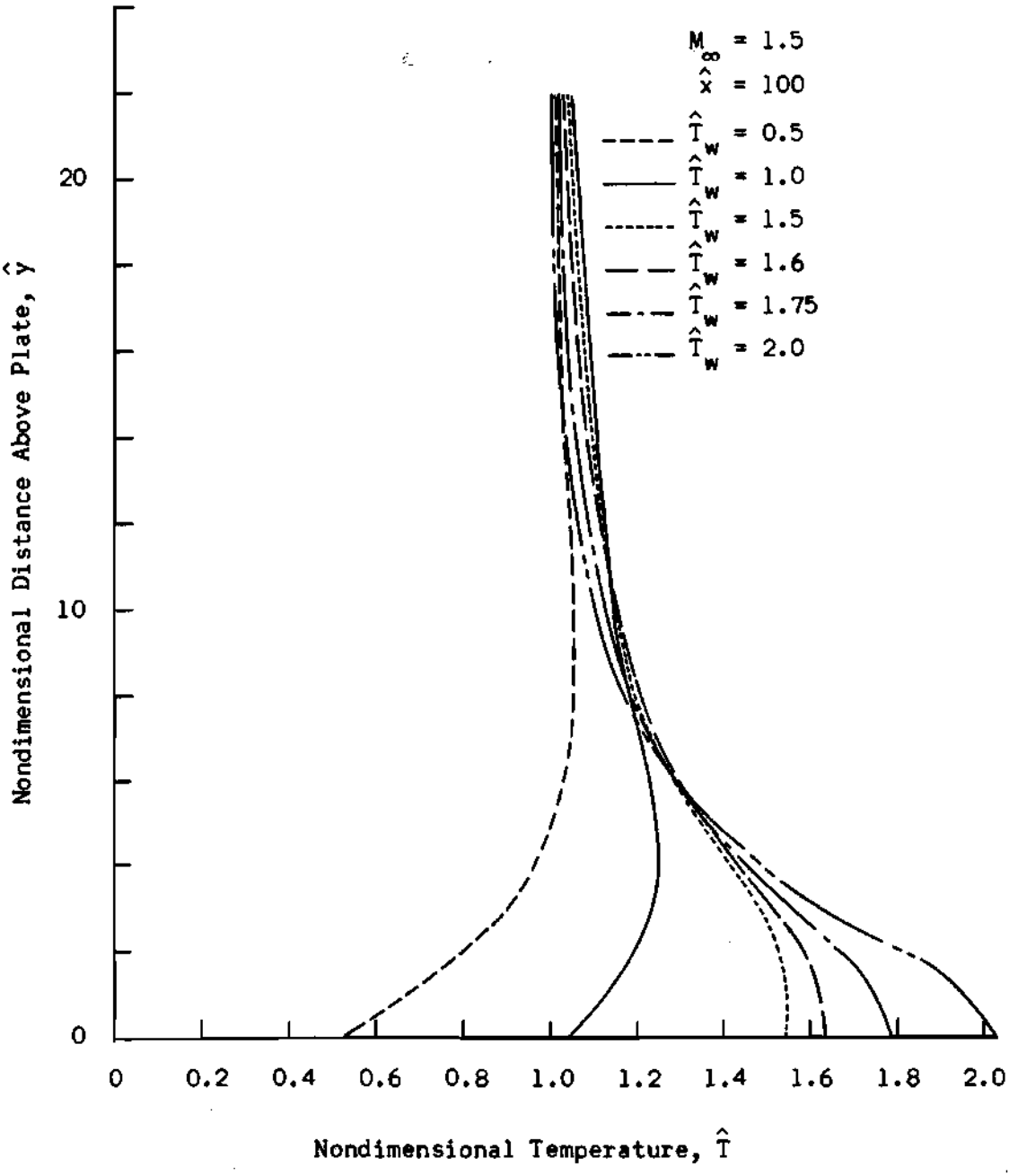

Figure 32. Temperature Profiles for Different Wall Temperatures, $\hat{x}$ = 100.

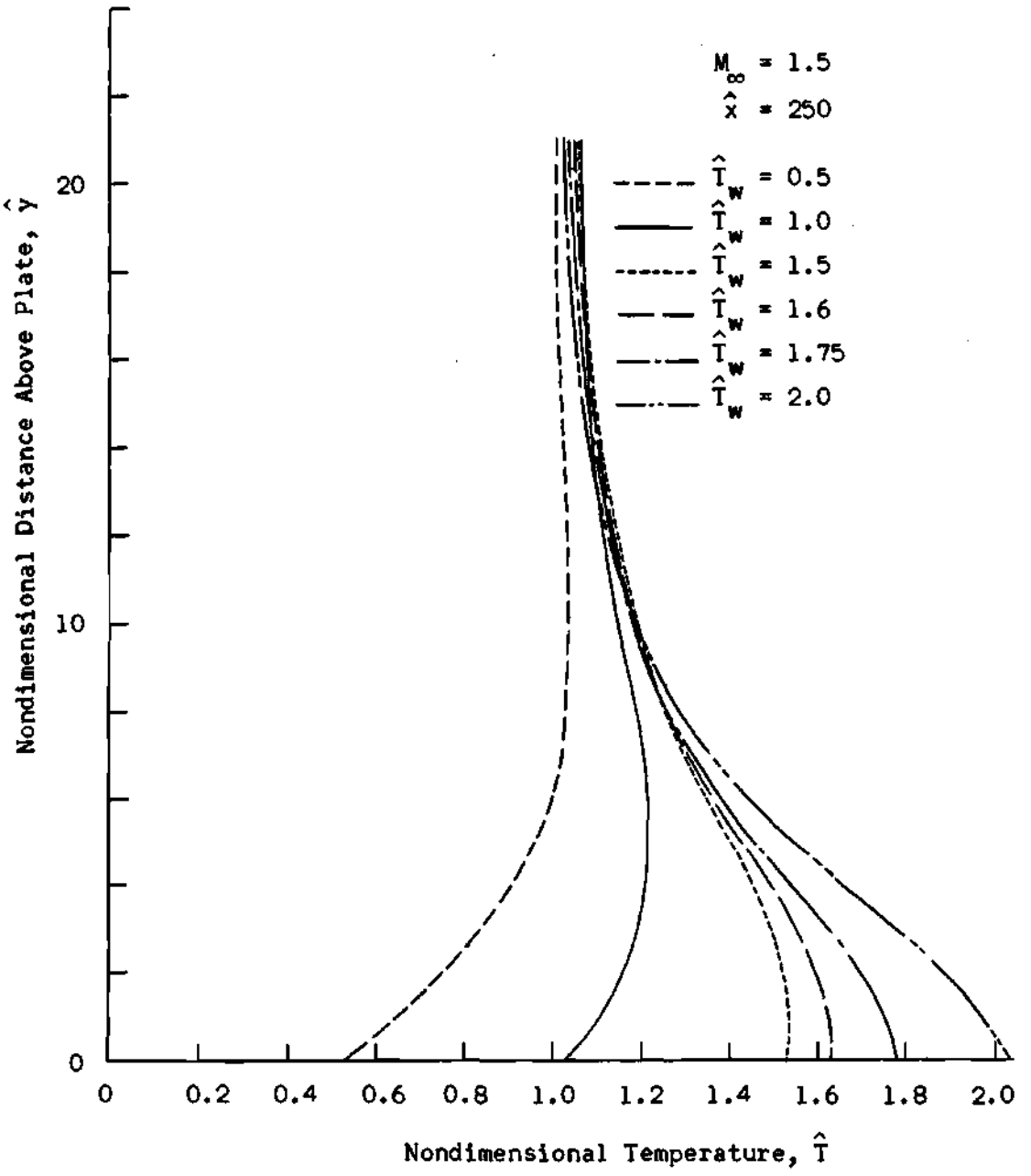

Figure 33. Temperature Profiles for Different Wall Temperatures, $\hat{x}$ = 250.

compared to the results of classical boundary layer theory [35], which gives

$$C_h = \frac{0.332}{\sqrt{Re_x}} \quad , \tag{26}$$

and to predicted results using skin friction data and Reynold's analogy as corrected by Li and Nagamatsu [56], which, for $\gamma = \frac{5}{3}$, is

$$\frac{2C_h}{C_f} = 0.71 \quad . \tag{27}$$

Also presented in Figure 34 for comparison are the experimental results of Nagamatsu, et.al. [47], Wallace and Burke [51], and Vidal and Wittliff [50].

Agreement with the boundary layer theory is quite good for small $\bar{V}_{\infty,x}$, and application of Reynold's analogy, Equation (27), gives excellent results for $\bar{V}_{\infty,x} \leq 0.35$. For positions within the transition and kinetic regions, however, the heat transfer drops sharply below the values predicted by either of the above theories. It is,of course, in this region where interaction theories based on continuum mechanics become invalid. The trend of the present solution agrees with the experimental results of Nagamatsu, et.al. [47], Wallace and Burke [51], and Vidal and Wittliff [50]. All of these experiments were conducted for conditions of $7 < M_\infty < 25$.

Vidal and Wittliff [50] noted that the location of the initial departures from interaction theories could be correlated by a single value of the rarefaction parameter, $\bar{V}_{\infty,x}$. Inspection of the various experimental results as well as the present solution in Figure 34 does reveal this departure to be within a common value of $0.4 \leq \bar{V}_{\infty,x} \leq 0.5$. It is important

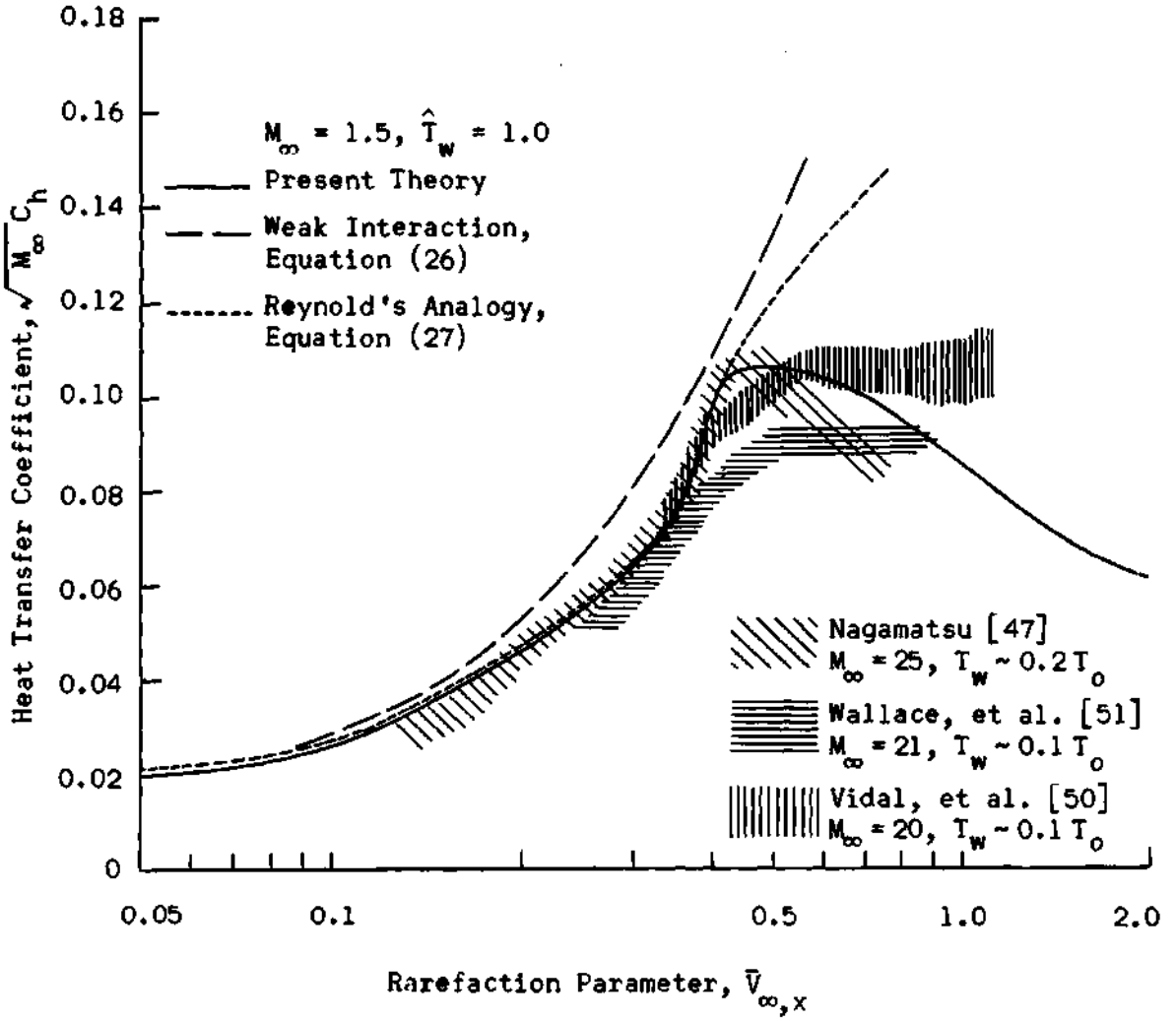

Figure 34. Heat Transfer Coefficient.

to note that this common transition point is also exhibited by the surface pressure and skin friction data, Figures 28 and 30.

Heat transfer results for other constant wall temperatures are presented in Figure 35. The cold wall curves are similar in character for all values of $\bar{V}_{\infty,x}$. The near-adiabatic wall results are dominated by strong gas heating in the transition and kinetic regions. This is because $\hat{T}_w \sim 1.6$ is near-adiabatic in the continuum limit only, and for regions of large slip influence the plate is actually very hot.

Based on the temperature ratio limitations discovered in the Couette flow solution, the results obtained for $\hat{T}_w \leq 0.75$ are assumed to be only qualitative for a low order quadrature solution and are presented here in that capacity.

Slip Velocity at the Wall

The decay of slip velocity along the plate is presented in Figure 36. Also presented for comparison are the experimental results of Becker and Boylan [48] for $M_\infty = 10.1$ and $T_w = 2T_\infty$, the theoretical prediction of Chow [68], and the theory of Oguchi [59] for $M_\infty = 1.5$ and $T_w = T_\infty$. The present solution agrees very well with the several other results except that at the leading edge itself the gas does not exhibit pure slip, $u_w = U_\infty$, but rather a near-free molecular value, $u_w = U_\infty/2$ for $T_w = T_\infty$. The practice of assuming pure slip at the leading edge is only valid for $M_\infty \to \infty$, i.e., when the random motion of molecules can be neglected.

The effects of different plate temperatures on the slip velocity is illustrated in Figure 37. Much as would be expected, the slip velocity increases almost linearly with increasing wall temperature. This trend agrees with the theoretical formulation of Oguchi [58].

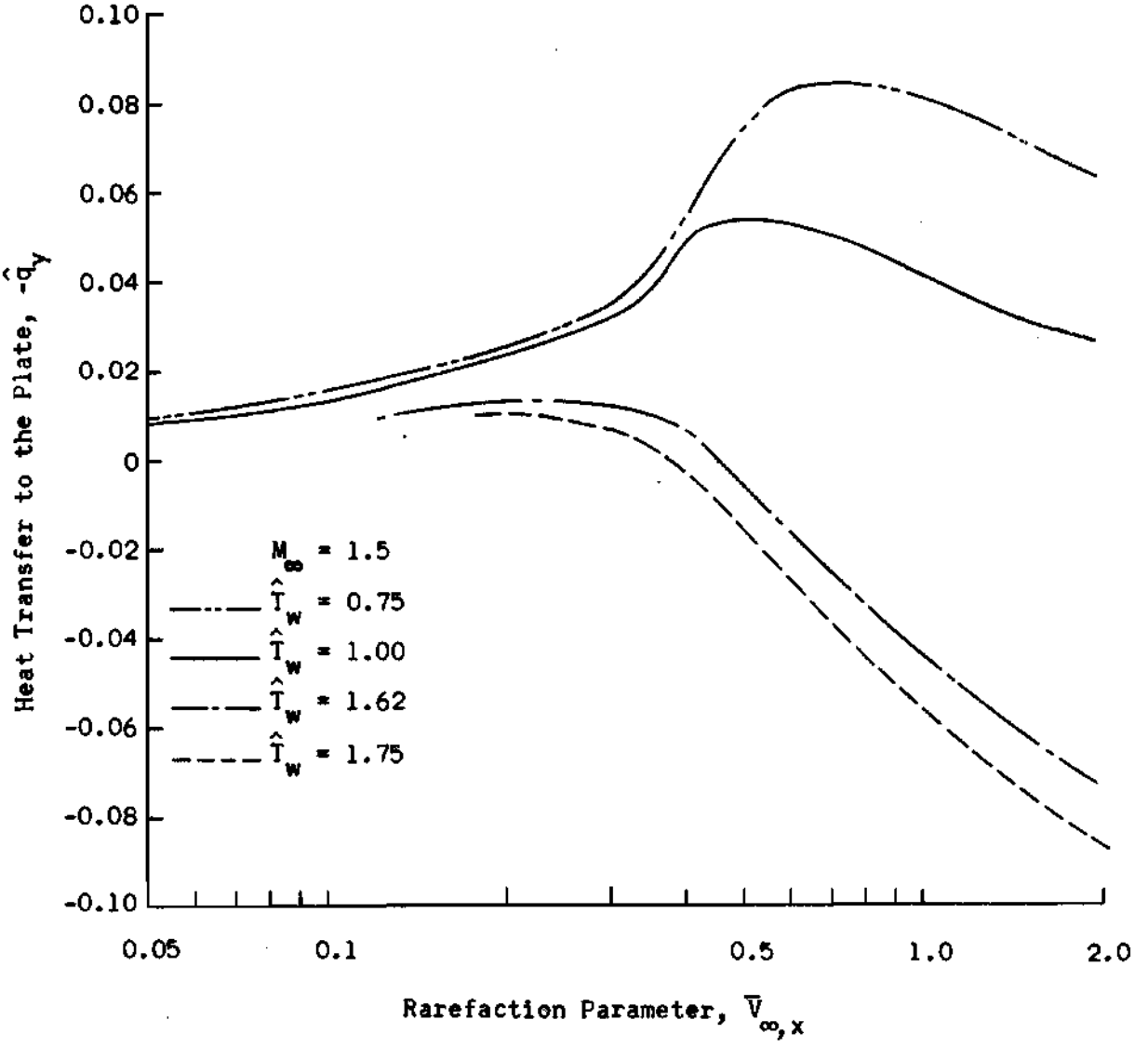

Figure 35. Effect of Plate Temperature on Heat Transfer.

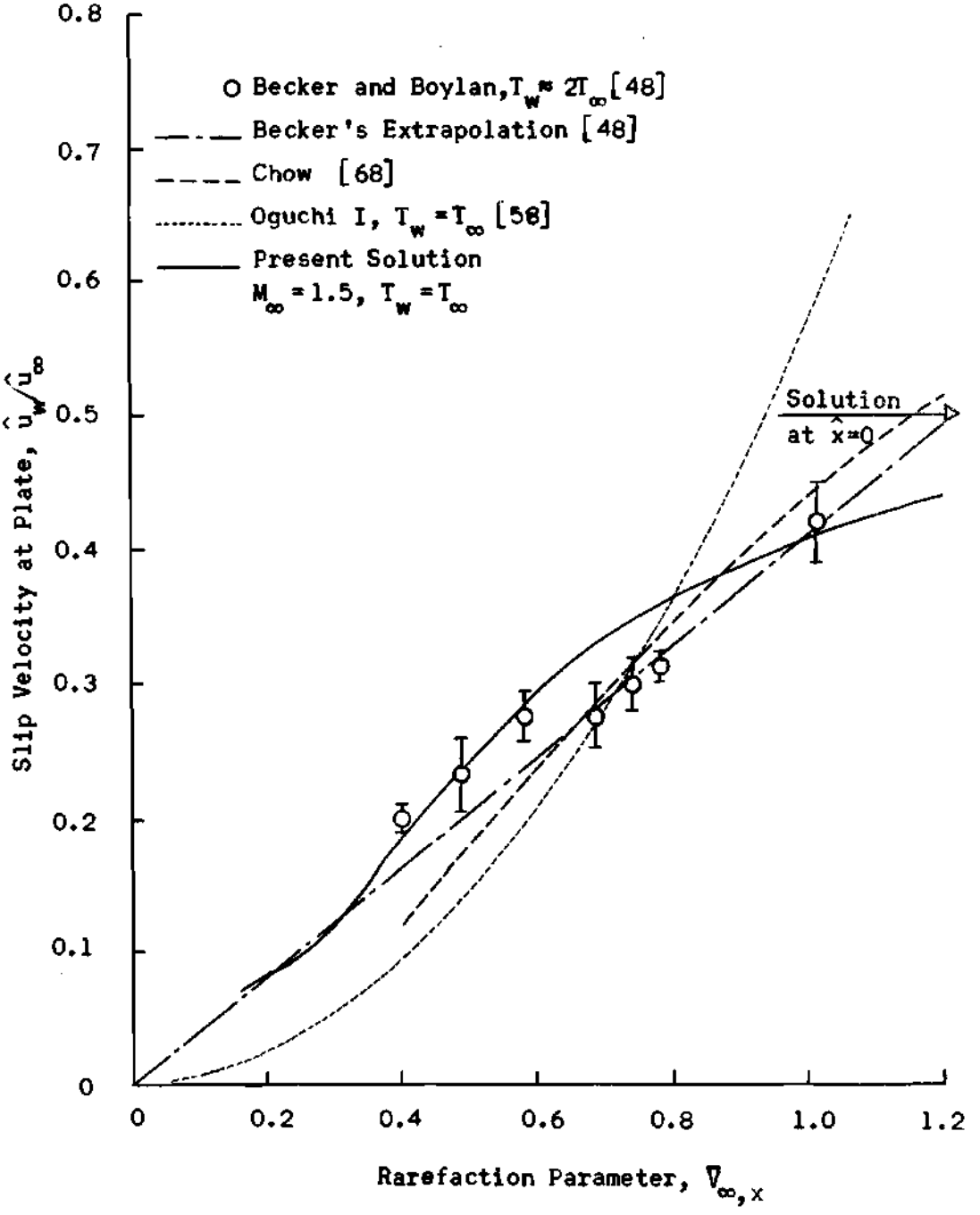

Figure 36. Slip Velocity at the Plate.

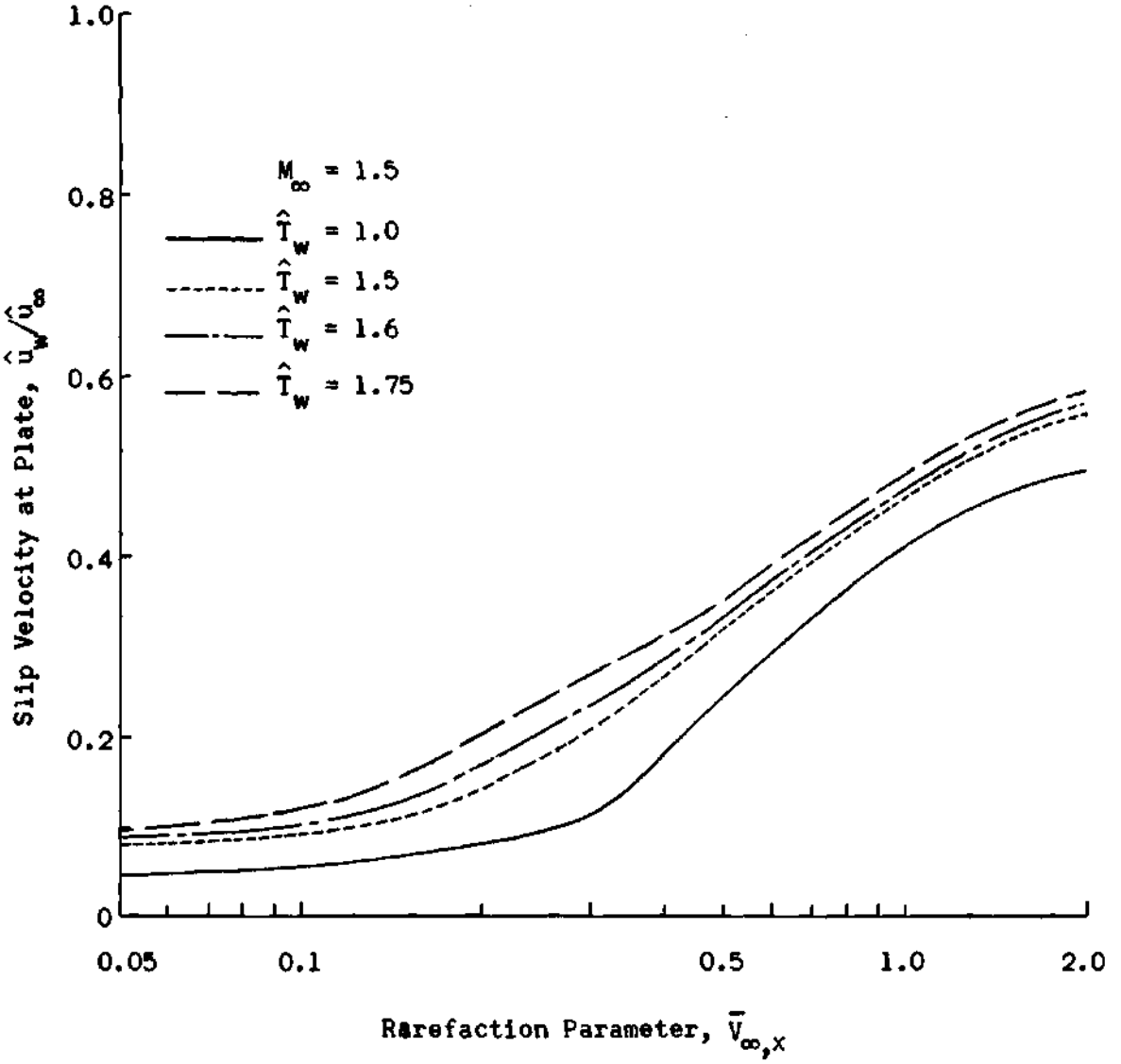

Figure 37. Effect of Plate Temperature on Slip Velocity.

Distribution Function in Kinetic Region

An interesting insight into the molecular behavior in the kinetic region can be obtained by looking at the distribution function near the plate where the velocity distribution is strongly non-Maxwellian; in fact, it is more nearly a two-sided Maxwellian. As an illustration of this phenomenon, the distribution function $\hat{g}(\hat{v}_x, \hat{v}_y; \hat{x}=0, \hat{y}=0)$ for $\hat{T}_w = 1$ is presented in Figure 38. The grid "net" covering the surface is the actual velocity grid used in the calculation. The two-stream distinction proposed by Gross, et.al., [7] is obvious. Under this condition, the flow phenomenon is largely governed by the molecule-surface collisions.

Farther downstream of the leading edge the increased number of molecule-molecule collisions will tend to drive the two-sided velocity distribution toward the single peak continuous velocity distribution characteristic of the continuum regime. The transition from the kinetic region velocity distribution to the continuum region velocity distribution is illustrated in Figure 39 where the transition region velocity distribution, $\hat{g}(\hat{v}_x, \hat{v}_y; \hat{x}=10, \hat{y}=0)$ is plotted for the case $\hat{T}_w = 1$. The tendency toward a continuous equilibrium distribution about a zero velocity is evident.

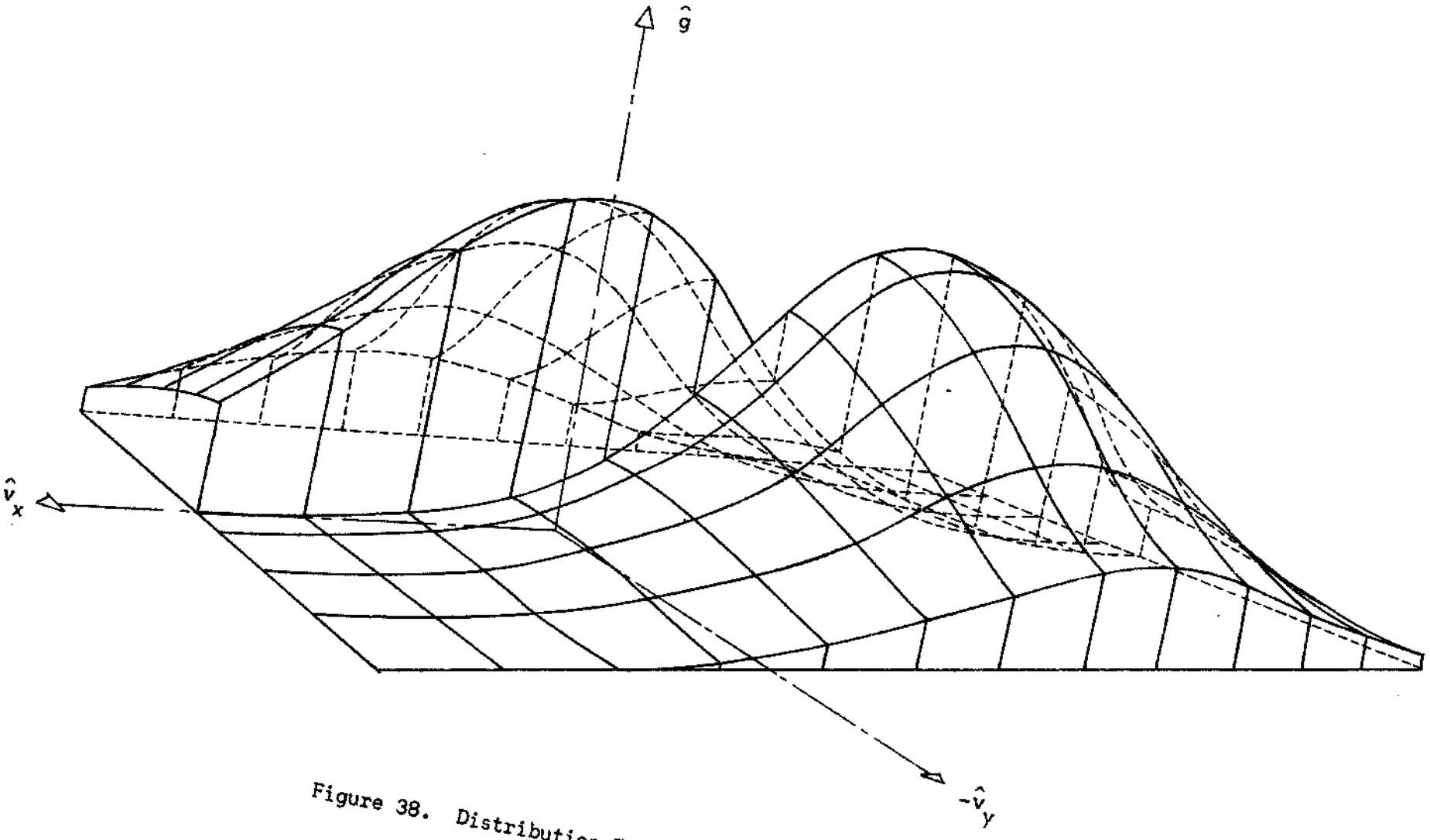

Figure 38. Distribution Function $\hat{g}(\hat{v}_x, \hat{v}_y; \hat{x} = 0, \hat{y} = 0)$.

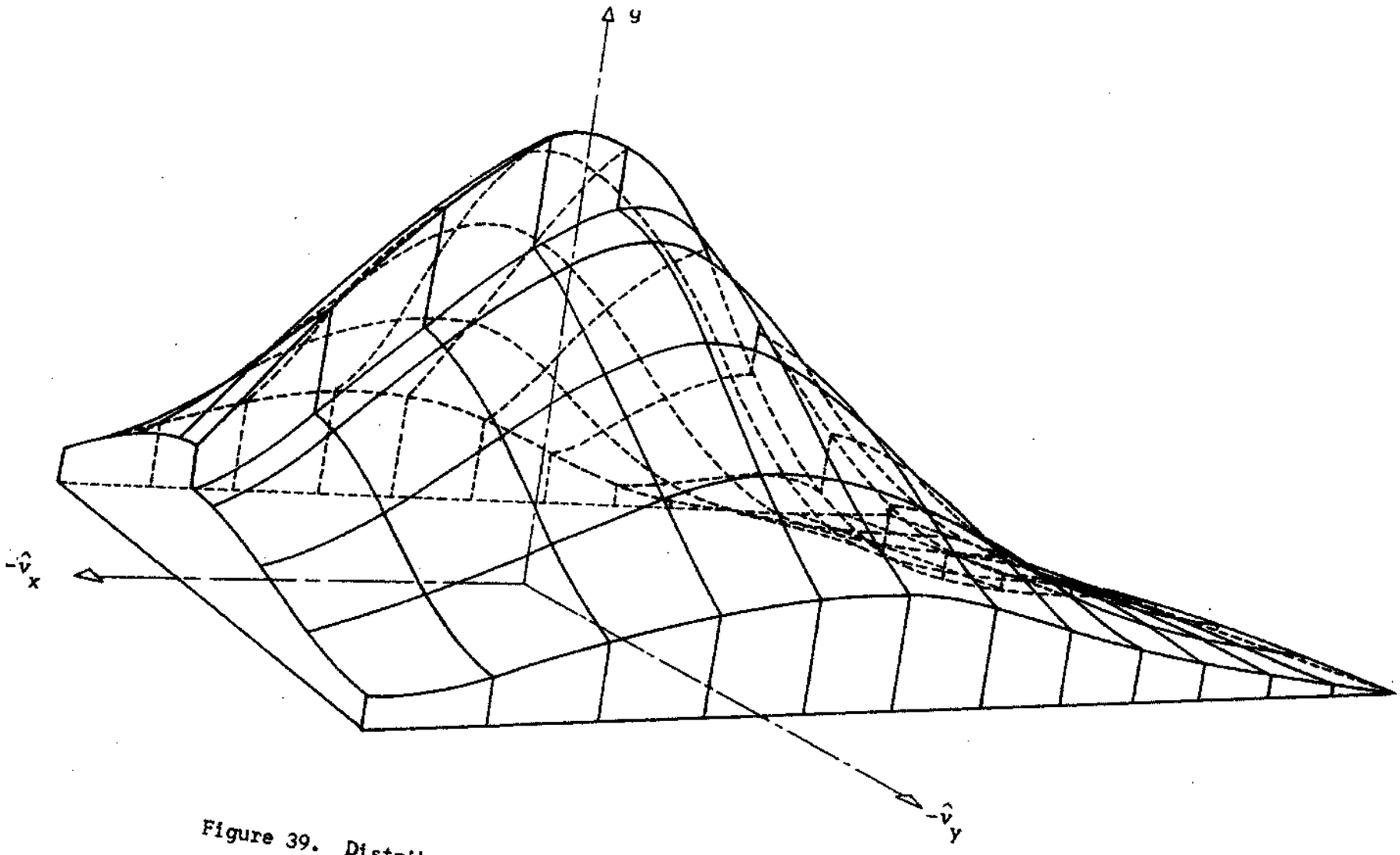

Figure 39. Distribution Function $\hat{g}(\hat{v}_x, \hat{v}_y; \hat{x} = 10, \hat{y} = 0)$.

CHAPTER IV

DISCUSSION AND CONCLUSIONS

The application of the discrete ordinate method for solving non-linear gasdynamic flow problems has been accomplished on a systematic basis. The usefulness and accuracy of the new quadrature was established in the solution of the problem of non-linear Couette flow with heat transfer. The results were compared with Anderson's exact numerical solution [14] and were found to be identical within graphical distinction. The method was then extended to the solution of the two-dimensional leading edge problem, and it achieved excellent results for all parameters studied. The success of this extension, using a low order quadrature, may lie partly in the fact that the moment integrals, which are solved by quadrature, are two-dimensional, and a low order quadrature (i.e. n=4, half-range) actually samples the integral at $(2n)^2$ discrete values of the argument. The accuracy of the leading edge solution then may be considered quite good.

Most theoretical treatments of viscous gasdynamics problems use simplifying assumptions to make the equations tractable for analysis. In contrast, the solutions achieved by the present technique utilized only the assumption of the BGK model; however, the method can be extended to other models. The approximation to the Boltzmann equation involved in the present research is made only in the sense of numerical truncations. Based on the success of the application of the proposed method to the solution of the leading edge problem, it appears that the method of

discrete ordinates, using the equally spaced quadrature, has suitable flexibility for adaptation to many practical situations which may arise in physical problems. For sufficiently higher Mach numbers, however, a higher order quadrature is necessary. The only limitation of the present leading edge solution is that of large computer storage requirements.

The results of the present investigation may be summarized in the following conclusions:

1. The discrete ordinate method has been shown to give accurate solutions over a wider range of Knudsen numbers for a given amount of computional effort than any other known existing method applied to the non-linear BBGK equation.

2. The flexibility of the discrete ordinate method, which has been extended to solve problems previously considered unapproachable from a computational standpoint, has been demonstrated in the solution of the leading edge problem. The results of the leading edge solution offer considerable insight into the behavior of a rarefied gas flow as it traverses the complete spectrum of flow regimes from near-free molecular to continuum, and presents a meaningful connection between the first-collision kinetic theory solutions at the leading edge and the extended continuum theories in the interaction regimes.

3. The successful extension of the method of discrete ordinates to non-linear problems is due to the development of the equally spaced quadratures.

4. The flow field generated for the leading edge problem presents a reasonable picture of the macroscopic properties and their spacial variations. The results indicate that the effect of wall temperature is

confined to the boundary layer region and significantly influences only the density and temperature profiles. The thickness of the shock wave is in qualitative agreement with the theories of Gilbarg and Paolucci [66] and of Liepman, et. al. [64]. The shock front position is slightly below the Mach wave, which agrees with the trend of Butler's numerical solution [60].

5. The surface pressures generated for the leading edge problem agree with the second order weak interaction theory of Hayes and Probstein [43] in the weak interaction range, $\bar{V}_{\infty,x} \lesssim 0.15$. The pressure results have the correct trend as indicated by available experimental data at nominal Mach numbers [40,48]. The pressure peak noted by several experimental investigators [47,48,49] is confirmed and, in fact, occurs in the transition range, $0.4 \leq \bar{V}_{\infty,x} \leq 0.6$, as pointed out by Becker and Boylan [48] and by Moulic [40]. The solution at the leading edge, $\hat{x} = 0$, does not achieve the free molecule limit and indicates that no true free molecule region exists. This was also pointed out by Kogan [62] and by Bird [63].

6. The skin friction results for the leading edge problem are in qualitative agreement with the Blassius solution in the interaction regime, $\bar{V}_{\infty,x} \lesssim 0.3$. The present solution also yields qualitative agreement with the experimental results of Wallace and Burke [51] and of Moulic [40] for interaction and merged regimes, $\bar{V}_{\infty,x} \lesssim 0.5$. The present results do not exhibit a "peak" of maximum skin friction behind the leading edge, but merely a reduction in slope of the skin friction curve as the leading edge is approached. This behavior agrees with the theoretical prediction of Mirels [67].

7. The heat transfer results for the leading edge problem are in

good agreement with boundary layer theory [35] for $\bar{V}_{\infty,x} < 0.1$. The application of Reynold's Analogy as corrected by Li and Nagamatsu [56] gives excellent results for $\bar{V}_{\infty,x} \lesssim 0.35$. The present results exhibit a heat transfer peak in the transition region, $0.4 \leq \bar{V}_{\infty,x} \leq 0.6$, which agrees with the experimental data of Nagamatsu, et.al. [47], of Wallace and Burke [51], and of Vidal and Wittliff [50].

8. The wall slip velocity for the leading edge problem agrees quite well with the theory of Chow [68] and of Oguchi [59], and with the experimental results of Becker and Boylan [48] for $\bar{V}_{\infty,x} < 1.0$. Nearer the leading edge, however, the gas does not exhibit pure slip, $u_w = U_\infty$, but rather a near-free molecular value, $u_w = U_\infty/2$ for $T_w = T_\infty$. The magnitude of the slip velocity is seen to increase almost linearly with increased plate temperature as predicted by Oguchi [59].

APPENDICES

APPENDIX A

THE "ODD" AND "EVEN" EQUALLY SPACED QUADRATURES

The idea of developing a quadrature for an integral of the type $\int_0^\infty e^{-v} f(v)dv$ based on difference formulas was introduced by Burgoyne [69]. This method involves equally spaced discrete ordinates but requires solution of the Newton difference operators first. This idea has been extended for the first time by incorporating the equivalent Lagrange formula to calculate the integrals of the type

$$\int_0^\infty e^{-\beta v^2} f(v)dv \tag{A-1}$$

where β is a real and positive constant. An important feature of the present formulation is the choice of the negative exponential weighting function, $e^{-\beta v^2}$. Most integrals formed in kinetic theory analyses contain an argument which is essentially a perturbation about a distribution function with exponential character. The present formulation then approximates the perturbation about the exponential argument rather than the entire argument of the integral. The discrete ordinate technique then consists of replacing the integration over molecular velocity space by a quadrature. This requires approximating the velocity dependence of the function, $f(v)$, by a set of functions, each evaluated at appropriate discrete points (equally distributed) in velocity space, i.e.,

$$\int_0^\infty e^{-\beta v^2} f(v)dv = \sum_{i=1}^{n} k_i f(\alpha_i) + E \tag{A-2}$$

where k_i are the weighting functions which are to be determined, α_i are the equally spaced discrete ordinates, n is the number of discrete points, and E is the error term which is instrumental in determining the optimum discrete ordinate spacing, w'.

The equally spaced quadratures are derived from two formulations. First, the "even" quadrature is derived for discrete ordinates equal to w, 2w, 3w, ..., nw. Second, the "odd" quadrature is derived for discrete ordinates equal to w/2, 3w/2, 5w/2, ..., etc. The "odd" and "even" quadratures are applied simultaneously for the solution of the Boltzmann equation with the hard sphere model (See Reference [29]). Either the "even" or "odd" quadrature can be applied to the problems in Chapter II and Chapter III, but the "odd" quadrature is used in the present solution for convenience.

The "Even" Equally Spaced Quadrature

The Lagrange formula gives [36]

$$f(v) = \sum_{i=1}^{n} \frac{P_i(v)}{P_i(\alpha_i)} f(\alpha_i) \tag{A-3}$$

where

$$P_i(v) = \frac{(v-w)(v-2w)\ldots(v-nw)}{(v-iw)} \tag{A-4}$$

where α_i's are taken to be w, 2w, 3w, ..., nw, for "even" quadrature.

Substituting Equation (A-3) into Equation (A-2) yields

$$\int_o^\infty e^{-\beta v^2} \sum_{i=1}^{\infty} \frac{P_i(v)}{P_i(\alpha_i)} f(\alpha_i)dv = \sum_{i=1}^{n} f(\alpha_i) \int_o^\infty e^{-\beta v^2} \frac{P_i(v)}{P_i(\alpha_i)} dv$$

$$= \sum_{i=1}^{n} f(\alpha_i)k_i \qquad \text{(A-5)}$$

such that the weighting coefficients are

$$k_i = \frac{1}{P_i(\alpha_i)} \int_o^\infty P_i(v)e^{-\beta v^2}dv \qquad \text{(A-6)}$$

Since $P_i(v)$ is a polynominal of degree n, the integral in Equation (A-6) for k_i can be solved analytically and thus the expressions for k_i are determined in terms of β and w once and for all. The k_i expressions for cases (n = 2, 3, ..., 8) are presented in the following:

$$n = 2,\ k_1 = \frac{\sqrt{\pi}}{\beta^{1/2}} - \frac{1}{2w\beta}$$

$$k_2 = -\frac{\sqrt{\pi}}{2\beta^{1/2}} + \frac{1}{2w\beta}$$

$$n = 3,\ k_1 = \frac{3\sqrt{\pi}}{2\beta^{1/2}} - \frac{5}{4w\beta} + \frac{\sqrt{\pi}}{8w^2\beta^{3/2}}$$

$$k_2 = -\frac{3\sqrt{\pi}}{2\beta^{1/2}} + \frac{2}{w\beta} - \frac{\sqrt{\pi}}{4w^2\beta^{3/2}}$$

$$k_3 = \frac{\sqrt{\pi}}{2\beta^{1/2}} - \frac{3}{4w\beta} + \frac{\sqrt{\pi}}{8w^2\beta^{3/2}}$$

$$n = 4,\quad K_1 = \frac{2\sqrt{\pi}}{\beta^{1/2}} - \frac{13}{6w\beta} + \frac{3\sqrt{\pi}}{8w^2\beta^{3/2}} - \frac{1}{12w^3\beta^2}$$

$$k_2 = -\frac{3\sqrt{\pi}}{\beta^{1/2}} + \frac{19}{4w\beta} - \frac{\sqrt{\pi}}{w^2\beta^{3/2}} + \frac{1}{4w^3\beta^2}$$

$$k_3 = \frac{2\sqrt{\pi}}{\beta^{1/2}} - \frac{7}{2w\beta} + \frac{7\sqrt{\pi}}{8w^2\beta^{3/2}} - \frac{1}{4w^3\beta^2}$$

$$k_4 = -\frac{\sqrt{\pi}}{2\beta^{1/2}} + \frac{11}{12w\beta} - \frac{\sqrt{\pi}}{4w^2\beta^{3/2}} + \frac{1}{12w^3\beta^2}$$

$$n = 5,\quad k_1 = \frac{5}{2}\frac{\sqrt{\pi}}{\beta^{1/2}} - \frac{77}{24}\frac{1}{w\beta} + \frac{71}{96}\frac{\sqrt{\pi}}{w^2\beta^{3/2}} - \frac{7}{24}\frac{1}{w^3\beta^2} + \frac{1}{64}\frac{\sqrt{\pi}}{w^4\beta^{5/2}}$$

$$k_2 = -5\frac{\sqrt{\pi}}{\beta^{1/2}} + \frac{107}{12}\frac{1}{w\beta} - \frac{59}{24}\frac{\sqrt{\pi}}{w^2\beta^{3/2}} + \frac{13}{12}\frac{1}{w^3\beta^2} - \frac{1}{16}\frac{\sqrt{\pi}}{w^4\beta^{5/2}}$$

$$k_3 = 5\frac{\sqrt{\pi}}{\beta^{1/2}} - \frac{39}{4}\frac{1}{w\beta} + \frac{49}{16}\frac{\sqrt{\pi}}{w^2\beta^{3/2}} - \frac{3}{2}\frac{1}{w^3\beta^2} + \frac{3}{32}\frac{\sqrt{\pi}}{w^4\beta^{5/2}}$$

$$k_4 = -\frac{5}{2}\frac{\sqrt{\pi}}{\beta^{1/2}} + \frac{61}{12}\frac{1}{w\beta} - \frac{41}{24}\frac{\sqrt{\pi}}{w^2\beta^{3/2}} + \frac{11}{12}\frac{1}{w^3\beta^2} - \frac{1}{16}\frac{\sqrt{\pi}}{w^4\beta^{5/2}}$$

$$k_5 = \frac{1}{2}\frac{\sqrt{\pi}}{\beta^{1/2}} - \frac{25}{24}\frac{1}{w\beta} + \frac{35}{96}\frac{\sqrt{\pi}}{w^2\beta^{3/2}} - \frac{5}{24}\frac{1}{w^3\beta^2} + \frac{1}{64}\frac{\sqrt{\pi}}{w^4\beta^{5/2}}$$

$$n = 6,\quad k_1 = 3\frac{\sqrt{\pi}}{\beta^{1/2}} - \frac{87}{20}\frac{1}{w\beta} + \frac{29}{24}\frac{\sqrt{\pi}}{w^2\beta^{3/2}} - \frac{31}{48}\frac{1}{w^3\beta^2} + \frac{1}{16}\frac{\sqrt{\pi}}{w^4\beta^{5/2}} - \frac{1}{120}\frac{1}{w^5\beta^3}$$

$$k_2 = -\frac{15}{2}\frac{\sqrt{\pi}}{\beta^{1/2}} + \frac{117}{8}\frac{1}{w\beta} - \frac{461}{96}\frac{\sqrt{\pi}}{w^2\beta^{3/2}} + \frac{137}{48}\frac{1}{w^3\beta^2} - \frac{19}{64}\frac{\sqrt{\pi}}{w^4\beta^{5/2}}$$

$$+ \frac{1}{24}\frac{1}{w^5\beta^3}$$

$$k_3 = 10\frac{\sqrt{\pi}}{\beta^{1/2}} - \frac{127}{6}\frac{1}{w\beta} + \frac{31}{4}\frac{\sqrt{\pi}}{w^2\beta^{3/2}} - \frac{121}{24}\frac{1}{w^3\beta^2} + \frac{9}{16}\frac{\sqrt{\pi}}{w^4\beta^{5/2}}$$

$$- \frac{1}{12}\frac{1}{w^5\beta^3}$$

$$k_4 = \frac{-15}{2}\frac{\sqrt{\pi}}{\beta^{1/2}} + \frac{33}{2}\frac{1}{w\beta} - \frac{307}{48}\frac{\sqrt{\pi}}{w^2\beta^{3/2}} + \frac{107}{24}\frac{1}{w^3\beta^2} - \frac{17}{32}\frac{\sqrt{\pi}}{w^4\beta^{5/2}}$$

$$+ \frac{1}{12}\frac{1}{w^5\beta^3}$$

$$k_5 = 3\frac{\sqrt{\pi}}{\beta^{1/2}} - \frac{27}{4}\frac{1}{w\beta} + \frac{65}{24}\frac{\sqrt{\pi}}{w^2\beta^{3/2}} - \frac{95}{48}\frac{1}{w^3\beta^2} + \frac{1}{4}\frac{\sqrt{\pi}}{w^4\beta^{5/2}} - \frac{1}{24}\frac{1}{w^5\beta^3}$$

$$k_6 = -\frac{1}{2}\frac{\sqrt{\pi}}{\beta^{1/2}} + \frac{137}{120}\frac{1}{w\beta} - \frac{15}{32}\frac{\sqrt{\pi}}{w^2\beta^{3/2}} + \frac{17}{48}\frac{1}{w^3\beta^2} - \frac{3}{64}\frac{\sqrt{\pi}}{w^4\beta^{5/2}}$$

$$+ \frac{1}{120}\frac{1}{w^5\beta^3}$$

$n = 7$, $k_1 = \frac{7}{2}\frac{\sqrt{\pi}}{\beta^{1/2}} - \frac{223}{40}\frac{1}{w\beta} + \frac{319}{180}\frac{\sqrt{\pi}}{w^2\beta^{3/2}} - \frac{37}{32}\frac{1}{w^3\beta^2} + \frac{59}{384}\frac{\sqrt{\pi}}{w^4\beta^{5/2}}$

$$- \frac{3}{80}\frac{1}{w^5\beta^3} + \frac{1}{768}\frac{\sqrt{\pi}}{w^6\beta^{7/2}}$$

$$k_2 = -\frac{21}{2}\frac{\sqrt{\pi}}{\beta^{1/2}} + \frac{879}{40}\frac{1}{w\beta} - \frac{3929}{480}\frac{\sqrt{\pi}}{w^2\beta^{3/2}} + \frac{71}{12}\frac{1}{w^3\beta^2} - \frac{27}{32}\frac{\sqrt{\pi}}{w^4\beta^{5/2}}$$

$$+ \frac{13}{60}\frac{1}{w^5\beta^3} - \frac{1}{128}\frac{\sqrt{\pi}}{w^6\beta^{7/2}}$$

$$k_3 = \frac{35}{2}\frac{\sqrt{\pi}}{\beta^{1/2}} - \frac{949}{24}\frac{1}{w\beta} + \frac{389}{24}\frac{\sqrt{\pi}}{w^2\beta^{3/2}} - \frac{1219}{96}\frac{1}{w^3\beta^2} + \frac{247}{128}\frac{\sqrt{\pi}}{w^4\beta^{5/2}}$$

$$- \frac{25}{48}\frac{1}{w^5\beta^3} + \frac{5}{256}\frac{\sqrt{\pi}}{w^6\beta^{7/2}}$$

$$k_4 = -\frac{35}{2}\frac{\sqrt{\pi}}{\beta^{1/2}} + 41\frac{1}{w\beta} - \frac{2545}{144}\frac{\sqrt{\pi}}{w^2\beta^{3/2}} + \frac{44}{3}\frac{1}{w^3\beta^2} - \frac{113}{48}\frac{\sqrt{\pi}}{w^4\beta^{5/2}}$$

$$+ \frac{2}{3}\frac{1}{w^5\beta^3} - \frac{5}{192}\frac{\sqrt{\pi}}{w^6\beta^{7/2}}$$

$$k_5 = \frac{21}{2}\frac{\sqrt{\pi}}{\beta^{1/2}} - \frac{201}{8}\frac{1}{w\beta} + \frac{67}{6}\frac{\sqrt{\pi}}{w^2\beta^{3/2}} - \frac{925}{96}\frac{1}{w^3\beta^2} + \frac{207}{128}\frac{\sqrt{\pi}}{w^4\beta^{5/2}}$$

$$- \frac{23}{48}\frac{1}{w^5\beta^3} + \frac{5}{256}\frac{\sqrt{\pi}}{w^6\beta^{7/2}}$$

$$k_6 = -\frac{7}{2}\frac{\sqrt{\pi}}{\beta^{1/2}} + \frac{1019}{120}\frac{1}{w\beta} - \frac{1849}{480}\frac{\sqrt{\pi}}{w^2\beta^{3/2}} + \frac{41}{12}\frac{1}{w^3\beta^2} - \frac{19}{32}\frac{\sqrt{\pi}}{w^4\beta^{5/2}}$$

$$+ \frac{11}{60}\frac{1}{w^5\beta^3} - \frac{1}{128}\frac{\sqrt{\pi}}{w^6\beta^{7/2}}$$

$$k_7 = \frac{1}{2}\frac{\sqrt{\pi}}{\beta^{1/2}} - \frac{49}{40}\frac{1}{w\beta} + \frac{203}{360}\frac{\sqrt{\pi}}{w^2\beta^{3/2}} - \frac{49}{96}\frac{1}{w^3\beta^2} + \frac{35}{384}\frac{\sqrt{\pi}}{w^4\beta^{5/2}}$$

$$- \frac{7}{240}\frac{1}{w^5\beta^3} + \frac{1}{768}\frac{\sqrt{\pi}}{w^6\beta^{7/2}}$$

$n = 8,$ $$k_1 = 4\frac{\sqrt{\pi}}{\beta^{1/2}} - \frac{481}{70}\frac{1}{w\beta} + \frac{349}{144}\frac{\sqrt{\pi}}{w^2\beta^{3/2}} - \frac{329}{180}\frac{1}{w^3\beta^2} + \frac{115}{384}\frac{\sqrt{\pi}}{w^4\beta^{5/2}}$$

$$- \frac{73}{720}\frac{1}{w^5\beta^3} + \frac{5}{768}\frac{\sqrt{\pi}}{w^6\beta^{7/2}} - \frac{1}{1680}\frac{1}{w^7\beta^4}$$

$$k_2 = -14\frac{\sqrt{\pi}}{\beta^{1/2}} + \frac{621}{20}\frac{1}{w\beta} - \frac{18353}{1440}\frac{\sqrt{\pi}}{w^2\beta^{3/2}} + \frac{15289}{1440}\frac{1}{w^3\beta^2} - \frac{179}{96}\frac{\sqrt{\pi}}{w^4\beta^{5/2}}$$

$$+ \frac{239}{360}\frac{1}{w^5\beta^3} - \frac{17}{384}\frac{\sqrt{\pi}}{w^6\beta^{7/2}} + \frac{1}{240}\frac{1}{w^7\beta^4}$$

$$k_3 = 28\frac{\sqrt{\pi}}{\beta^{1/2}} - \frac{2003}{30}\frac{1}{w\beta} + \frac{2391}{80}\frac{\sqrt{\pi}}{w^2\beta^{3/2}} - \frac{134}{5}\frac{1}{w^3\beta^2} + \frac{639}{128}\frac{\sqrt{\pi}}{w^4\beta^{5/2}}$$

$$- \frac{149}{80} \frac{1}{w^5\beta^3} + \frac{33}{256} \frac{\sqrt{\pi}}{w^6\beta^{7/2}} - \frac{1}{80} \frac{1}{w^7\beta^4}$$

$$k_4 = - 35 \frac{\sqrt{\pi}}{\beta^{1/2}} + \frac{691}{8} \frac{1}{w\beta} - \frac{1457}{36} \frac{\sqrt{\pi}}{w^2\beta^{3/2}} + \frac{10993}{288} \frac{1}{w^3\beta^2} - \frac{179}{24} \frac{\sqrt{\pi}}{w^4\beta^{5/2}}$$

$$+ \frac{209}{72} \frac{1}{w^5\beta^3} - \frac{5}{24} \frac{\sqrt{\pi}}{w^6\beta^{7/2}} + \frac{1}{48} \frac{1}{w^7\beta^4}$$

$$k_5 = 28 \frac{\sqrt{\pi}}{\beta^{1/2}} - \frac{141}{2} \frac{1}{w\beta} + \frac{4891}{144} \frac{\sqrt{\pi}}{w^2\beta^{3/2}} - \frac{1193}{36} \frac{1}{w^3\beta^2} + \frac{2581}{384} \frac{\sqrt{\pi}}{w^4\beta^{5/2}}$$

$$- \frac{391}{144} \frac{1}{w^5\beta^3} + \frac{155}{768} \frac{\sqrt{\pi}}{w^6\beta^{7/2}} - \frac{1}{48} \frac{1}{w^7\beta^4}$$

$$k_6 = - 14 \frac{\sqrt{\pi}}{\beta^{1/2}} + \frac{2143}{60} \frac{1}{w\beta} - \frac{561}{32} \frac{\sqrt{\pi}}{w^2\beta^{3/2}} + \frac{2803}{160} \frac{1}{w^3\beta^2} - \frac{117}{32} \frac{\sqrt{\pi}}{w^4\beta^{5/2}}$$

$$+ \frac{61}{40} \frac{1}{w^5\beta^3} - \frac{15}{128} \frac{\sqrt{\pi}}{w^6\beta^{7/2}} + \frac{1}{80} \frac{1}{w^7\beta^4}$$

$$k_7 = 4 \frac{\sqrt{\pi}}{\beta^{1/2}} - \frac{103}{10} \frac{1}{w\beta} + \frac{3689}{720} \frac{\sqrt{\pi}}{w^2\beta^{3/2}} - \frac{469}{90} \frac{1}{w^3\beta^2} + \frac{427}{384} \frac{\sqrt{\pi}}{w^4\beta^{5/2}}$$

$$- \frac{343}{720} \frac{1}{w^5\beta^3} + \frac{29}{768} \frac{\sqrt{\pi}}{w^6\beta^{7/2}} - \frac{1}{240} \frac{1}{w^7\beta^4}$$

$$k_8 = - \frac{1}{2} \frac{\sqrt{\pi}}{\beta^{1/2}} + \frac{363}{280} \frac{1}{w\beta} - \frac{469}{720} \frac{\sqrt{\pi}}{w^2\beta^{3/2}} + \frac{967}{1440} \frac{1}{w^3\beta^2} - \frac{7}{48} \frac{\sqrt{\pi}}{w^4\beta^{5/2}}$$

$$+ \frac{23}{360} \frac{1}{w^5\beta^3} - \frac{1}{192} \frac{\sqrt{\pi}}{w^6\beta^{7/2}} + \frac{1}{1680} \frac{1}{w^7\beta^4}$$

It is noted that exact numerical values of the weighting coefficients, k_i, can be easily computed for particular β and w. More weighting coefficients for higher order approximations can easily be determined by the method described above.

The "Odd" Equally Spaced Quadrature

Another extension of this method is the "odd" equally spaced quadrature where the discrete ordinates, α_i, are taken to be w/2, 3w/2, 5w/2, 7w/2, ..., etc. The weighting functions of this "odd" quadrature can be obtained exactly as for the "even" equally spaced quadrature and the corresponding expressions are presented as follows:

$$n = 2,\ k_1 = \frac{3\sqrt{\pi}}{4\beta^{1/2}} - \frac{1}{2w\beta}$$

$$k_2 = -\frac{\sqrt{\pi}}{4\beta^{1/2}} + \frac{1}{2w\beta}$$

$$n = 3,\ k_1 = \frac{15\sqrt{\pi}}{16\beta^{1/2}} - \frac{1}{w\beta} + \frac{\sqrt{\pi}}{8w^2\beta^{3/2}}$$

$$k_2 = -\frac{5\sqrt{\pi}}{8\beta^{1/2}} + \frac{3}{2w\beta} - \frac{\sqrt{\pi}}{4w^2\beta^{3/2}}$$

$$k_3 = \frac{3\sqrt{\pi}}{16\beta^{1/2}} - \frac{1}{2w\beta} + \frac{\sqrt{\pi}}{8w^2\beta^{3/2}}$$

$$n = 4,\ k_1 = \frac{35}{32}\frac{\sqrt{\pi}}{\beta^{1/2}} - \frac{71}{48w\beta} + \frac{5\sqrt{\pi}}{16w^2\beta^{3/2}} - \frac{1}{12w^3\beta^2}$$

$$k_2 = -\frac{35\sqrt{\pi}}{32\beta^{1/2}} + \frac{47}{16w\beta} - \frac{13\sqrt{\pi}}{16w^2\beta^{3/2}} + \frac{1}{4w^3\beta^2}$$

$$k_3 = \frac{21\sqrt{\pi}}{32\beta^{1/2}} - \frac{31}{16w\beta} + \frac{11\sqrt{\pi}}{16w^2\beta^{3/2}} - \frac{1}{4w^3\beta^2}$$

$$k_4 = -\frac{5\sqrt{\pi}}{32\beta^{1/2}} + \frac{23}{48w\beta} - \frac{3\sqrt{\pi}}{16w^2\beta^{3/2}} + \frac{1}{12w^3\beta^2}$$

$$n = 5,\ k_1 = 1.2304687500\ \frac{\sqrt{\pi}}{\beta^{1/2}} - 1.9375000000\ \frac{1}{w\beta} + 0.5364583333\ \frac{\sqrt{\pi}}{w^2\beta^{3/2}}$$

$$- 0.2500000000\ \frac{1}{w^3\beta^2} + 0.0156250000\ \frac{\sqrt{\pi}}{w^4\beta^{5/2}}$$

$$k_2 = - 1.6406250000\ \frac{\sqrt{\pi}}{\beta^{1/2}} + 4.7708333333\ \frac{1}{w\beta} - 1.7083333333\ \frac{\sqrt{\pi}}{w^2\beta^{3/2}}$$

$$+ 0.9166666667\ \frac{1}{w^3\beta^2} - 0.0625000000\ \frac{\sqrt{\pi}}{w^4\beta^{5/2}}$$

$$k_3 = 1.4765625000\ \frac{\sqrt{\pi}}{\beta^{1/2}} - 4.6875000000\ \frac{1}{w\beta} + 2.0312500000\ \frac{\sqrt{\pi}}{w^2\beta^{3/2}}$$

$$- 1.2500000000\ \frac{1}{w^3\beta^2} + 0.0937500000\ \frac{\sqrt{\pi}}{w^4\beta^{5/2}}$$

$$k_4 = - 0.7031250000\ \frac{\sqrt{\pi}}{\beta^{1/2}} + 2.3125000000\ \frac{1}{w\beta} - 1.0833333333\ \frac{\sqrt{\pi}}{w^2\beta^{3/2}}$$

$$+ 0.7500000000\ \frac{1}{w^3\beta^2} - 0.0625000000\ \frac{\sqrt{\pi}}{w^4\beta^{5/2}}$$

$$k_5 = 0.1367187500\ \frac{\sqrt{\pi}}{\beta^{1/2}} - 0.4583333333\ \frac{1}{w\beta} + 0.2239583333\ \frac{\sqrt{\pi}}{w^2\beta^{3/2}}$$

$$- 0.166666667\ \frac{1}{w^3\beta^2} + 0.0156250000\ \frac{\sqrt{\pi}}{w^4\beta^{5/2}}$$

$$n = 6,\ k_1 = 1.3535156250\ \frac{\sqrt{\pi}}{\beta^{1/2}} - 2.3773437500\ \frac{1}{w\beta} + 0.7838541667\ \frac{\sqrt{\pi}}{w^2\beta^{3/2}}$$

$$- 0.4895833333\ \frac{1}{w^3\beta^2} + 0.0546875000\ \frac{\sqrt{\pi}}{w^4\beta^{5/2}}$$

$$- 0.0083333333\ \frac{1}{w^5\beta^3}$$

$$k_2 = -2.2558593750 \frac{\sqrt{\pi}}{\beta^{1/2}} + 6.9700520834 \frac{1}{w\beta} - 2.9453125000 \frac{\sqrt{\pi}}{w^2\beta^{3/2}}$$
$$+ 2.1145833333 \frac{1}{w^3\beta^2} - 0.2578125000 \frac{\sqrt{\pi}}{w^4\beta^{5/2}}$$
$$+ 0.0416666667 \frac{1}{w^5\beta^3}$$

$$k_3 = 2.7070312500 \frac{\sqrt{\pi}}{\beta^{1/2}} - 9.0859375000 \frac{1}{w\beta} + 4.5052083333 \frac{\sqrt{\pi}}{w^2\beta^{3/2}}$$
$$- 3.6458333333 \frac{1}{w^3\beta^2} + 0.4843750000 \frac{\sqrt{\pi}}{w^4\beta^{5/2}}$$
$$- 0.0833333333 \frac{1}{w^5\beta^3}$$

$$k_4 = -1.9335937500 \frac{\sqrt{\pi}}{\beta^{1/2}} + 6.7109375000 \frac{1}{w\beta} - 3.5572916667 \frac{\sqrt{\pi}}{w^2\beta^{3/2}}$$
$$+ 3.1458333333 \frac{1}{w^3\beta^2} - 0.4531250000 \frac{\sqrt{\pi}}{w^4\beta^{5/2}}$$
$$+ 0.0833333333 \frac{1}{w^5\beta^3}$$

$$k_5 = 0.7519531250 \frac{\sqrt{\pi}}{\beta^{1/2}} - 2.6575520833 \frac{1}{w\beta} + 1.4609375000 \frac{\sqrt{\pi}}{w^2\beta^{3/2}}$$
$$- 1.3645833333 \frac{1}{w^3\beta^2} + 0.2109375000 \frac{\sqrt{\pi}}{w^4\beta^{5/2}}$$
$$- 0.0416666667 \frac{1}{w^5\beta^3}$$

$$k_6 = -0.1230468750 \frac{\sqrt{\pi}}{\beta^{1/2}} + 0.4398437500 \frac{1}{w\beta} - 0.2473958333 \frac{\sqrt{\pi}}{w^2\beta^{3/2}}$$
$$+ 0.2395833333 \frac{1}{w^3\beta^2} - 0.0390625000 \frac{\sqrt{\pi}}{w^4\beta^{5/2}}$$

$$+ 0.0083333333 \frac{1}{w^5\beta^3}$$

$$n = 7,\ k_1 = 1.4663085938 \frac{\sqrt{\pi}}{\beta^{1/2}} - 2.801041667 \frac{1}{w\beta} + 1.0472873264 \frac{\sqrt{\pi}}{w^2\beta^{3/2}}$$

$$- 0.7916666667 \frac{1}{w^3\beta^2} + 0.1204427083 \frac{\sqrt{\pi}}{w^4\beta^{5/2}}$$

$$- 0.0333333333 \frac{1}{w^5\beta^3} + 0.0013020833 \frac{\sqrt{\pi}}{w^6\beta^{7/2}}$$

$$k_2 = - 2.9326171875 \frac{\sqrt{\pi}}{\beta^{1/2}} + 9.5122395833 \frac{1}{w\beta} - 4.5259114583 \frac{\sqrt{\pi}}{w^2\beta^{3/2}}$$

$$+ 3.9270833333 \frac{1}{w^3\beta^2} - 0.6523437500 \frac{\sqrt{\pi}}{w^4\beta^{5/2}}$$

$$+ 0.1916666667 \frac{1}{w^5\beta^3} - 0.0078125000 \frac{\sqrt{\pi}}{w^6\beta^{7/2}}$$

$$k_3 = 4.3989257813 \frac{\sqrt{\pi}}{\beta^{1/2}} - 15.4414062500 \frac{1}{w\beta} + 8.4567057291 \frac{\sqrt{\pi}}{w^2\beta^{3/2}}$$

$$- 8.1770833334 \frac{1}{w^3\beta^2} + 1.4707031250 \frac{\sqrt{\pi}}{w^4\beta^{5/2}}$$

$$- 0.4583333333 \frac{1}{w^5\beta^3} + 0.0195312500 \frac{\sqrt{\pi}}{w^6\beta^{7/2}}$$

$$k_4 = - 4.1894531250 \frac{\sqrt{\pi}}{\beta^{1/2}} + 15.1848958334 \frac{1}{w\beta} - 8.8259548611 \frac{\sqrt{\pi}}{w^2\beta^{3/2}}$$

$$+ 9.1875000000 \frac{1}{w^3\beta^2} - 1.7682291667 \frac{\sqrt{\pi}}{w^4\beta^{5/2}}$$

$$+ 0.5833333333 \frac{1}{w^5\beta^3} - 0.0260416667 \frac{\sqrt{\pi}}{w^6\beta^{7/2}}$$

$$k_5 = 2.4438476563 \frac{\sqrt{\pi}}{\beta^{1/2}} - 9.0130208334 \frac{1}{w\beta} + 5.4124348958 \frac{\sqrt{\pi}}{w^2\beta^{3/2}}$$

$$- 5.8958333333 \frac{1}{w^3\beta^2} + 1.1972656250 \frac{\sqrt{\pi}}{w^4\beta^{5/2}}$$

$$- 0.4166666667 \frac{1}{w^5\beta^3} + 0.0195312500 \frac{\sqrt{\pi}}{w^6\beta^{7/2}}$$

$$k_6 = - 0.7998046875 \frac{\sqrt{\pi}}{\beta^{1/2}} + 2.9820312500 \frac{1}{w\beta} - 1.8279947917 \frac{\sqrt{\pi}}{w^2\beta^{3/2}}$$

$$+ 2.0520833333 \frac{1}{w^3\beta^2} - 0.4335937500 \frac{\sqrt{\pi}}{w^4\beta^{5/2}}$$

$$+ 0.1583333333 \frac{1}{w^5\beta^3} - 0.0078125000 \frac{\sqrt{\pi}}{w^6\beta^{7/2}}$$

$$k_7 = 0.1127929688 \frac{\sqrt{\pi}}{\beta^{1/2}} - 0.4236979167 \frac{1}{w\beta} + 0.2634331597 \frac{\sqrt{\pi}}{w^2\beta^{3/2}}$$

$$- 0.3020833333 \frac{1}{w^3\beta^2} + 0.0657552083 \frac{\sqrt{\pi}}{w^4\beta^{5/2}}$$

$$- 0.0250000000 \frac{1}{w^5\beta^3} + 0.0013020833 \frac{\sqrt{\pi}}{w^6\beta^{7/2}}$$

$$n = 8,\ k_1 = 1.5710449219 \frac{\sqrt{\pi}}{\beta^{1/2}} - 3.2105887277 \frac{1}{w\beta} + 1.3221679688 \frac{\sqrt{\pi}}{w^2\beta^{3/2}}$$

$$- 1.1474392361 \frac{1}{w^3\beta^2} + 0.2138671875 \frac{\sqrt{\pi}}{w^4\beta^{5/2}}$$

$$- 0.0815972222 \frac{1}{w^5\beta^3} + 0.0058593750 \frac{\sqrt{\pi}}{w^6\beta^{7/2}}$$

$$- 0.0005952381 \frac{1}{w^7\beta^4}$$

$$k_2 = - 3.6657714844 \frac{\sqrt{\pi}}{\beta^{1/2}} + 12.3790690105 \frac{1}{w\beta} - 6.4500759549 \frac{\sqrt{\pi}}{w^2\beta^{3/2}}$$

$$+ 6.4174913195 \frac{1}{w^3\beta^2} - 1.3063151042 \frac{\sqrt{\pi}}{w^4\beta^{5/2}}$$

$$+ 0.5295138889 \frac{1}{w^5\beta^3} - 0.0397135417 \frac{\sqrt{\pi}}{w^6\beta^{7/2}}$$

$$+ 0.0041666667 \frac{1}{w^7\beta^4}$$

$$k_3 = 6.5983886719 \frac{\sqrt{\pi}}{\beta^{1/2}} - 24.0418945312 \frac{1}{w\beta} + 14.2291992188 \frac{\sqrt{\pi}}{w^2\beta^{3/2}}$$

$$- 15.6483072917 \frac{1}{w^3\beta^2} + 3.4326171875 \frac{\sqrt{\pi}}{w^4\beta^{5/2}}$$

$$- 1.4718750000 \frac{1}{w^5\beta^3} + 0.1152343750 \frac{\sqrt{\pi}}{w^6\beta^{7/2}}$$

$$- 0.0125000000 \frac{1}{w^7\beta^4}$$

$$k_4 = - 7.8552246094 \frac{\sqrt{\pi}}{\beta^{1/2}} + 29.5190429689 \frac{1}{w\beta} - 18.4467773438 \frac{\sqrt{\pi}}{w^2\beta^{3/2}}$$

$$+ 21.6395399306 \frac{1}{w^3\beta^2} - 5.0380859375 \frac{\sqrt{\pi}}{w^4\beta^{5/2}}$$

$$+ 2.2725694445 \frac{1}{w^5\beta^3} - 0.1855468750 \frac{\sqrt{\pi}}{w^6\beta^{7/2}}$$

$$+ 0.0208333333 \frac{1}{w^7\beta^4}$$

$$k_5 = 6.1096191406 \frac{\sqrt{\pi}}{\beta^{1/2}} - 23.3471679689 \frac{1}{w\beta} + 15.0332573785 \frac{\sqrt{\pi}}{w^2\beta^{3/2}}$$

$$- 18.3478732640 \frac{1}{w^3\beta^2} + 4.4671223958 \frac{\sqrt{\pi}}{w^4\beta^{5/2}}$$

$$- 2.1059027778 \frac{1}{w^5\beta^3} + 0.1790364583 \frac{\sqrt{\pi}}{w^6\beta^{7/2}}$$

$$- 0.0208333333 \frac{1}{w^7\beta^4}$$

$$k_6 = -2.9992675781\frac{\sqrt{\pi}}{\beta^{1/2}} + 11.5825195313\frac{1}{w\beta} - 7.6004882813\frac{\sqrt{\pi}}{w^2\beta^{3/2}}$$
$$+ 9.5233072917\frac{1}{w^3\beta^2} - 2.3955078125\frac{\sqrt{\pi}}{w^4\beta^{5/2}}$$
$$+ 1.1718750000\frac{1}{w^5\beta^3} - 0.1035156250\frac{\sqrt{\pi}}{w^6\beta^{7/2}}$$
$$+ 0.0125000000\frac{1}{w^7\beta^4}$$

$$k_7 = 0.8459472656\frac{\sqrt{\pi}}{\beta^{1/2}} - 3.2905273437\frac{1}{w\beta} + 2.1875976563\frac{\sqrt{\pi}}{w^2\beta^{3/2}}$$
$$- 2.7924913194\frac{1}{w^3\beta^2} + 0.7197265625\frac{\sqrt{\pi}}{w^4\beta^{5/2}}$$
$$- 0.3628472222\frac{1}{w^5\beta^3} + 0.0332031250\frac{\sqrt{\pi}}{w^6\beta^{7/2}}$$
$$- 0.0041666667\frac{1}{w^7\beta^4}$$

$$k_8 = -0.1047363281\frac{\sqrt{\pi}}{\beta^{1/2}} + 0.4095470610\frac{1}{w\beta} - 0.2748806424\frac{\sqrt{\pi}}{w^2\beta^{3/2}}$$
$$+ 0.3557725694\frac{1}{w^3\beta^2} - 0.0934244792\frac{\sqrt{\pi}}{w^4\beta^{5/2}}$$
$$+ 0.0482638889\frac{1}{w^5\beta^3} - 0.0045572917\frac{\sqrt{\pi}}{w^6\beta^{7/2}}$$
$$+ 0.0005952381\frac{1}{w^7\beta^4}$$

It can be noted that exact numerical values of the weighting coefficients, k_i, for the "odd" quadrature can easily be calculated for particular β and w. The expressions for k_i are presented to ten significant figures; however, due to the accumulation of round off error in the computer

it is felt that no claim should be laid to an accuracy greater than nine decimal places.

The Optimum Spacing

The optimum spacing is determined from the Lagrange error term [36]. The Lagrange formula gives

$$f(v) = \sum_{i=1}^{n} \frac{P_i(v)}{P_i(a_i)} f(a_i) + R_{n-1}(v) \qquad (A-7)$$

where $R_{n-1}(v)$ is the error term,

$$R_{n-1}(v) = \pi_{n-1}(v) \frac{f^{(n)}(\xi)}{n!} , \quad v_1 \leq \xi \leq v_n , \qquad (A-8)$$

and

$$\pi_{n-1}(v) = (v - a_1)(v - a_2)\cdots\cdots(v - a_n)$$

Thus, the error term in Equation (A-2) becomes

$$E = \frac{1}{n!} \int_0^{\infty} e^{-\beta v^2} \pi_{n-1}(v) f^{(n)}(\xi) dv \qquad (A-9)$$

where, for both "odd" and "even" equally spaced quadratures, $\pi_{n-1}(v)$ is a function of spacing, w, i.e.,

$$\pi_{n-1}(v) = (v-w)(v-2w)(v-3w)\cdots\cdots(v-nw) .$$

To obtain the optimum spacing which will minimize the error, one must minimize E, or,

$$\frac{dE}{dw} = \frac{1}{n!} \int_0^\infty e^{-\beta v^2} \frac{d}{dw} [\pi_{n-1}(v)] f^{(n)}(\xi(v))dv = 0 \qquad (A-10)$$

Equation (A-10) yields a polynomial of degree n-1 in w from which the zeros for w yield the optimum, or minimum error, spacing, w'.

For an arbitrary unknown function f(v), the optimum spacing is found from the relation

$$\int_0^\infty e^{-\beta v^2} \frac{d}{dw} [\pi_{n-1}(v)]dv = 0 \qquad (A-11)$$

for any order of approximation n.

The optimum spacings obtained for cases n = 2, 3, 4, 5, 6, 7, and 8 are respectively 0.421, 0.426, 0.32, 0.316, 0.27, 0.262, and 0.23.

APPENDIX B

ON THE CONVERGENCE OF THE TWO-DIMENSIONAL FINITE DIFFERENCE FORMULATION IN CHAPTER III

The numerical formulation of the non-linear BBGK equation requires the solution of a system composed of a large number of simultaneous non-linear algebraic equations. Since a closed form solution of such a system is intractable, an iterative scheme is required. The procedure proposed in Chapter III to solve the difference equations is a Gauss-Seidel type formulation, and the question of convergence of the technique is based to a large extent on a knowledge of the eigenvalues of the matrix B in the system

$$\bar{f}^{(m+1)} = B\bar{f}^{(m)} + D \qquad (B\text{-}1)$$

where $\bar{f}$ is the column vector of the dependent variable.

For a large and complicated matrix B, the difficulty in finding the eigenvalues is of the same order of magnitude as that encountered in finding the dependent variable. However, a feeling for the rate of convergence can be attained by employing a linear analysis to find an approximate value for the largest Gauss-Seidel eigenvalue.

To the iterative method proposed in Equation (B-1), one can associate error vectors $\bar{\varepsilon}^{(m)}$ defined by

$$\bar{\varepsilon}^{(m)} = \bar{f}^{(m)} - \bar{f} \qquad (B\text{-}2)$$

where $\bar{f}$ is the unique solution of Equation (B-1), and from the very

definition of the iterative method, the error vectors can be expressed as

$$\bar{\varepsilon}^{(m)} = B\bar{\varepsilon}^{(m-1)} = \ldots = B^{m}\bar{\varepsilon}^{(o)} \quad , \quad m > 0 \tag{B-3}$$

where B is the corresponding iteration matrix for the method. The error vectors $\bar{\varepsilon}$ tend to the zero vector if and only if the spectral radius $\rho(B)$ of the matrix B is less than unity [65]. The spectral radius is defined as

$$\rho(B) = \max_{0 \leq i \leq n} |\lambda_i| \tag{B-4}$$

where λ_i are the eigenvalues of the matrix B. Hence, if the eigenvalues of B are less than unity the method will converge.

Equation (B-3) can be written approximately for a component of the error vector as [70]

$$\varepsilon_i^{(m)} \approx \lambda_{G.S.}\, \varepsilon_i^{(m-1)} \tag{B-5}$$

where $\lambda_{G.S.}$ is the largest eigenvalue of the Gauss-Seidel matrix B. Combining Equation (B-5) with a similar equation for $\varepsilon^{(m-1)}$ one obtains

$$\lambda_{G.S.} \approx \frac{\varepsilon_i^{(m)} - \varepsilon_i^{(m-1)}}{\varepsilon_i^{(m-1)} - \varepsilon_i^{(m-2)}} \approx \frac{\bar{f}_i^{(m)} - \bar{f}_i^{(m-1)}}{\bar{f}_i^{(m-1)} - \bar{f}_i^{(m-2)}} \quad . \tag{B-6}$$

The independent variable for the present solution is the velocity distribution function. However, the final solution is based on velocity moments of the distribution function, and these moments can be applied to Equation (B-6). A random sampling of all moments for several $\hat{x}$ stations and for several iterations of the results of Chapter III was performed.

The approximate value of $\lambda_{G.S.}$ was found to be

$$\lambda_{G.S.} \lesssim 0.2 \qquad \text{(B-7)}$$

Based on this finding as well as the intuitively correct nature of the solution, the finite difference formulation and iterative scheme outlined in Chapter III are assumed to be convergent.

BIBLIOGRAPHY

1. S. Chapman and T. G. Cowling, The Mathematical Theory of Non-Uniform Gases, Cambridge University Press, London (1958).

2. D. Burnett, "The Distribution of Velocities in a Slightly Non-Uniform Gas," Proc. Math. Soc. 2, 385 (1933).

3. H. Grad, "On the Kinetic Theory of Rarefied Gases," Pure Appl. Math. 2, 331 (1949).

4. H. Yang and L. Lees, "Rayleigh's Problem at Low Mach Numbers According to the Kinetic Theory of Gases," J. of Math. and Phys. 35, 195 (1956).

5. H. M. Mott-Smith, "A New Approach in the Kinetic Theory of Gases," M.I.T., Lincoln Lab. Group Report V-2 (1952).

6. C. S. Wang Chang and G. E. Uhlenbeck, "The Couette Flow Between Two Parallel Plates as a Function of Knudsen Number," University of Michigan Engineering Research Institute, Report Number 119-1-T (1954).

7. E. P. Gross, E. A. Jackson, and S. Ziering, "Boundary Value Problems in Kinetic Theory of Gases," Annals of Physics 1, 141 (1957).

8. A. B. Huang and R. L. Stoy, "Rarefied Gas Channel Flows for Three Molecular Models," Physics of Fluids 9, 2327 (1966).

9. D. Mintzer, "Generalized Orthogonal Polynomial Solutions of the Boltzmann Equation," Physics of Fluids 8, 1076 (1965).

10. L. Lees, "Kinetic Theory Description of Rarefied Gas Flow," J. Soc. Indust. Appl. Math. 13, 278 (1965).

11. D. R. Willis, "Comparison of Kinetic Theory Analyses of Linearized Couette Flow," Physics of Fluids 5, 127 (1962).

12. M. Krook, "Continuum Equations in the Dynamics of Rarefied Gases," J. of Fluid Mech. 6, 523 (1959).

13. P. L. Bhatnagar, E. P. Gross, and M. Krook, "A Model for Collision Processes in Gases," Physical Review 94, 511 (1954).

14. D. Anderson, "Numerical Solutions of the Krook Kinetic Equation," J. of Fluid Mech. 25, 271 (1966).

15. H. K. Macomber, "Moment Methods for Non-Linear Problems in Kinetic Theory," Harvard University, Engineering Science Laboratory, Technical Report Number 13 (1965).

16. D. R. Willis, "On the Flow of Gases Under Nearly Free Molecular Flow Conditions," Princeton University, Aeronautical Engineering Report Number 442 (1958).

17. C. Cercignani and C. D. Pagani, "Variational Approach to Boundary Value Problems in Kinetic Theory," Physics of Fluids 9, 1167 (1966).

18. C. K. Chu, "Kinetic Theory Description of Shock Wave Formation II," Physics of Fluids 8, 1450 (1965).

19. C. K. Chu, "The High Mach Number Rayleigh Problem According to the Krook Model," in Rarefied Gas Dynamics, ed. by C. L. Brundin, 589 (Academic Press, New York, 1967).

20. S. Chandrasekhar, Radiative Transfer, Dover Publishing Company, New York (1960).

21. A. B. Huang and D. P. Giddens, "Kinetic Theory of the Transient Development of Couette Flow Between Parallel Plates," Physics of Fluids, (to be published).

22. A. B. Huang and D. P. Giddens, "The Discrete Ordinate Method for the Linearized Boundary Value Problems in Kinetic Theory of Gases," in Rarefied Gas Dynamics, ed. by C. L. Brundin, 481 (Academic Press, New York, 1967).

23. A. B. Huang, D. P. Giddens, and C. W. Bagnal, "Rarefied Gas Flow Between Parallel Plates Based on the Discrete Ordinate Method," Physics of Fluids 10, 498 (1967).

24. A. B. Huang and D. P. Giddens, "The Discrete Ordinate Method for Unsteady Linearized Boltzmann-Bhatnagar-Gross-Krook Equation," Physics of Fluids 10, 232 (1967).

25. A. B. Huang and D. P. Giddens, "Rayleigh's Problem at Low Mach Numbers Based on Kinetic Theory," J. AIAA 5, 1354 (1967).

26. A. B. Huang, "Slip Coefficient of a Gas," Physics of Fluids (to be published).

27. A. B. Huang, "Evaluation of the Integral $\int_0^\infty u^m \exp(-u^2-x/u)du$ by the Discrete Ordinate Method," J. of Math. and Phys. 46, 107 (1967).

28. D. P. Giddens, "Study of Rarefied Gas Flows by the Discrete Ordinate Method," Georgia Institute of Technology, Ph.D. Thesis (1966).

29. A. B. Huang, "General Discrete Ordinate Method for the Dynamics of Rarefied Gases," Georgia Institute of Technology, School of Aerospace Engineering, Rarefied Gasdynamics Report Number 4 (1967), also Physics of Fluids (to be published).

30. A. B. Huang and D. P. Giddens, "A New Table for a Modified (Half-Range) Gauss-Hermite Quadrature with an Evaluation of the Integral $\int_0^\infty \exp(-u^2-x/u)du$," J. of Math. and Phys., (to be published).

31. A. B. Huang and D. L. Hartley, "The Odd and Even Equally Spaced Quadratures for the Non-Linear Boltzmann Equation," (to be published).

32. J. E. Broadwell, "Study of Rarefied Shear Flow by the Discrete Velocity Method," J. of Fluid Mech. 19, 401 (1964).

33. B. B. Hamel and M. Wachman, "A Discrete Ordinate Technique for the Linearized Boltzmann Equation with Application to Couette Flow," General Electric Report R64SD53 (1964), also in Rarefied Gas Dynamics, ed. by J. H. deLeeuw, 370 (Academic Press, New York, 1965).

34. N. G. Van Kampen, "On the Theory of Stationary Waves in Plasmas," Physica 21, 949 (1955).

35. H. Schlichting, Boundary Layer Theory, McGraw-Hill Book Company, Inc., New York, Fourth Edition (1962).

36. Z. Kopal, Numerical Analysis, Wiley and Sons, New York, Chapters 2,4 (1961).

37. H. M. DeGroff, "On Viscous Heating," JAS 23, 395 (1956).

38. Y. S. Pan and R. F. Probstein, "Rarefied Flow Transition at a Leading Edge," M.I.T., Fluid Mech. Lab. Report 64-8 (1964).

39. L. Talbot, "Criterion for Slip Near the Leading Edge of a Flat Plate in Hypersonic Flow," J. AIAA 1, 1169 (1963).

40. E. S. Moulic, Jr., "Local Skin Friction and Induced Pressure Measurements on a Sharp-Edged Insulated Flat Plate in Low Density Hypersonic Flow," Univ. Calif. (Berkeley) Tech. Report on NSF Grant GP-2520, Series 7, Number 3 (1966).

41. J. L. Potter, "The Transitional Rarefied-Flow Regime," in Rarefied Gas Dynamics, ed. by C. L. Brundun, 881 (Academic Press, New York, 1967).

42. J. V. Becker, "Results in Recent Hypersonic and Unsteady Research at the Langley Aeronautical Laboratory," J. of Applied Phys. 21, 622 (1950).

43. W. D. Hayes and R. F. Probstein, Hypersonic Flow Theory, Academic Press, New York, Chapter 9 (1959).

44. S. A. Schaaf, F. C. Hurlburt, L. Talbot, and J. Aroesty, "Viscous Interaction Experiments at Low Reynolds Numbers," J. ARS 29, 527 (1959).

45. J. A. Laurmann, "Free Molecule Probe and Its Use for the Study of Leading Edge Flows," Physics of Fluids 1, 469 (1958).

46. H. T. Nagamatsu and R. E. Sheer, Jr., "Hypersonic Shock Wave Boundary Layer Interaction with Leading Edge Slip," J. ARS 30, 454 (1960).

47. H. T. Nagamatsu, J. A. Weil, and R. E. Sheer, Jr., "Heat Transfer in High Temperature Rarefied Ultra-high Mach Number Flow," J. ARS 32, 533 (1962).

48. M. Becker and D. E. Boylan, "Experimental Flow Field Investigations Near the Sharp Leading Edge of a Cooled Flat Plate in a Hypervelocity, Low-Density Flow," in Rarefied Gas Dynamics, ed. by C. L. Brundin, 993 (Academic Press, New York, 1967).

49. W. J. McCroskey, "An Experimental Model for the Sharp Leading Edge Problem in Rarefied Hypersonic Flow," ARL Report 66-0101 (1966).

50. R. J. Vidal and C. E. Wittliff, "Hypersonic Low Density Studies of Blunt and Slender Bodies," in Rarefied Gas Dynamics, ed. by J. A. Laurmann, 343 (Academic Press, New York, 1963).

51. J. E. Wallace and A. F. Burke, "Skin Friction, Heat Transfer and Pressure Distributions Over a Flat Plate and Highly Swept Delta Wings with Sharp and Blunt Leading Edges at Angles of Attack in Hypersonic Flow," in Rarefied Gas Dynamics, ed. by J. H. deLeeuw, 487 (Academic Press, New York, 1965).

52. R. L. Chuan and S. A. Waiter, "Experimental Study of Hypersonic Rarefied Flow Near the Leading Edge of a Thin Flat Plate," in Rarefied Gas Dynamics, ed. by J. A. Laurmann, 328 (Academic Press, New York, 1963).

53. L. Lees and R. F. Probstein, "Hypersonic Viscous Flow over a Flat Plate," Princeton University, Dept. of Aero. Engineering Report 195 (1952).

54. J. Aroesty, "Slip Flow and Hypersonic Boundary Layers," J. AIAA 2, 189 (1964).

55. J. A. Laurmann, "Structure of the Boundary Layer at the Leading Edge of a Flat Plate in Hypersonic Slip Flow," J. AIAA 2, 1655 (1964).

56. T. Y. Li and H. T. Nagamatsu, "Hypersonic Viscous Flow on a Non-Insulated Flat Plate," Proc. Fourth Midwestern Conf. on Fluid Mech., Purdue Univ., Number 128 (1955).

57. R. Garvine, "On Hypersonic Viscous Flow Near a Sharp Leading Edge," Princeton University, Dept. of Aerospace and Mechanical Sciences Report 755 (1965).

58. H. Oguchi, "The Sharp Leading Edge Problem in Hypersonic Flow," in Rarefied Gas Dynamics, ed. by L. Talbot, 501 (Academic Press, New York, 1961).

59. H. Oguchi, "Leading Edge Slip Effects in Rarefied Hypersonic Flow," in Rarefied Gas Dynamics, ed. by J. A. Laurmann, 181 (Academic Press, New York, 1963).

60. T. D. Butler, "Numerical Solutions of the Hypersonic Sharp-Leading-Edge Flows," Los Alamos Scientific Laboratory Report LA-DC-8250 (1967), also Physics of Fluids 10, 1205 (1967).

61. A. F. Charwat, "Theoretical Analysis of Near Free Molecular Hypersonic Flow at the Sharp Leading Edge of a Flat Plate," in Rarefied Gas Dynamics, ed. by J. A. Laurmann, 553 (Academic Press, New York, 1963).

62. M. N. Kogan, "On Hypersonic Flows of a Rarefied Gas," NASA TTF-8286 (1962), translated from Prikladnaya matematika i mekhanika, Tom 26, 520, O.T.N.A.N. USSR (1962).

63. G. A. Bird, "Aerodynamic Properties of Some Simple Bodies in the Hypersonic Transition Regime," J. AIAA 4, 55 (1966).

64. H. W. Liepmann, R. Narasimha, and M. Chahine, "Structure of a Plane Shock Layer," Physics of Fluids 5, 1313 (1962).

65. R. S. Varga, Matrix Iterative Analysis, Prentice-Hall, Inc., Englewood Cliffs, N. J., 59 (1962).

66. D. Gilbarg and D. Paolucci, "The Structure of Shock Waves in the Continuum Theory of Fluids," J. Rat. Mech. Anal. 2, 617 (1953).

67. H. Mirels, "Estimate of Slip Effects on Compressible Laminar-Boundary-Layer Skin Friction," NACA TN 2609 (1952).

68. W. L. Chow, "Hypersonic Flow Past the Leading Edge of a Flat Plate," J. AIAA 4, 2062 (1966).

69. F. D. Burgoyne, "Quadrature Formulas Over Infinite Intervals in Terms of Differences," Math. of Comp. 16, 298 (1962).

70. V. N. Faddeeva, Computational Methods of Linear Algebra, Dover Publications, Inc., New York, 205 (1959).

VITA

Danny Lynn Hartley was born in North Little Rock, Arkansas, on September 10, 1941. His parents are Edward L. and Hally Hartley. He attended forty-eight different elementary schools in thirty states. His high school education was begun at Balboa, Panama Canal Zone, and was completed at the American High School, Monterrey, Mexico, where he was graduated valedictorian in June, 1959.

In September of 1959, he entered the Georgia Institute of Technology, and in June of 1963, was graduated with honor as a Bachelor of Aerospace Engineering.

In the summer of 1962 he was employed by Douglas MSSD in Santa Monica, California. In June of 1963 he was employed by Lockheed MSSD in Sunnyvale, California, as an associate engineer.

He returned to the Georgia Institute of Technology in September of 1964 as a graduate student. He was awarded an NDEA fellowship to study under the doctoral program. The degree of Master of Science in Aerospace Engineering was awarded him in June of 1966. He is a member of Sigma Gamma Tau, Tau Beta Pi, Phi Kappa Phi, Phi Eta Sigma, Pi Delta Epsilon, Sigma Xi, and Delta Tau Delta; was selected to appear in Who's Who Among Students in American Colleges and Universities, 1963-64; and has been chosen to attend the von Karman Institute for Fluid Dynamics as a Research Fellow during 1967-68.

On June 10, 1963, he married the former Barbara Ann White of Louisville, Kentucky; they have one child, Dana Elizabeth.